SANTA PAULA-MOUND-FOREBAY BASIN BOUNDARY TDEM GEOPHYSICAL SURVEY

Open-File Report 2020-01
March 2020

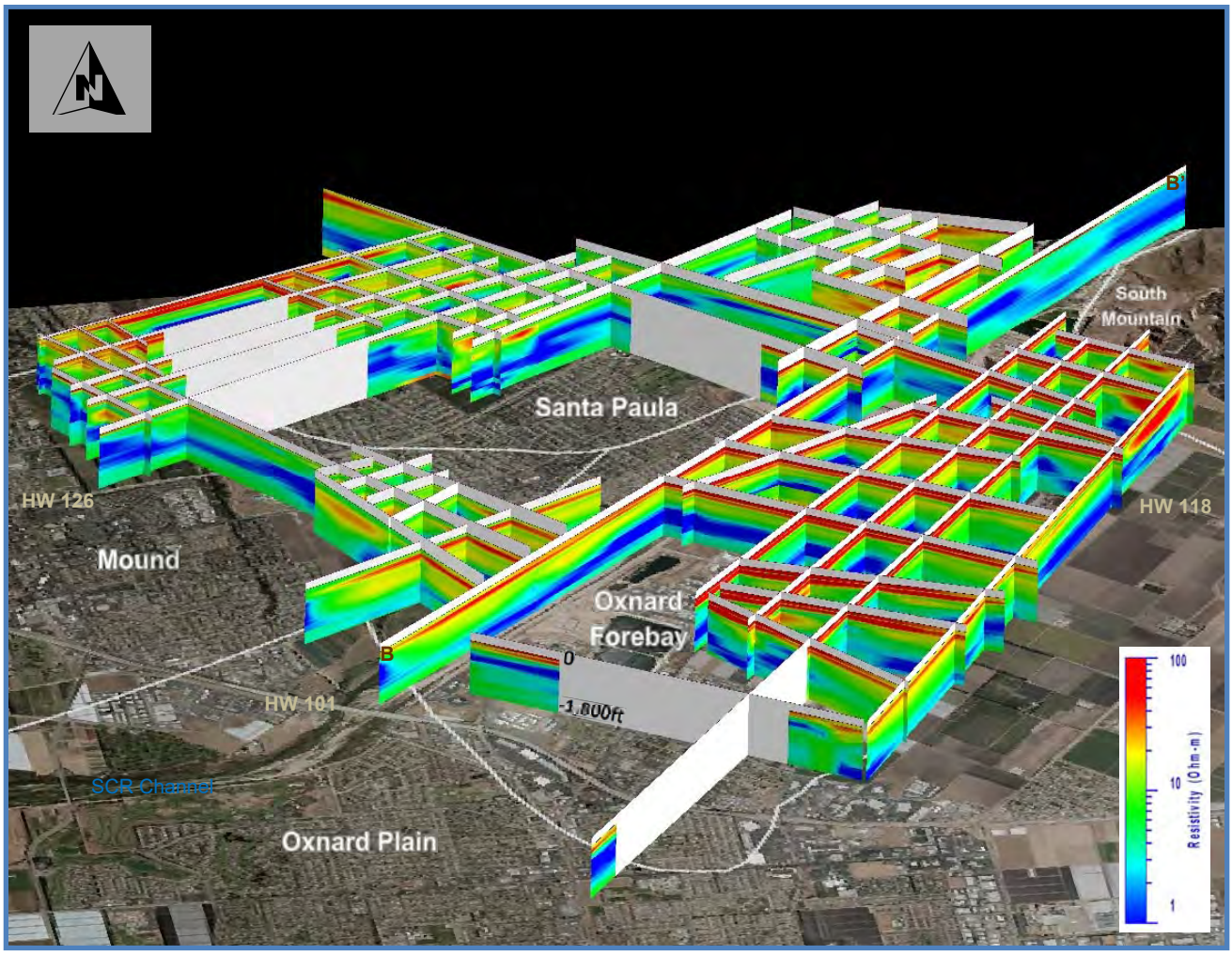

THIS REPORT IS PRELIMINARY AND IS SUBJECT TO MODIFICATION BASED UPON FUTURE ANALYSIS AND EVALUATION

PREPARED BY
GROUNDWATER
RESOURCES
DEPARTMENT

United Water
CONSERVATION DISTRICT

SANTA PAULA-MOUND-FOREBAY BASIN BOUNDARY TDEM GEOPHYSICAL SURVEY

United Water Conservation District
Open-File Report 2020-01

PREPARED BY

GROUNDWATER RESOURCES DEPARTMENT

MARCH 2020

THIS REPORT IS PRELIMINARY AND IS SUBJECT TO MODIFICATION BASED UPON FUTURE ANALYSIS AND EVALUATION

Cover Photo: Fence diagram of 2011-2014 TDEM soundings with 1 to 100 Ohm-m color ramp looking obliquely north.

Preferred Citation: United Water Conservation District, 2020, Santa Paula-Mound-Forebay Basin Boundary TDEM Geophysical Survey, United Water Conservation District Open-File Report 2020-01.

Principal Authors: Tim Moore, PG, CHG, Eric Elliott, Martin Miele, PGP, PG

SANTA PAULA-MOUND-FOREBAY BASIN BOUNDARY TDEM GEOPHYSICAL SURVEY

UWCD OPEN-FILE REPORT 2020-01

EXECUTIVE SUMMARY / ABSTRACT

United Water Conservation District (United) conducted a Time Domain Electromagnetics (TDEM) surface geophysical survey in the Mound and Santa Paula groundwater basins in summer-fall 2013 and winter 2014. TDEM data collected in fall 2011 and summer 2012 in the adjacent Oxnard Forebay (Forebay) groundwater basin were subsequently published as UWCD Open-File Report 2013-06. The purpose of this present study is to advance understanding of subsurface geologic conditions such as the depth and continuity of hydrostratigraphic units that affect groundwater flow at and near the boundaries between Santa Paula and Mound basins and the adjacent Forebay basin.

The study area covered approximately nine square miles consisting of agricultural fields, orchards and open private land within and near the Santa Paula and Mound basins. A total of 116 high-quality soundings were obtained in 2013 and 2014 in the study area. Geophysical software was used to model the data associated with each sounding and the model results were used to correlate the individual soundings in 32 resistivity cross-sections. The distinguishable zones or layers apparent in the modeled soundings correlated in cross-section are referred to as “geoelectric layers”.

The modeled depths of geoelectric layers may not coincide with aquifer depths. Permeable coarse-grained material such as sand and gravel is typically more resistive than less permeable fine-grained materials such as silt and clay. The TDEM method provides an indication of grain size and porosity of various beds at depth, but there is not a direct relationship between resistivity, grain size and porosity due to the many variables that influence the measured resistivity for a given sounding.

Aquifer delineation can be difficult using TDEM surface geophysical methods alone. The large TDEM transmitter loop laid on the ground surface required to obtain the desired depth of investigation for this project is subject to significant lateral influence (averaging) of the modeled geoelectric layers. However, in this study the TDEM method was particularly useful for showing the degree of lateral continuity of units. Other sources of data such as borehole electrical resistivity logs (electrical logs) are useful for comparison when interpreting surface geophysical data.

The resistivity data from this project can be roughly divided into three geoelectric layers; these layers may not coincide with previously mapped hydrostratigraphic horizons but are useful for interpretation of the TDEM data. Geoelectric Layer 1 is represented by the Semi-perched, Oxnard and Upper Mugu aquifers, and other age-equivalent material; Layer 2 is represented by the Lower Mugu and Upper Hueneme aquifers, and other age-equivalent hydrostratigraphic units in the study area; and Layer 3 is represented by the Lower Hueneme and Fox Canyon aquifers (San Pedro Formation), the Santa Barbara Formation, and other age-equivalent material.

Several of the cross-sections show offset in the low resistivity intervals in geoelectric Layers 2 and 3, but the offset is less apparent or absent in geoelectric Layer 1. Changes in the resistivity of the geoelectric layers are apparent in the cross-sections that transverse the mapped Mound-Forebay basin boundary. The geoelectric changes are interpreted to reflect changes in depositional/erosional environments and/or suspected faulting. Highly resistive features interpreted to be coarse-grained paleo-channel deposits of the Santa Clara River were observed in the Forebay near the Santa Paula basin boundary. Geoelectric layer changes across the mapped Santa Paula-Forebay basin boundary show faulting and thinning of the shallow resistive zones near South Mountain.

The TDEM data confirm the location of several geologic features recognized by previous investigators in the study area. Evidence of the alignments of the Oak Ridge Fault and the axis of the Montalvo anticline to the south are readily apparent in the TDEM data. Highly resistive ancestral channel deposits of the Santa Clara River were also observed near and along the Forebay's northwestern boundary adjacent the Mound basin.

The mapped traces of the Country Club Fault, which form the Santa Paula-Mound basin boundary, are located almost entirely beneath developed land, preventing the collection of useful TDEM data. One cross-section (located in an adjacent undeveloped area) does, however, show a low-resistivity anomaly that may correspond with the northwest portion of the fault zone.

The TDEM sections also show evidence of a previously unmapped extension of the Ventura Fault extending farther east into the Santa Paula basin than has traditionally been recognized. Further investigation is required to confirm if this geoelectric anomaly is an extension of the Ventura Fault or results from other, as yet undetermined, subsurface conditions.

SANTA PAULA-MOUND-FOREBAY BASIN BOUNDARY TDEM GEOPHYSICAL SURVEY

TABLE OF CONTENTS

LIST OF FIGURES

1 INTRODUCTION AND PROJECT PURPOSE

United Water Conservation District (United) acknowledges and thanks the many landowners that permitted access to their property and various other accommodations that made the collection of the field data possible.

1.1 UNITED WATER CONSERVATION DISTRICT

United is a public agency within Ventura County, California that is governed by a seven-person board of directors elected by region. The District is charged with managing, protecting, conserving and enhancing the water resources of the Santa Clara River, its tributaries and associated aquifers, including those portions of the Santa Paula, Mound, and Oxnard basins that are within the study area for the geophysical survey described in this report. After completion of field data collection and data analysis discussed in this report, groundwater subbasin boundaries were modified by local agencies for geologic, hydrologic or jurisdictional reasons. The final basin boundary modifications were released by the California Department of Water Resources in February 2019. Fig. 1.1-1 is a location map showing the recently modified basin boundaries together with the former basin boundaries. It should be noted that the subsequent figures in this report show the former basin boundaries (as they were located when the fieldwork for this geophysical survey was conducted). The modifications of basin boundaries do not change the overall conclusions reached in this report. Figure 1.1-2 is a location map of the former basin boundaries and select facilities.

United encompasses nearly 213,000 acres of central Ventura County, including the Ventura County portion of the Santa Clara River Valley and the Oxnard Plain. The developed areas within United's district boundaries are a mix of agriculture and urban areas, with prime agricultural land supporting high-dollar crops such as avocados, strawberries, row crops, lemons, and flowers. More than 370,000 people live within United's district boundaries, including those living in the cities of Oxnard, Port Hueneme, Santa Paula, Fillmore and eastern Ventura.

United is authorized under the California Water Code to conduct water resource investigations, acquire water rights, build facilities to store and recharge water, construct wells and pipelines for water deliveries, commence actions involving water rights and water use, and prevent interference with or diminution of stream/river flows and their associated natural subterranean supply of water (California Water Code, section 74500 et al.).

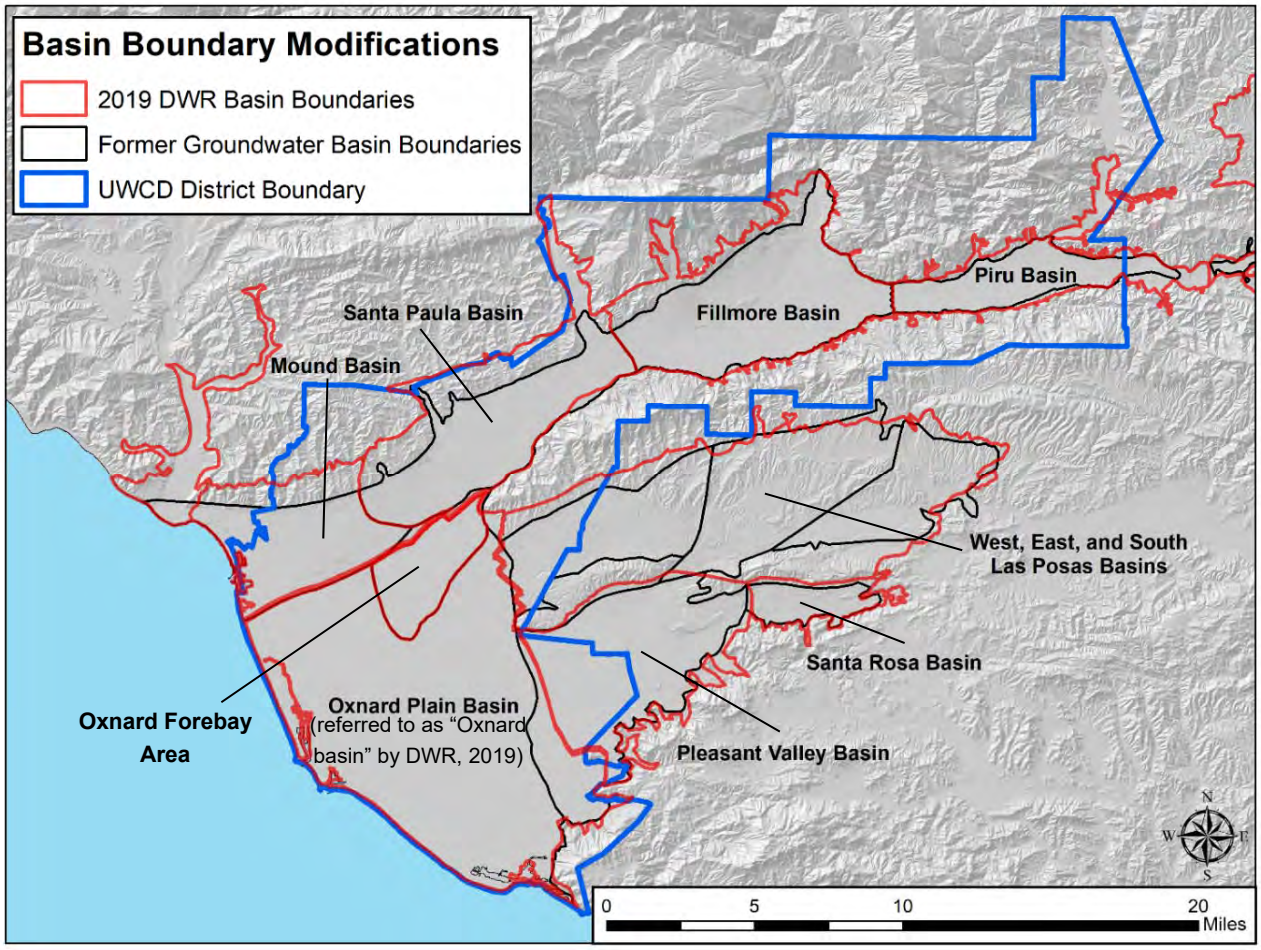

Figure 1.1-1. – Location map for basin boundary modifications and former basin boundaries within and near United Water Conservation District.

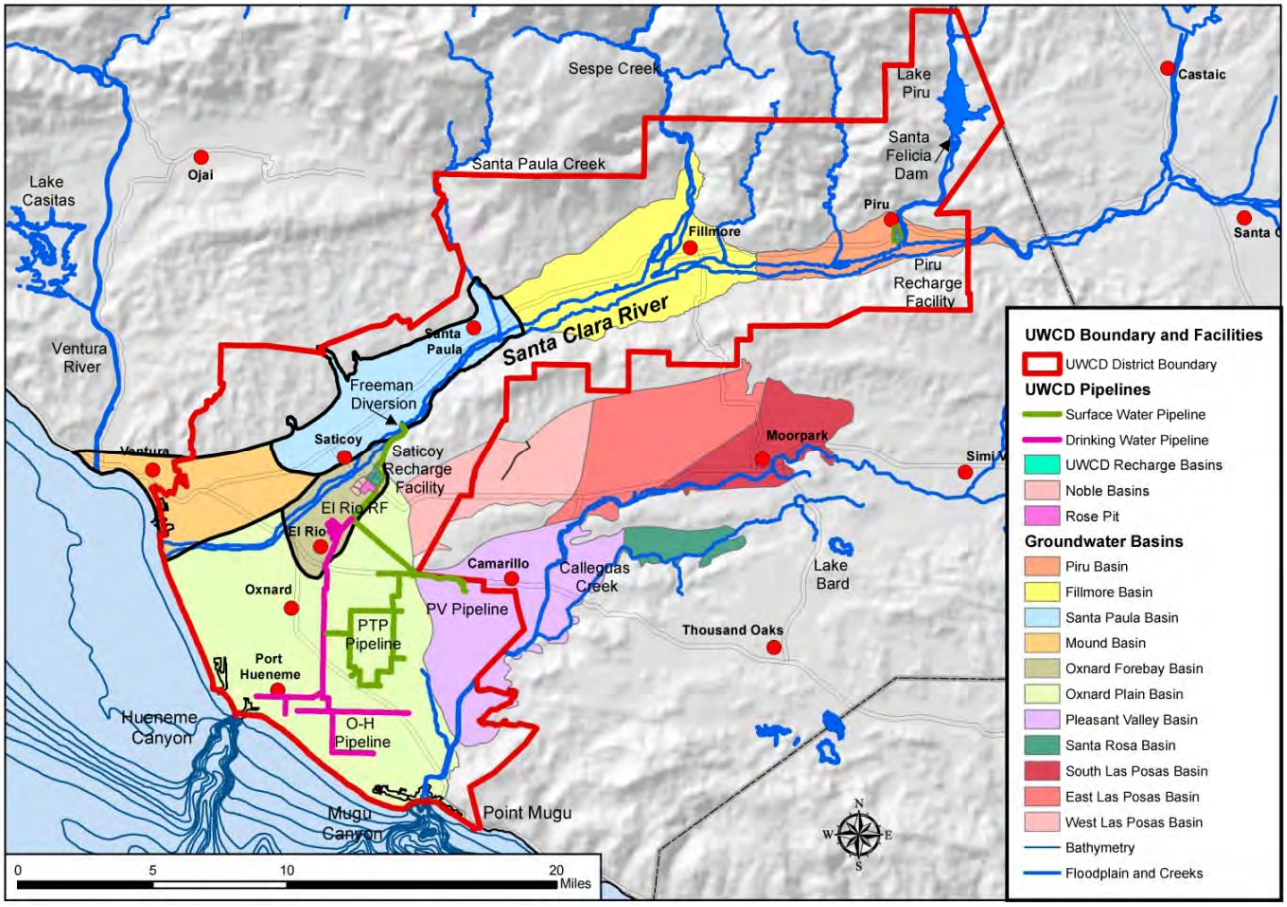

Figure 1.1-2. Location map for the Santa Paula, Mound, Oxnard basins and other groundwater basins, and United Water Conservation District.

1.2 PROJECT PURPOSE

This investigation is an extension of United's fall 2011 and summer 2012 TDEM survey in the Forebay area of the Oxnard basin. Those data were published as UWCD Open-File Report 2013-06 (UWCD, 2013) and examined the occurrence of low-permeability (low resistivity) units in the Forebay, and how thickness and continuity of those units change across the Forebay-Oxnard Plain basin boundary. The 2013 Forebay TDEM Open-File Report includes a cursory examination of geoelectric changes across the Mound-Forebay basins boundary.

The purpose of this present study is to advance understanding of subsurface geologic conditions that affect groundwater flow at and near the boundaries between Santa Paula and Mound basins and the adjacent Forebay area (the study area), such as depth and continuity of hydrostratigraphic units.

The groundwater basins within United's district boundaries are hydrogeologically connected (UWCD, 2014). Activities in one basin can affect adjacent up-gradient and down-gradient basins. A significant portion of groundwater recharge to the Mound basin is thought to be underflow from Santa Paula basin and to a lesser extent from the Forebay when groundwater levels are high. United conducts managed aquifer recharge activities, including the distribution water from the Santa Clara River to

recharge facilities in the Forebay. These recharge activities raise groundwater elevations in the Forebay and promote increased groundwater flow to adjacent basins.

Understanding the complex boundaries between the Santa Paula, Mound and Forebay basins is important for future planning and management of the groundwater resources. Moreover, one of the requirements of California's Sustainable Groundwater Management Act (SGMA) is consideration of conditions in adjacent basins.

In addition to improving the general knowledge of flow across basin boundaries in the study area, United has developed a detailed basin conceptual model that serves as the basis for construction of a numerical groundwater flow model. The conceptual model relies on a large number of oil and water well borehole electrical resistivity logs and other sources of information. This TDEM survey encompassing the greater Santa Paula-Mound-Forebay basin boundary area provides additional detail and potential refinement to the existing conceptual model. SGMA requires that detailed hydrogeologic conceptual models be included in the Groundwater Sustainability Plans (GSPs) that must be developed for all high- and medium-priority basins within the State.

2 GEOLOGIC / HYDROLOGIC SETTING

An overview of the geologic setting and hydrogeologic conditions of the study area and vicinity is provided in this section.

The basins within United's boundary are part of the Transverse Ranges geomorphic province, in which the mountain ranges and basins are oriented east-west rather than the typical northwest-southeast trend over much of California. Geologic structure within the Transverse Ranges is dominated by north-south compression, resulting in east-west trending folds and thrust faults that create the elongate mountains and valleys that dominate Ventura and Santa Barbara County landscape. The study area is within the regional Ventura basin, which is an elongate east-to-west trending, structurally-complex syncline within the Transverse Ranges province (Yeats, et. al., 1981). Land surface elevation of the study area ranges about 500 feet above mean sea level (amsl) near Brown Barranca in Santa Paula basin to about 70 feet amsl at the southern end of the Santa Clara River floodplain in the Forebay.

Active thrust faults border the basins of the Santa Clara River valley, causing uplift of the adjacent mountains and down-dropping of the basins. The total stratigraphic thickness of upper Cretaceous, Tertiary, and Quaternary strata exceeds 55,000 feet in places (Sylvester and Brown, 1988). The sediments were deposited in both marine and terrestrial settings. Figure 2-1 is a geologic map of the region showing surface geology, major faults and location of the basins.

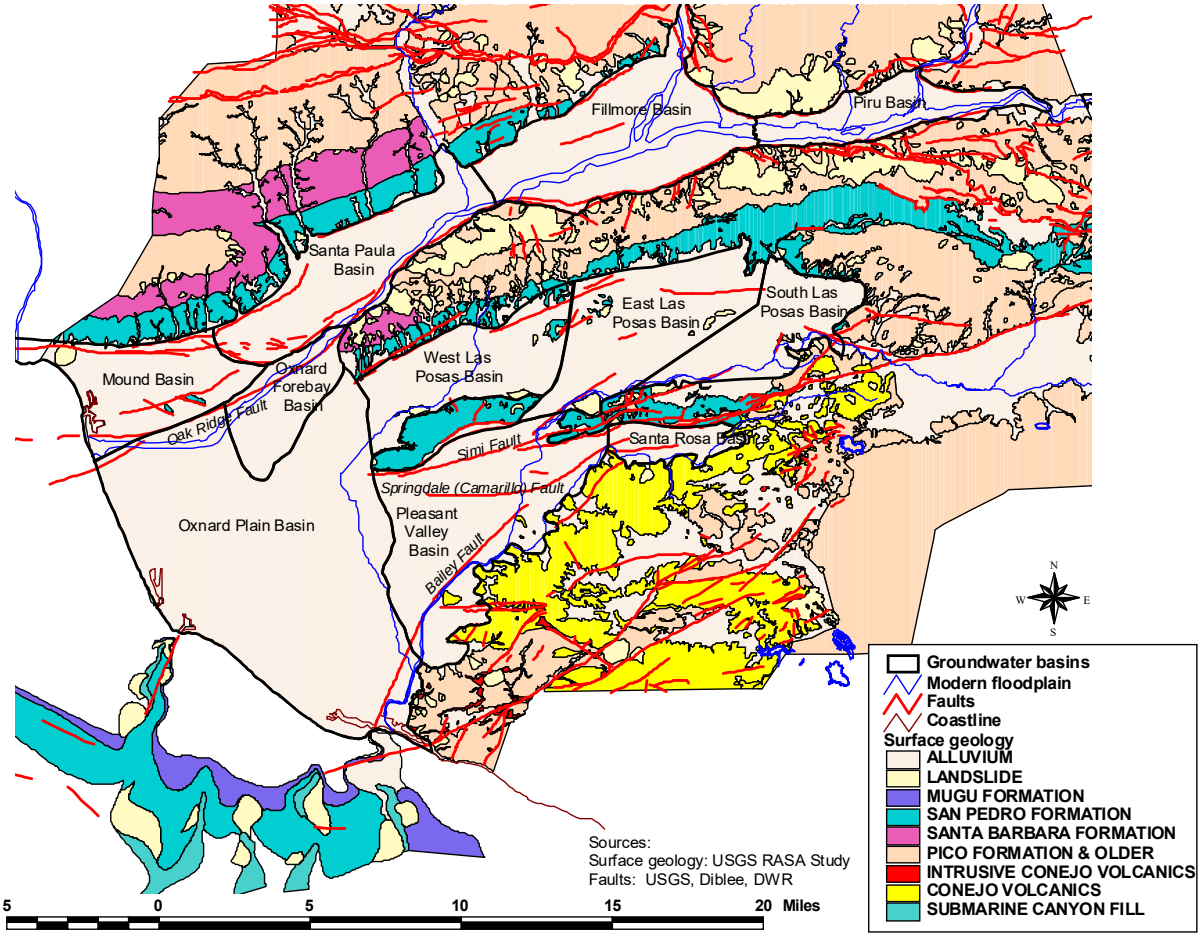

Figure 2-1. Surface geology, major faults and groundwater basins of the western Ventura basin.

Figure 2-2 is a schematic showing typical depths and relationships between the major hydrostratigraphic units (i.e., aquifers and aquifer systems) and their geologic formations and ages as typically defined in the Oxnard basin. The aquifers and aquitards of the study area are generally grouped into the Upper Aquifer System (UAS) and Lower Aquifer System (LAS) (Turner, 1975; Mukae and Turner, 1975).

In general the Oxnard and Mugu aquifers comprise the UAS; and the LAS includes the Hueneme, Fox Canyon, and Grimes Canyon aquifers. The aquifers consist primarily of gravel and sand deposited in fluvial and deltaic environments by the ancestral Santa Clara River, and in alluvial fans along the flanks of the mountains by smaller streams. The Santa Clara River has formed a large coastal plain between the mountains of the Transverse Ranges in the north and the Pacific Ocean to the southwest. The aquifers are recharged by infiltration of streamflow (primarily the Santa Clara River), artificial recharge (diverted stream flow), mountain-front recharge along the exterior boundary of the basins, direct infiltration of precipitation on the valley floors and on bedrock outcrops in adjacent mountain fronts, and irrigation return flow in agricultural areas.

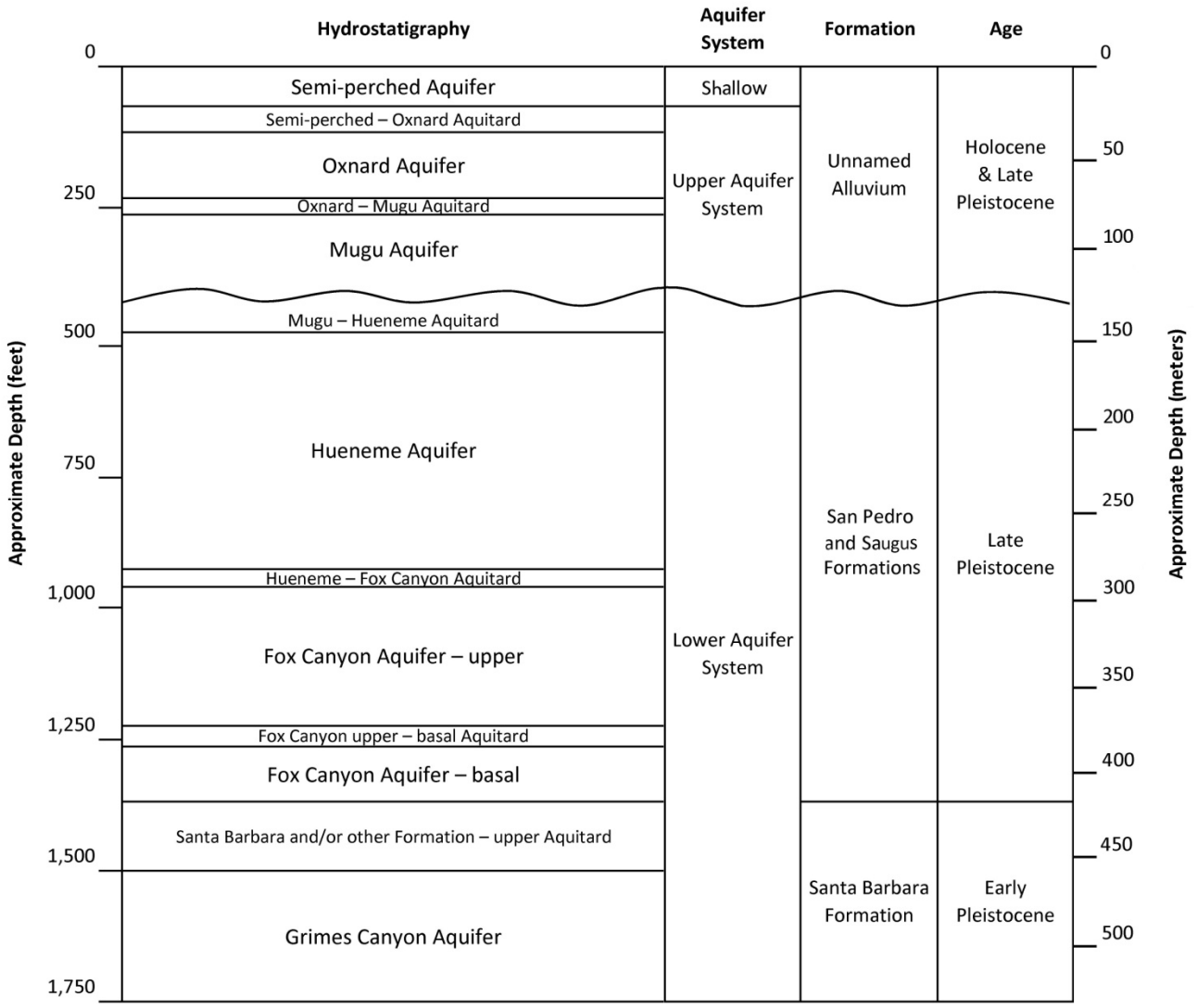

Figure 2-2. Schematic diagram of Upper and Lower aquifer systems in the Oxnard basin.

Some previous investigators have carried this aquifer nomenclature into the basins of the Santa Clara River valley (north of the Oak Ridge Fault). The hydrostratigraphic units extend into the Mound basin from the Oxnard Plain and Forebay, however, they change character (e.g., lithology, thickness, degree of interbedding) in places (UWCD, 2012). The qualifying term “age-equivalent” is used in this report to signify that hydrostratigraphic units mapped in the Mound and Santa Paula basins may be quite different in character from their time-equivalent counterparts on the Oxnard Plain, but new terms for these units are not proposed. The most pronounced differences are seen in the UAS, where thick Holocene clays are present in the Mound basin but not on the Oxnard Plain.

The LAS in the Mound and Santa Paula basins consists of the age-equivalent Hueneme and Fox Canyon aquifers. These LAS aquifers are part of the San Pedro and Saugus formations of Pleistocene age (Hanson et al, 2003). The Hueneme aquifer overlies the Fox Canyon aquifer. In some areas the aquifers of the LAS may be isolated from each other vertically by low-permeability units. The LAS is folded and tilted in many areas and has been eroded along an unconformity that

separates the Upper and Lower Aquifer Systems. The Grimes Canyon Aquifer is not present in the study area.

The UAS of the Oxnard Plain consists of the Mugu and Oxnard aquifers of Late Pleistocene and Holocene age. The UAS rests unconformably on the LAS, with basal conglomerates in many areas (Hanson et al, 2003). In the Oxnard Plain and Oxnard Forebay basins these coarse-grained basal deposits are referred to as the Mugu aquifer (Turner, 1975). The Oxnard aquifer rests unconformably on the Mugu aquifer and is a highly-permeable assemblage of sand and gravel generally found at depths that range between approximately 100 feet to 250 feet below land surface elevation. Recent river channel deposits comprise the uppermost water-bearing units along portions of the Santa Clara River basins.

In the Forebay, the low-permeability confining layers present in the Oxnard Plain are absent or discontinuous resulting in less isolation between the UAS and LAS aquifers. In the area between United's El Rio and Saticoy Recharge Facilities (see Figure 2-3) at the central east edge of the project area, the LAS has been uplifted and truncated along its contact with the UAS. The Mugu and Hueneme aquifers are interpreted to pinch out near the northeast boundary of the Forebay at the base of South Mountain. The Fox Canyon aquifer outcrops at several locations on South Mountain.

In many places in Mound basin and the western portion of Santa Paula basin, the uppermost silt and clay deposits of the age-equivalent Oxnard aquifer are overlain by sand and silt layers that comprise a shallow alluvial "aquifer". United routinely measures water levels in one well screened in the shallow alluvial aquifer in Mound basin, located one and a half miles west (down-gradient) of the study area in roughly the center of the basin. Water levels in this well were around 17 feet below land surface (feet bls) during the study period. The depth to water measured in three UAS wells screened below the shallow alluvial aquifer in Mound and Santa Paula basins near and in the study area ranged from approximately 120 to 180 feet bls. As mentioned above, clay aquitards are generally absent or discontinuous in the Oxnard Forebay, permitting the deep percolation of natural and artificial groundwater recharge. As such, a Semi-perched aquifer is not present in the Oxnard Forebay.

The shallow alluvial aquifer in the Mound basin generally contains poor-quality water as shown by the following data. Available groundwater samples from a Mound basin shallow alluvial aquifer well show total dissolved solids (TDS) by total filterable residue (TFR) ranging from 2,990 (shortly after construction of the well) to 5,264 milligrams per liter (mg/L) over the period of record from 1995 through 2016. The average TDS for this well is 4,646 mg/L. A search on California State Water Resources Control Board's GeoTracker located 15 shallow monitoring wells at one site, located a half mile west of the study area in roughly the center of the basin, that had an average TDS of 2,211 mg/L, with samples dating from 2005 to 2009 (CA SWRCB, 2017). TDS in three shallow wells located in west Santa Paula basin range from 1,710 to 2,080 mg/L over the period of record from 1980 through 1994. GeoTracker data indicated an average TDS of 2,867 mg/L at shallow monitoring wells at a site in the western Santa Paula basin in 2007 and 2008 (CA SWRCB, 2017). The State of California has promulgated a "Secondary Maximum Contaminant Level – Consumer Acceptance Contaminant Level Range" for TDS of 500 mg/L (recommended) to 1,500 mg/L (short-term).

The axis of the Ventura syncline (also called the Santa Clara River syncline by some researchers) trends through the Mound and Santa Paula basins. In Mound basin it generally trends in an east-west direction and in Santa Paula basin it is oriented in a northeast-southwest direction, roughly paralleling Highway 126 (Yeats, et. al., 1981). The syncline is structurally complex and plunges gradually to the west. The Montalvo anticline trends approximately parallel to the Ventura syncline and is located south of the syncline, and is the structural feature that delineates the southern boundary of the Mound basin (Geotechnical Consultants, Inc., 1972).

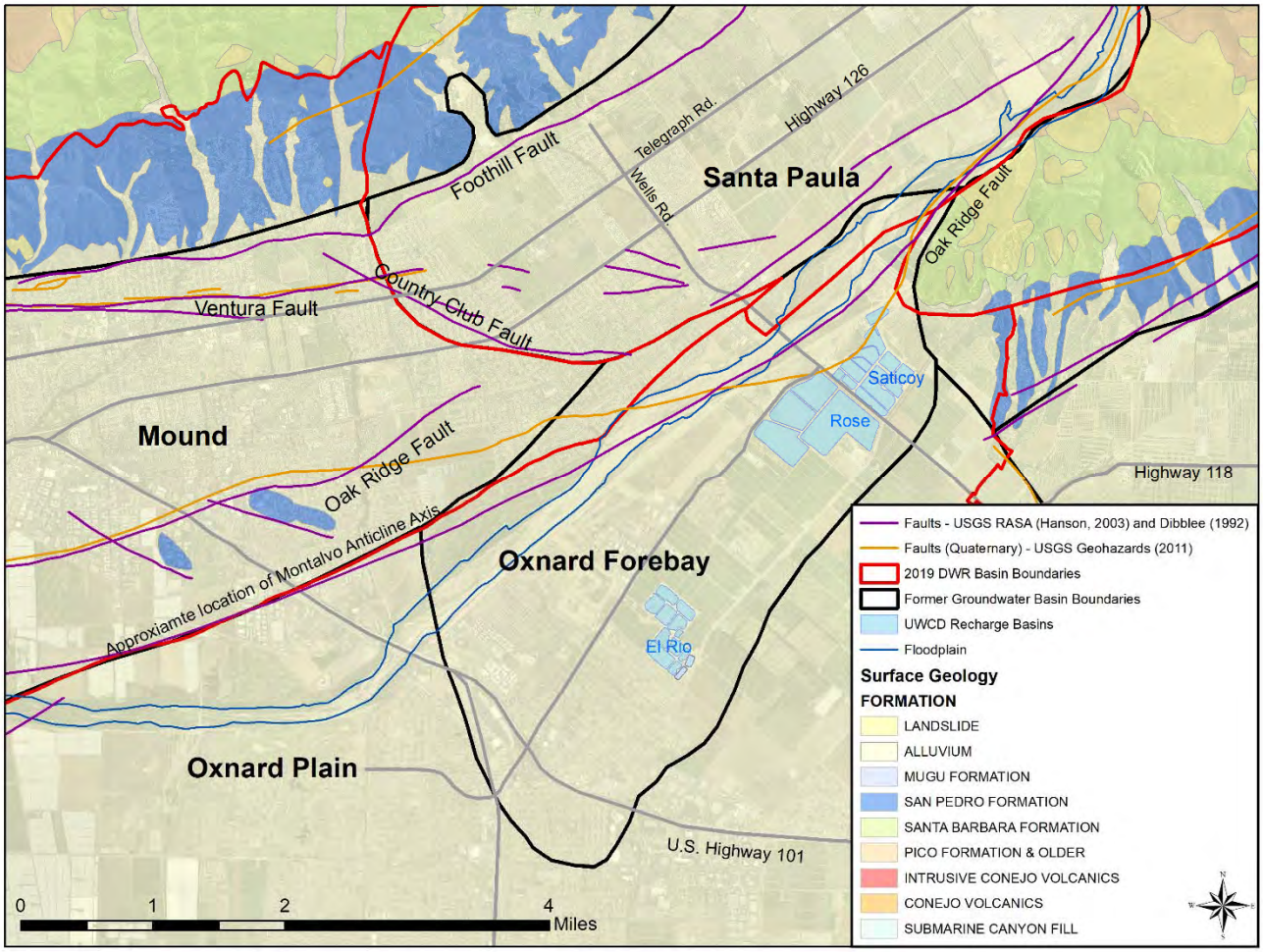

Figure 2-3. Mapped faults in and near the study area.

Mapped faults roughly align with the mapped boundaries between the Mound and Santa Paula basins and the Forebay area. These faults generally align with the basin boundaries which are based on the extent of shallow alluvium and the outcrop of the San Pedro Formation (Figure 2-3). The Montalvo anticline is often mapped as the Mound-Forebay basin boundary with the Oak Ridge Fault running sub-parallel to the basin boundary. The Country Club Fault roughly forms the mapped boundary between Mound and Santa Paula basins. Faults in the Mound basin may be conduits or barriers to groundwater flow (UWCD, 2012).

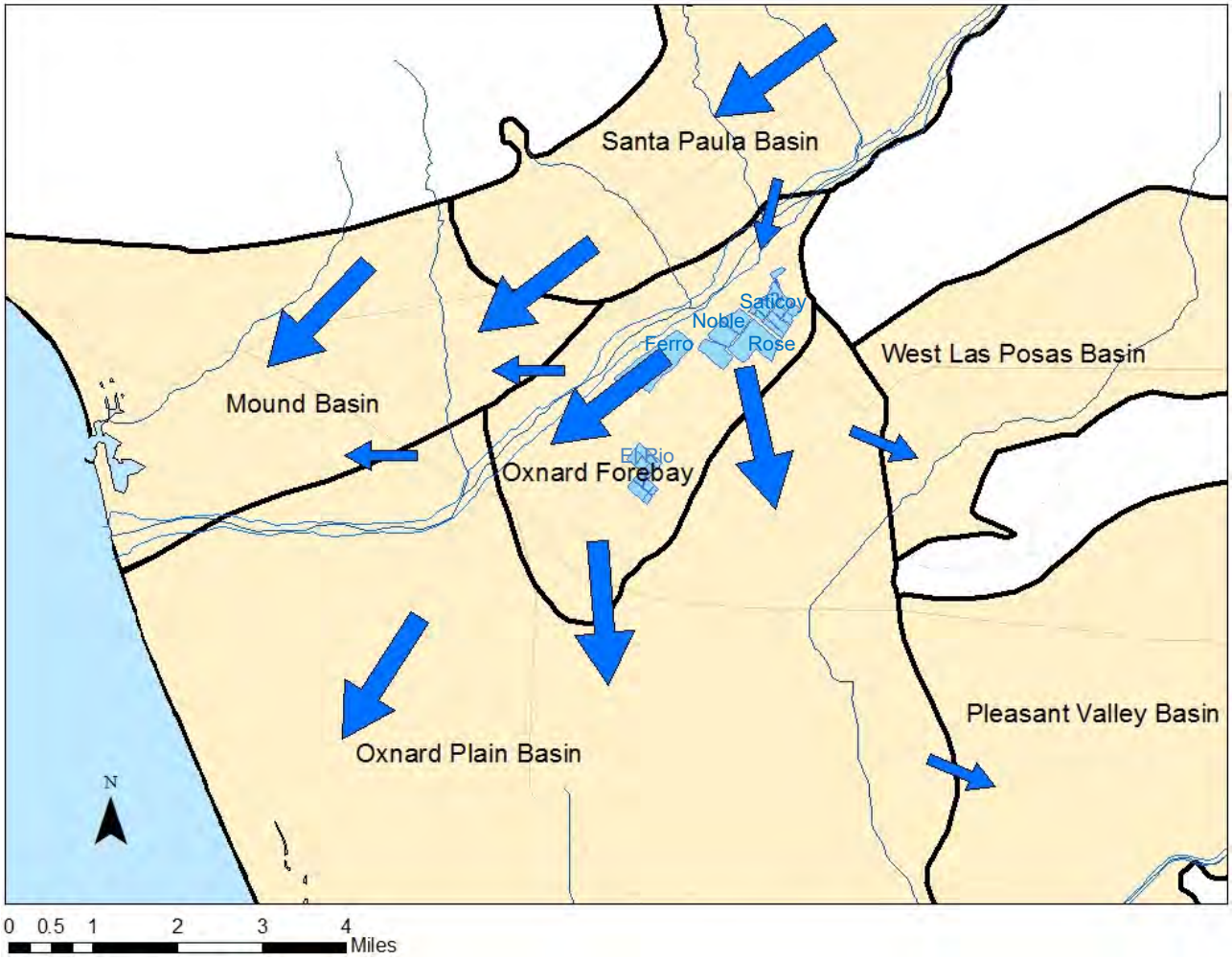

Figure 2-4. Generalized conceptual groundwater flow paths.

The Forebay is an important source of recharge to adjacent groundwater basins, including the Mound basin when groundwater levels are high in the Forebay. Sources of recharge to the Forebay include: percolation of Santa Clara River flows (Figure 2-4), artificial recharge from United's recharge facilities, irrigation return flows, percolation of rainfall, and lesser amounts of underflow from adjacent basins.

3 METHODS

In order to refine the current understanding of the subsurface geologic conditions at and near the Santa Paula-Mound and adjacent Forebay basin boundaries, a surface geophysical survey was designed and conducted. The survey area (Figure 3.3-1) encompassed approximately nine square miles. Agricultural, commercial, residential and native/vacant land uses are common in the survey area. In all, 116 high quality soundings were collected on agricultural fields, orchards and open land within and near the Mound and Santa Paula basins in summer-fall 2013 and winter 2014. A portion of the study area contains streets, houses, commercial buildings and other structures that completely cover the land surface, making collection of usable data impossible due to electromagnetic interference. An overview of TDEM methodology, field procedures and data interpretation/modeling are presented below (an expanded explanation is included in Appendix A).

3.1 TDEM METHODOLOGY AND DATA INTERPRETATION

TDEM surface geophysical methods allow for rapid, cost-effective data collection compared to borehole geophysical surveys, such as electrical resistivity logging that requires an open, uncased, fluid-filled borehole. TDEM measures electrical resistivity of underlying sediment and rock materials at depths from about 30 feet to more than a thousand feet. Resistivity is the reciprocal of conductivity, which is a measure of a material's ability to conduct electrical current. TDEM is a powerful tool for mapping soils and changes in soil type and groundwater conditions in this depth range, because electrical resistivity of underlying sediment and rock materials correlate strongly with soil and aquifer properties. TDEM can be used to investigate saline water intrusion, depth to bedrock, leachate plumes, mineral exploration, the depth and extent of sand and gravel aquifers, and subsurface clay layers (Northwest Geophysical Associates, 2002).

TDEM techniques induce electrical currents in the underlying sediment and rock using electromagnetic induction. A time-varying magnetic field is created using a loop of wire laid on the earth's surface. Faraday's Law of induction indicates that a changing magnetic field will produce an electric field, which will in turn create an electric current. Thus the primary magnetic field from the transmitter loop is used to create a secondary electric current in the underlying sediment and rock. Additional instrumentation (a receiver) measures the secondary magnetic field produced by those secondary electric currents (eddy currents) in the underlying sediment and rock. Modeling of the field data may reveal layers of varying resistivity at depth, allowing interpretations related to geologic structure and the resistivity (salinity) of groundwater at various depths.

The TDEM receiver measures voltage against time for the decaying secondary magnetic field associated with the eddy currents produced by the primary current transmitter. An inversion must be performed on the raw data to calculate apparent resistivity, and then the apparent resistivity is modeled to generate "true" depth-dependent resistivity values for each sounding. The methodology relies on modeling of resistivity values, which may or may not correspond with vertical aquifer boundaries. The distinguishable zones or layers apparent in the modeled soundings are termed "geoelectric layers". The data are useful for showing the degree of horizontal continuity of geoelectric layers, but not absolute vertical depths of individual aquifers. The depths of the geoelectric layers generally do not coincide exactly with actual aquifer depths. There is, however, reasonable agreement between the broader aquifer system observed from this study and data derived from other sources (i.e. geophysical logs, see Figure 5.1-2 presented later in this report). This is demonstrated in greater detail in UWCD Open-File Report 2013-06, where TDEM results within the Forebay consistently indicated similar depths of hydrostratigraphic units as determined by downhole lithologic and geophysical logging.

IX1D 3.51 modeling software (Interpex, Inc.) was used to model the data. A consistent automatically-generated smooth modeling approach was used to process all of the soundings in the study area. The modeled results for each sounding location produced from 26 to 37 depth intervals, with a corresponding resistivity value for each interval. Cross-sections were then constructed based on

correlations between the individual soundings to a depth of approximately 1,800 feet below land surface.

Modeled resistivity values from the deepest few hundred feet displayed on the cross-sections approach the limit of investigation for the TDEM geophysical method as configured for this study. Modeled data corresponding to these deepest depths have large error bars (Appendix D) and are less reliable than those displayed on the shallower portions of the cross-sections. Further explanation of the methodology and data interpretation are included in Appendix A, and a discussion of apparent resistivity in TDEM soundings is included in Appendix B.

Data were collected, modeled and interpreted in the same manner as was previously published in UWCD Open-File Report 2013-06. This consistency in methodology allows data collected in the previous Forebay geophysical study to be directly compared with data processed for this investigation.

3.2 FIELD PROCEDURES

Figure 3.2-1 shows a typical layout for a central loop TDEM sounding. United used a Monex GeoScope terraTEM Time-Domain Electromagnetic Surveying System and a terraTX-50 External terraTEM Transmitter. The system is battery powered and uses marine deep cycle 12-volt batteries, connected in series, as the transmitter power source. The external transmitter allows additional amperage (maximum of 50 amperes) to be generated, allowing a greater depth of investigation before the signal-to-noise ratio decays to below an acceptable level.

Field procedures involved placing a square transmitter "loop" of wire on the ground surface. There is a tradeoff between signal resolution and depth of investigation associated with the loop size. A smaller loop is easier to handle in the field and produces higher-resolution data, but the depth of investigation is proportionately shallower. A 350-foot (per side) square loop of 10-gauge wire was determined to be the optimal loop size to meet the depth and resolution goals for this investigation.

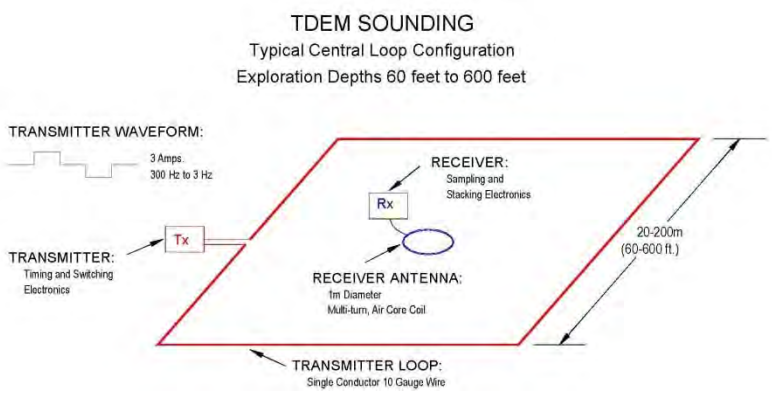

Figure 3.2-1. General TDEM field setup (from Northwest Geophysical Associates, 2002).

The transmitter generates square wave current for the transmitter loop, which is abruptly turned off and on, generating electrical eddy currents in the subsurface. Decay of the eddy currents and their

secondary magnetic fields are detected by the receiver antenna and recorded. Measurements are made with a receiver coil in the center of the transmitter loop, as the induced eddy currents penetrate and diffuse through the underlying sediment and rock. The receiver may also be placed outside of the transmitter loop in an "offset" configuration, but this configuration was not employed in this study. For typical groundwater investigations the measurement times range from 0.006 to 50 milliseconds (ms) after the primary transmitter current is turned off.

The receiver averages recordings from hundreds to thousands of repetitious measurements ("stacks") to improve the signal-to-noise ratio of the sounding. Data are recorded digitally, reviewed in the field and stored in memory. Data are downloaded at the end of the day's survey for further processing and interpretation at the office.

The large transmitter loop required to obtain the desired depth of investigation for this project introduced notable lateral influence (averaging) of the modeled geoelectric layers. The TDEM equipment configuration used for this project was selected to balance depth of investigation with the vertical resolution of bedding.

A number of soundings were made with a smaller transmitter loop in an attempt to enhance horizontal (less lateral averaging) and vertical resolution of bedding. The data were nosier and the depth of investigation was reduced. In general, the same features were apparent in both the big loop and small loop data, but the modeled depth-dependent resistivity values of the small loop were more extreme and the observed features were shallower.

3.3 STUDY AREA AND DATA ACQUISTION

Figure 3.3-1 is a map showing the location of the 116 TDEM soundings (indicated by yellow squares) obtained during the data acquisition phase of the project. An additional 19 TDEM soundings (orange squares on Figure 3.3-1) were collected in 2011 and 2012 for the earlier Forebay project and are included to tie the current project to that earlier work. The sounding locations are unevenly spaced due to access restrictions imposed by various infrastructure, including metallic irrigation pipe and power lines, which can "short-circuit" the natural pathways for the electrical currents generated (and received) by the TDEM instrumentation.

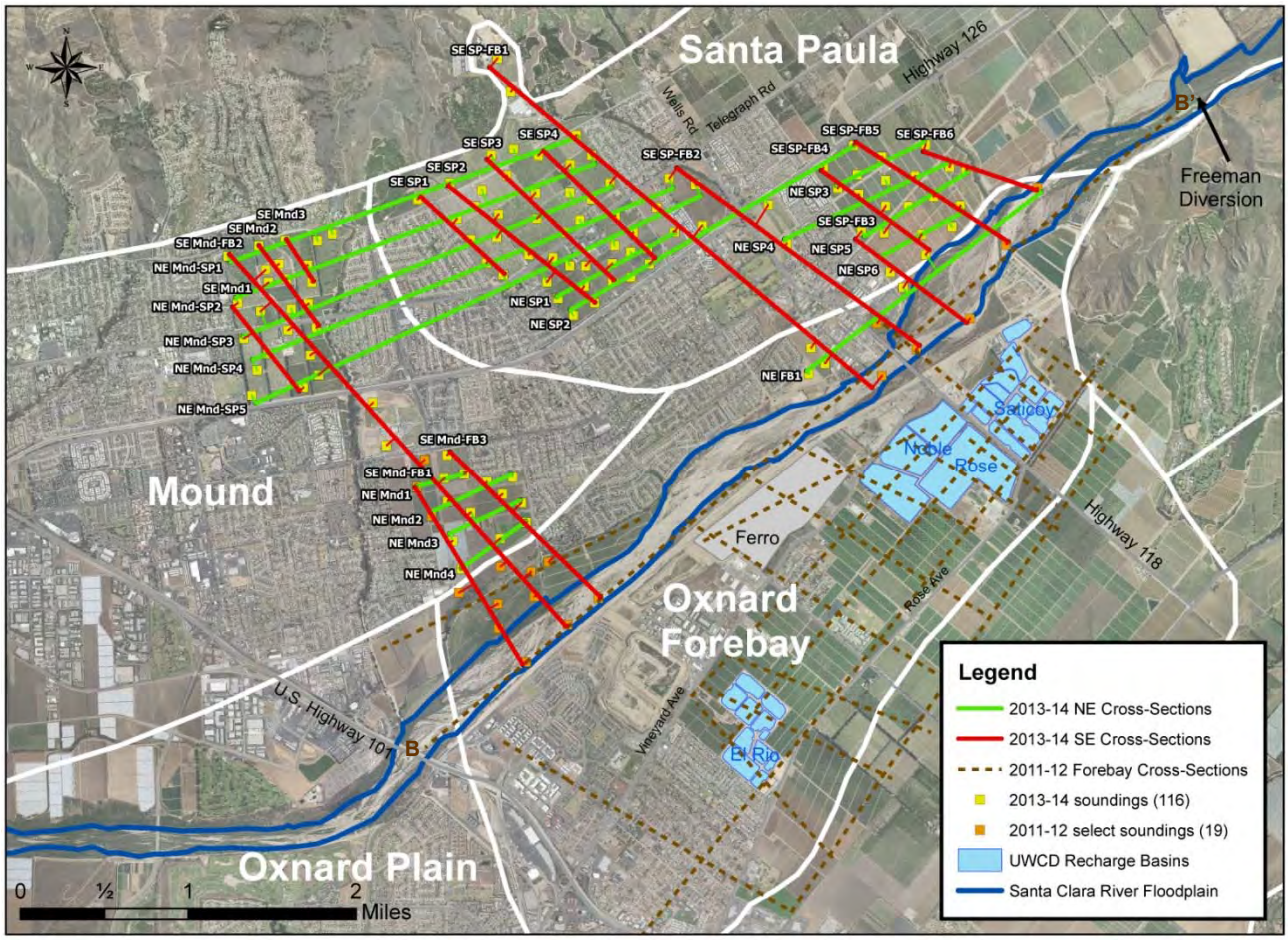

Figure 3.3-1. Location map, TDEM soundings collected during summer/fall 2013 and winter 2014, and cross-section lines.

Some of the soundings were collected in actively-farmed strawberry fields. There is a short window of time to conduct surface geophysical surveys in summer, after berries have been harvested and aluminum irrigation pipes have been removed from the fields and before fields are prepared for subsequent cropping. A concentrated field effort was performed in the summer of 2013 during this window. United worked closely with land owners and ranch managers to access fields between crop rotations. Voluntary cooperation from many individuals made this project possible. There were, however, a couple of fields and areas where United could not gain access to collect data. In general, a good distribution of data points was achieved by working in all areas that were accessible.

The location of each sounding was determined with a handheld Global Positioning System (GPS) unit. The GPS points shown on maps in this report represent the receiver coil location near the center of the transmitting loop for each sounding. The receiver coil is the theoretical location for a given sounding; the data are assumed to be from directly below the receiver coil. Accuracy of the GPS position (laterally on the land surface) varies depending on field conditions and satellite reception. The GPS unit reported that location accuracy was generally within 10 to 20 feet of the true location.

The naming convention for soundings collected for this project incorporated the date, site and run. An example sounding name is “130719s1r1” which translates to July 19th, 2013, site 1, run 1. Data

were stored on the instrument receiver console throughout a given field day. At the end of the day the data were downloaded for processing back in the office. One day's worth of data typically consisted of three to six soundings. Prior to performing the modeling, the raw data were converted to Universal Sounding Format (USF). This process takes the raw data and formats it for import into a modeling program.

The terraTEM Time-Domain Electromagnetic Surveying System has a filter that is able to remove some of the effects of the background noise from power lines. The frequency of the waveform oscillations in transmitted alternating current (AC) through power lines in North America is 60 Hertz (Hz). Power lines and high voltage lines trended through parts of the field area, and data collected close to power lines were often deemed to be unusable due to significant ambient electrical noise.

Limiting electrical interference from power lines was achieved by collecting data as far away from power lines as possible, while attempting to maintain an evenly-spaced distribution of sounding locations. Up to 2048 stacks per sounding were used during data acquisition to increase the signal-to-noise ratio. The use of an external transmitter also helped improve the signal-to-noise ratio by generating a stronger signal (up to 50 amperes). A distinguishable signal-to-noise ratio was achieved for all soundings represented in this report.

The selected transmitter loop size and the programmed instrument parameters also affect the measured resistivity values at a given location. All of the data for this project were collected using consistent instrument parameters, transmitter loop size, and field methods.

Quality control of the data was conducted both in the field and in the office. Careful inspection of the data in the field allowed real time identification of possible interferences, so that sounding positions could be relocated if necessary without returning to the site at a later date. Problems were typically discovered and resolved in the field. Data obtained on a given day were usually evaluated that same day back in the office. If there were any apparent problem with the data (e.g., interference, wrong settings, instrument malfunction, etc.) not detected in the field, the sounding was recollected and/or relocated (when possible) and data were obtained properly.

4 STUDY RESULTS

The collection and modeling of 135 soundings in the study area allowed the construction of 32 cross-sections that correlate units of similar resistivity as identified in the individual soundings (see Figure 3.3-1). All individual cross-sections are included in Appendix C, and individual modeled soundings are included in Appendix D.

4.1 RESISTIVITY VALUES

In this study, modeled resistivity values for subsurface materials ranged from less than 1 Ohm-m to over 100 Ohm-m. Coarse-grained material (sand, gravel, etc.) is typically more resistive than fine-grained materials (silt, clay, etc.) (Aquifer Science & Technology, 2008). The modeled soundings provide an indication of grain size and porosity of various beds at depth (sands and gravels are

relatively less porous but more permeable than silts and clays) but there is not a direct relationship due to the many variables that influence the measured resistivity for a given sounding.

Solid, dry rock has a very high resistivity, and composition also plays a significant factor in resistivity. However, the presence of water significantly reduces the resistivity of all underlying sediment and rock materials. Water quality can also affect the measured resistivity values, as water with a high salinity has very low resistivity. Conversely, water with a low concentration of salts or salinity is characterized by relatively higher resistivity. Measured resistivity values are influenced by water content, water type, and host materials (Aquifer Science & Technology, 2008). Where the groundwater has low salinity, the water table may not be apparent in the soundings collected for this study.

In the Mound and western Santa Paula basins water quality tends to be poor (high salinity) in the shallow alluvial aquifer, and the modeled soundings suggest salinity generally does not vary significantly in the center portions of the basins within this uppermost unconfined zone. The poor-quality water of the shallow alluvial aquifer likely increases the conductivity of the shallow sediments, which may influence the resistivity data obtained below this zone. Further investigation would be required to determine what affects water quality has on the TDEM data collected for this study in other areas and deeper zones.

4.2 GEOELECTRIC CHARACTERISTICS OF GEOLOGIC FEATURES

TDEM measures lateral and vertical variability in electrical resistivity of underlying sediment and rock materials. When a color ramp is applied to the range of resistivity values present in the dataset, geospatial variability produces patterns and contrasts in color, allowing individual soundings to be correlated in cross-sections. As mentioned in section 4.1, measured resistivity at a given site is dependent on a variety of factors, but certain patterns of geoelectric variability are recognized as indicative of certain geologic features.

Geoelectric layers may be discernible and may correlate to specific geologic formations or groundwater aquifers. These layers may be tilted or offset by geologic structure, and a number of geoelectric layers appear to be discontinuous. These patterns reveal changes in the characteristics of the subsurface. Care must be taken when interpreting geoelectric layering and geoelectric anomalies within a dataset, as very different geologic features can be represented by similar resistivity patterns in cross-section (e.g. fine-grained soils with low-TDS groundwater adjacent to coarse-grained soils with high-TDS groundwater).

Within the study area faults often appear in cross-section as sub-vertical high- or low-resistivity anomalies. This may be due to the offset of geologic material or formations, or it may be a function of water chemistry. Differences in water chemistry along a fault plane could produce this effect, or if a fault acts as a barrier to flow, water chemistry may be different on opposite sides of the fault. Faults identified as part of this project are presented later in the report.

Another prominent set of geologic features observed in this study are high-energy alluvial deposits in paleo-channels of the ancestral Santa Clara River. These appear in cross-section as zones with very high resistivity. These channel deposits can be mapped and visualized in three dimensions by preparing a series of georeferenced cross-sections (fence diagrams) that transect the channel deposits. Channel deposits mapped as part of this project are presented later in the report.

4.3 STUDY CROSS-SECTIONS

Cross-sections were constructed to evaluate vertical and horizontal relationships between modeled resistivity values for each sounding. In all, 16 southwest-to-northeast trending cross-sections and 16 northwest-to-southeast trending cross-sections were produced from 135 soundings. The vertical range of each of the cross-sections was standardized for easy comparison (approximately +490 feet (+150m) to -1475 feet (-450m) of elevation above mean sea level (amsl)). Due to software constraints, cross-sections were prepared with scales in metric units (meters). The number of soundings used to construct each cross-section ranges from 3 to 18, and the horizontal length of each cross-section varies.

The 32 cross-section locations are identified in Figure 3.3-1. The red lines on the figure represent the 16 northeast-trending cross-sections and the green lines represent the 16 southeast-trending cross-sections. The brown dashed cross-section lines are from the previous Forebay study. The individual cross-section figures are included in Appendix C. Plan view cross-section alignments displayed in Figure 3.3-1 are best-fit lines drawn through the soundings included (correlated) on a cross-section. The IX1D modeling software projects the selected soundings onto a cross-section line; therefore, the sounding sampling grid was not as uniform as represented in Figure 3.3-1. All soundings shown on individual cross-sections were located within 750 feet of the section line.

Figures 4.3-1 and 4.3-2 are fence diagrams showing the cross-sections in three dimensions, offset vertically (approximately 1,475 feet) to display above sea level. Cross-sections are to scale (no vertical or horizontal exaggeration) and show modeled geoelectric data from the ground surface to a depth of approximately 1,800 feet below land surface. The blanked-out areas in cross-sections NE Mnd-SP2, NE Mnd-SP3, NE Mnd-SP4, NE Mnd-SP5 and SE SP-FB1 are due to large data gaps between soundings.

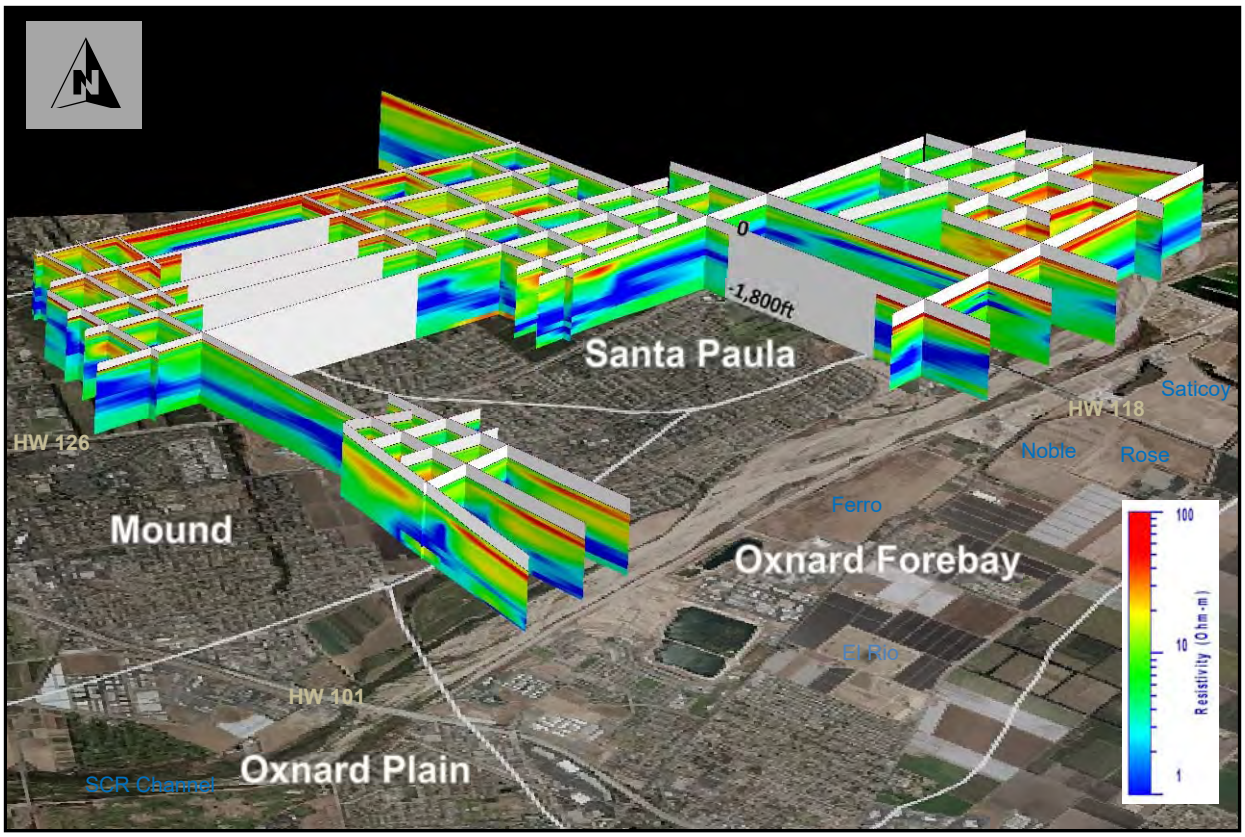

Figure 4.3-1. Fence diagram with 1 to 100 Ohm-m color ramp (blue to red) looking obliquely north.

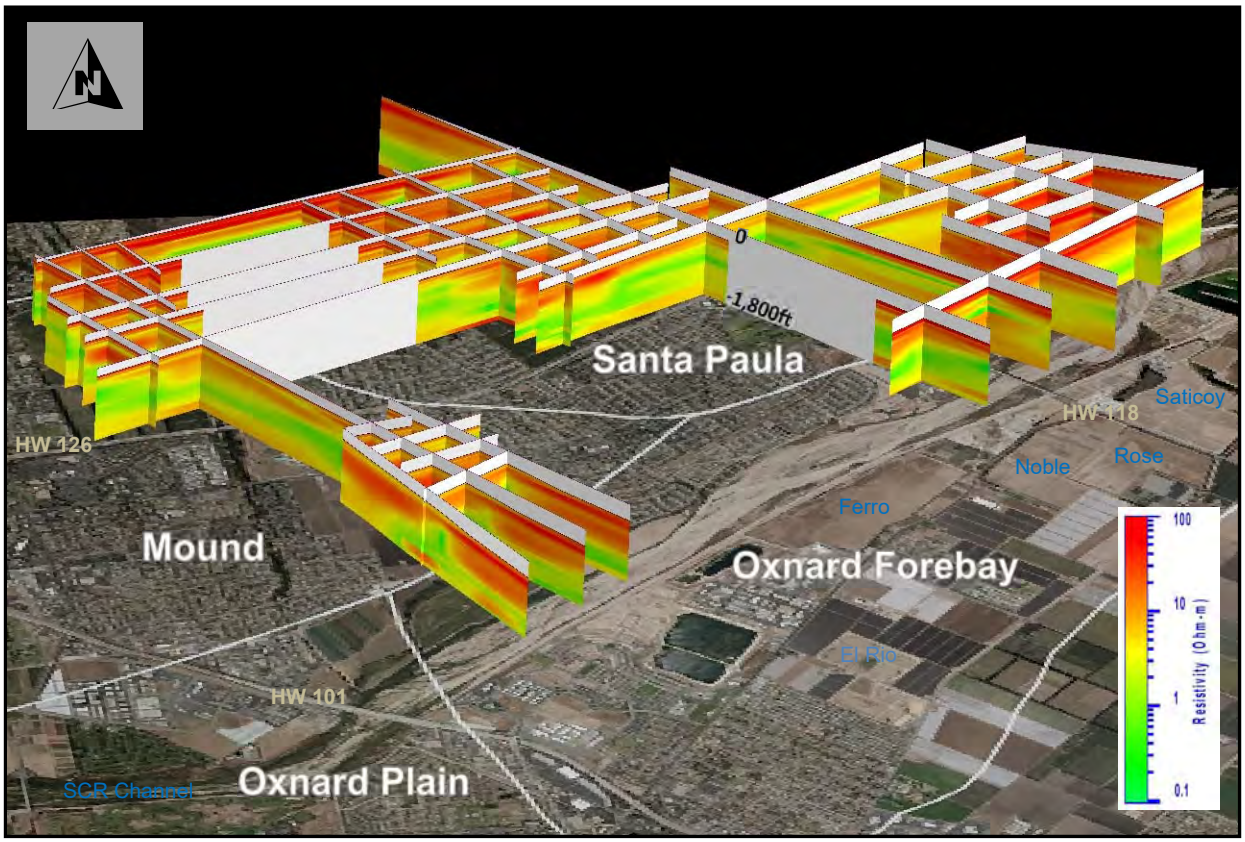

Figure 4.3-2. Fence diagram with 0.1 to 100 Ohm-m color ramp (green to red) looking obliquely north.

Two different color ramps were used to correlate the individual soundings represented in each of the cross-sections (Appendix C). In both color ramps, warm colors correspond with higher resistivity and cool colors correspond with lower resistivity. Log scales were used for both color ramps. A 1 to 100 Ohm-m range was selected for one color ramp (blue to red), and 0.1 to 100 Ohm-m was selected for the other (coarser) color ramp (green to red). Because some modeled resistivity values were higher than 100 Ohm-m for a few soundings, those values were filled with the color that represents the highest-resistivity values for the color ramp (red). The 1 to 100 Ohm-m color ramp reveals smaller vertical and lateral differences in resistivity, while the 0.1 to 100 Ohm-m color ramp better displays the coarser features of the geoelectric layers observed in the dataset.

5 DISCUSSION

The discussion of the study results are presented in this section of the report. Included in this section are selected cross-section figures with annotation where appropriate.

5.1 GEOELECTRIC LAYERS DELINEATION

The common resistivity patterns (geoelectric layers) modeled from the soundings and labeled in Figure 5.1-1 can generally be grouped into three layers. Layer 1 and Layer 3 can be further divided into sub-layers (“a” and “b”) in some areas. This three-layer grouping does not hold true for all of the soundings, especially in Santa Paula basin, but it is useful for general interpretation of the data. Figure 5.1-1 employs the 1-100 Ohm-m color ramp (blue to red), but these same general layers can also be seen with the 0.1-100 Ohm-m color ramp (green to red) with less color contrast (Figure 5.1-2). Thickness and occurrence of these layers vary significantly within the project area. In the Forebay TDEM report, the observed geoelectric layers were categorized and divided in a way similar to that depicted here.

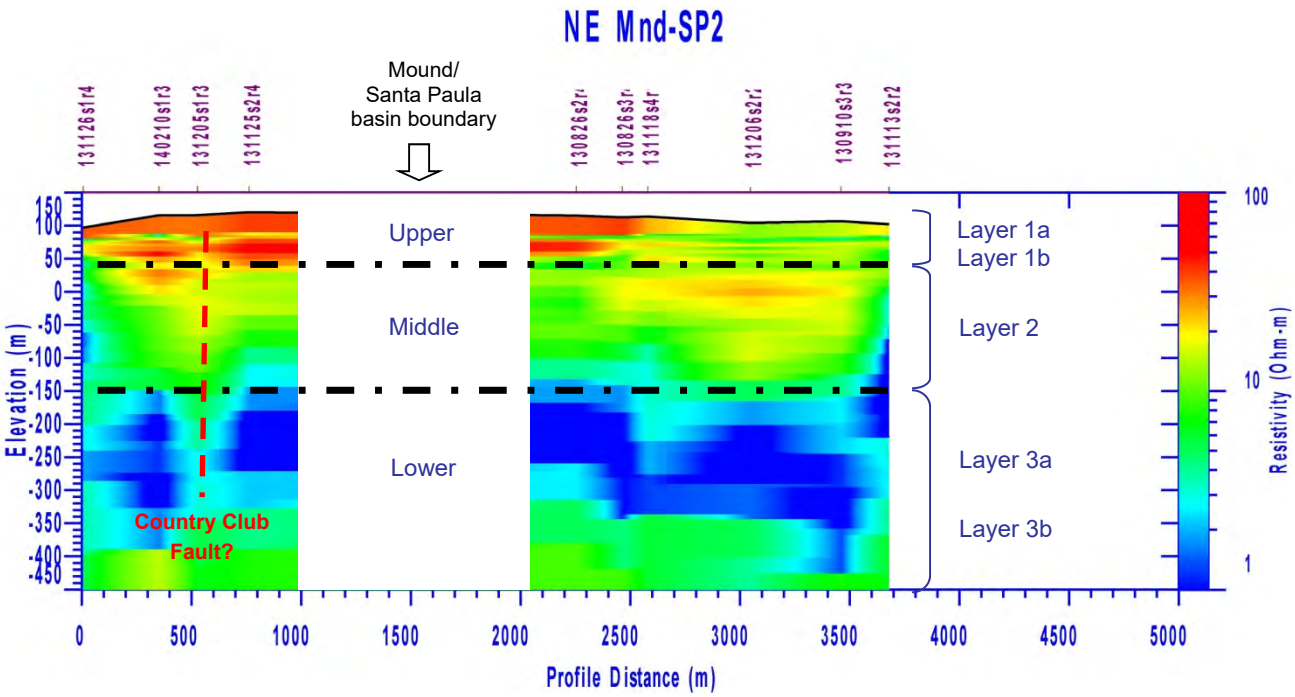

Figure 5.1-1. Cross-section NE Mnd-SP2 (with annotation); a portion of the section is blanked due to sparse data.

The high-resistivity (warm-colored) upper geoelectric layer (further divided into “Layer 1a” and “Layer 1b” in Figure 5.1-1) is continuous throughout the Forebay (UWCD, 2013) and is present in the northern portion of Mound and Santa Paula basins, but not in the middle and southern portions of these basins. This could be related to differences within the study area of geologic depositional environments such as fanglomerate material near the foothills; or as mentioned in Section 2, the shallow alluvial aquifer of Mound basin and west Santa Paula basin containing poor quality water. It may be a shallow clay/silt confining layer and/or the shallow poor-quality semi-perched water that is causing this low resistivity effect displayed in the cross-sections in these basins.

There is a thin, continuous, conductive layer that roughly bisects this upper geoelectric layer, resulting in the interpreted delineation of resistive geoelectric Layers 1a and 1b. This thin conductive zone does not correlate with any recognized aquifer boundary and runs through much of the dataset at an approximate depth of 100 to 165 feet (30 to 50 meters) below land surface. It is most pronounced in the 1-100 Ohm-m color ramp (blue to red) used in Figure 5.1-1. It is unclear if it is geologic in nature, or an artifact of the imaging or data processing.

The intermediate-colored (yellow and green) geoelectric Layer 2 identified in Figure 5.1-1 is interpreted to roughly correspond to the age-equivalent Lower Mugu and Upper Hueneme aquifers (UWCD, 2013). Geoelectric Layer 2 contains several noticeable anomalies. The warm-colored anomalies are interpreted to be relatively coarse-grained deposits (sand and gravel) and the cool-colored anomalies are interpreted as fine-grained deposits (silts and clays).

Geoelectric Layer 3 is interpreted to correspond with the age-equivalent Lower Hueneme and Fox Canyon aquifers, and the Santa Barbara Formation (UWCD, 2013), which is often considered to be the deepest local unit containing fresh water. As stated in Section 2, the Grimes Canyon aquifer does

not exist in the study area. Layer 3 can be divided into two sub-layers. Layer 3a is a low-resistivity layer resting on top of the comparatively more resistive Layer 3b (blue and green in color respectively in Figure 5.1-1).

The modeled resistivity throughout the project area generally tends to decrease with increasing depth (see Figure 5.1-1). The age-equivalent Lower Hueneme and Fox Canyon aquifers (Layer 3) have similar resistivity values to the clay lenses (aquitards) present within the study area. This is likely due to the composition of the age-equivalent Lower Hueneme and Fox Canyon aquifers (San Pedro Formation) containing more fine-grained marine sands, in contrast to the predominately coarse-grained terrestrial deposits (with intermixed marine deposits due to changes in sea level) of the age-equivalent Upper Hueneme, Mugu and Oxnard aquifers (Hanson et al, 2003).

Silts and clays may be displayed as the same color when cross-sections are constructed based on the correlated resistivity values from each sounding. Shallow clay lenses are often discontinuous and appear as low-resistivity anomalies within the dataset (see the fence diagram cross-sections located in the northeast portion of the study area from Figure 4.3-1 and Figure 4.3-2). The deeper age-equivalent Lower Hueneme and Fox Canyon aquifers appear as a somewhat continuous geoelectric layer (Layer 3). The deeper clay lenses, if present, may not be distinguishable from the age-equivalent Lower Hueneme and Fox Canyon aquifers using the TDEM surface geophysical technique in the project area.

Aquifer delineation using surface geophysical methods is best accomplished by using complementary sources of data. Borehole electrical resistivity logs (electrical logs) are useful for comparison and validation when interpreting surface geophysical data. A detailed discussion of borehole resistivity electrical log comparison to TDEM data was prepared as part of the Forebay TDEM report (UWCD, 2013).

Since the Forebay TDEM report was published, new sources of data have become available as a result of further development and refinement of the Ventura Regional Groundwater Flow Model (VRGFM). Hydrostratigraphic cross-sections consisting of geophysical and lithologic logs were used to identify and correlate stratigraphic boundaries and elevations, which the VRGFM discretely simulates as individual aquifer and aquitard model layers. These stratigraphic sections were digitally interpolated using kriging methods to create contoured elevation surfaces which may aid in defining hydrostratigraphic units between available electrical log data (UWCD OFR 2018-02).

Borehole resistivity data can provide a high degree of vertical detail of the geologic formation material but only within a few feet laterally of the borehole wall; the interpolated aquifer and aquitard elevation surfaces aid in generally relating and projecting these geometries between boreholes. In an effort to better correlate between geoelectric layers and hydrostratigraphic units, UWCD-interpolated aquifer and aquitard elevation surfaces were superimposed (as well as nearby borehole electrical logs) and compared to select TDEM transects (Figure 5.1-2).

Figure 5.1-2 includes the modeled surface elevation profiles for the age-equivalent Mugu, Hueneme, and Fox Canyon aquifers; also included is the modeled surface elevation of the age-equivalent San

Pedro aquitard. Hydrostratigraphic units below the Fox Canyon aquifer were not included. The hydrostratigraphic surface elevation profiles were generated with GIS software using the modeled elevation data previously described. The elevation surfaces generally reflect the larger structural controls of the basin, with the Montalvo anticline and Ventura syncline well represented in the data.

The geoelectric Layer 1 resistivity signature is reflected in the borehole electrical logs superimposed on Fig. 5.1-2, however changes in resistivity are evident near the basin boundary where the more resistive channel alluvium deposits occur. This may also be indicative of changes in water quality and decreased mineral content of groundwater. Geoelectric Layer 2 roughly coincides with the age-equivalent Oxnard and Mugu aquifers near the foothills and due to offset near the Oak Ridge fault/Montalvo anticline coincides more closely with the top of Hueneme aquifer near the basin boundary. Vertical offset near the possible Oak Ridge Fault trace can be interpreted from the soundings but is more readily apparent in the hydrostratigraphic profiles and borehole electrical logs. Geoelectric Layer 3 includes older and more fine-grained deposits of the Fox Canyon and lower Hueneme aquifers and marks the boundary between the more resistive deposits near the basin boundary.

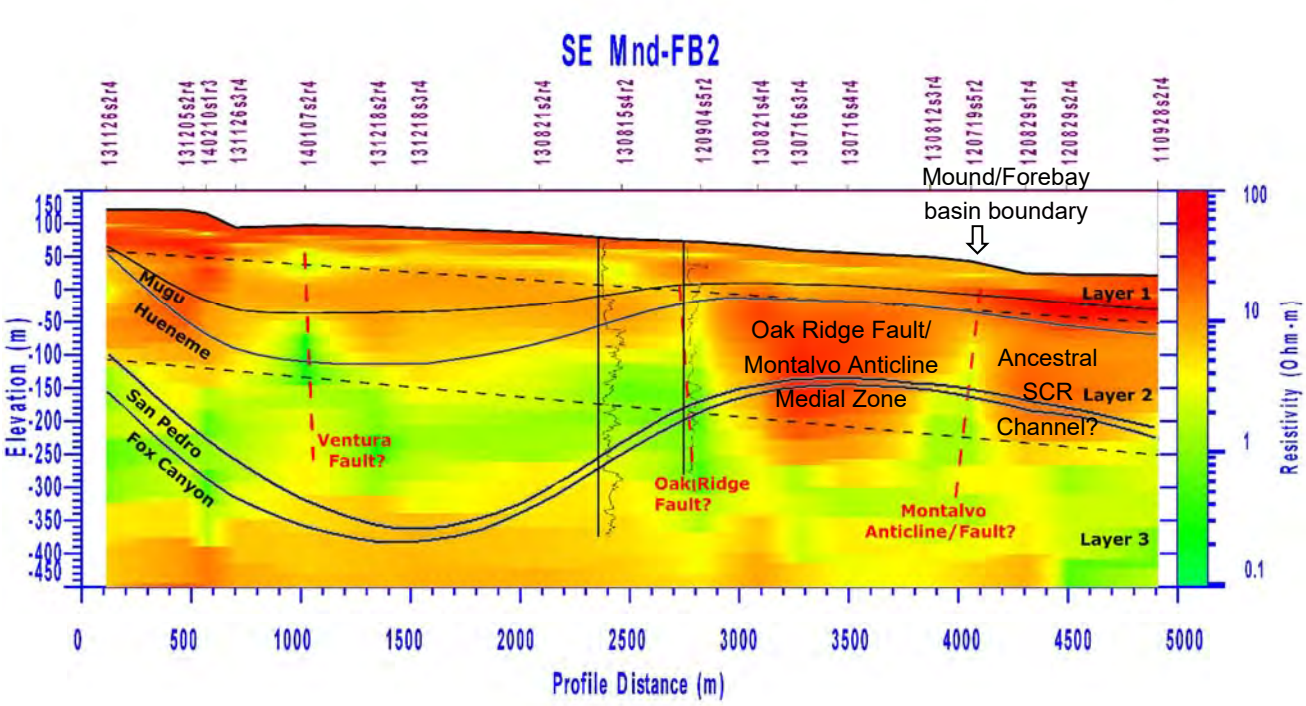

Figure 5.1-2. Cross-section SE Mnd-FB2 (with annotation), superimposed nearby borehole resistivity electrical logs and hydrostratigraphic surface elevation profiles.

Results indicate that the geoelectric groupings correspond more closely with recognized hydrostratigraphic units within the Forebay study area, and less so with soundings collected near the Forebay boundary (UWCD, 2013). Figure 5.1-2 may indicate that the more structurally complex boundaries in this area are less conducive to aquifer delineation using TDEM data. The TDEM data

does however provide insight into lateral continuity of geoelectric layers, particularly in the vicinity of structural features.

5.2 FAULTING

Figure 5.2-1 combines Figure 2-3 (mapped faults in and near the study area) and Figure 3.3-1 (location map, TDEM soundings collected during summer/fall 2013 and winter 2014, and cross-section lines) into a single figure.

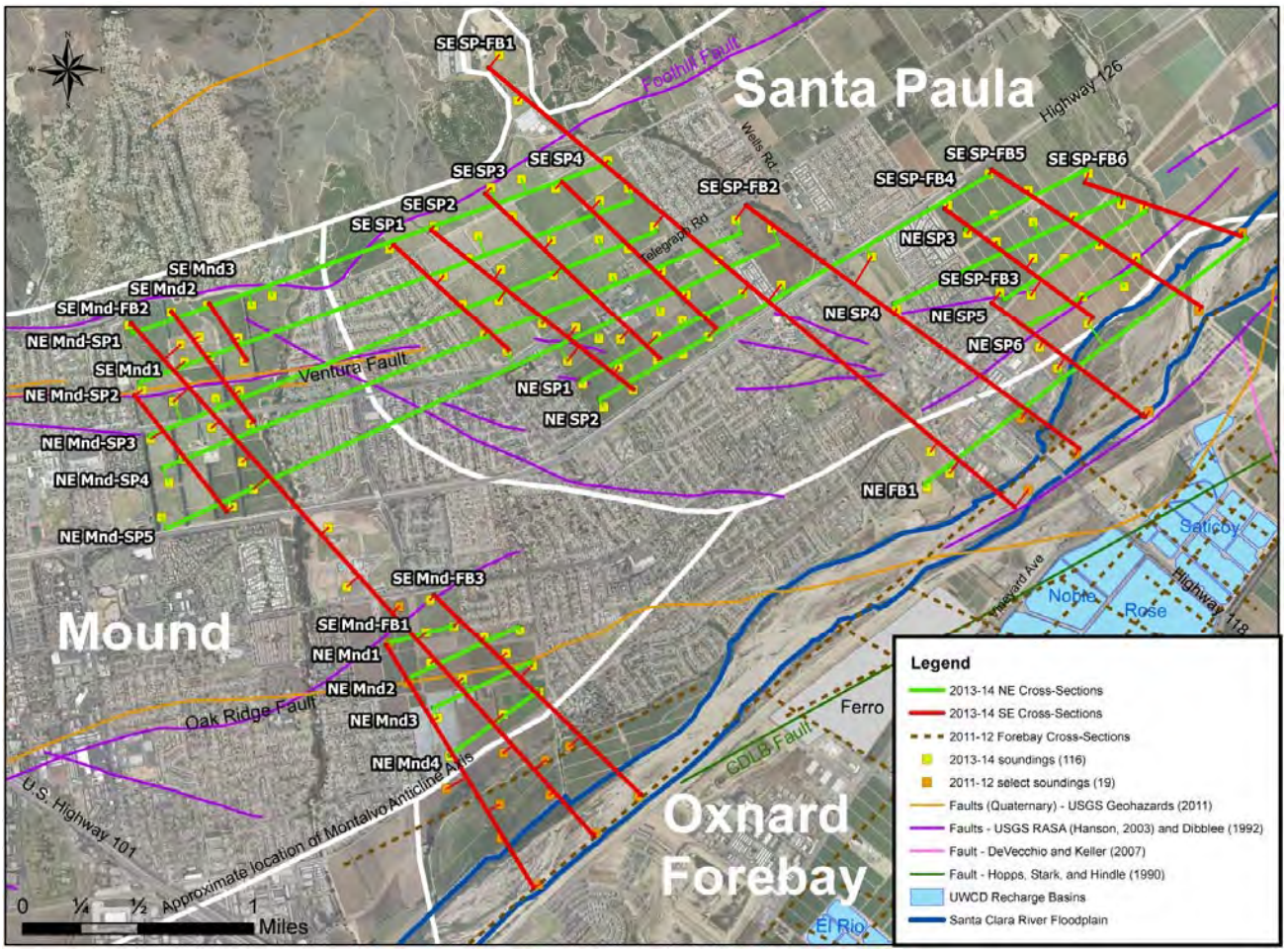

Figure 5.2-1. Location map, TDEM soundings collected during summer/fall 2013 and winter 2014, cross-section lines, and mapped faults.

Cross-section SE Mnd-FB2 (Figure 5.1-2 and Appendix C) correlates resistivity from 18 soundings collected in the Mound and Forebay basins. The section runs southeast from the northeast margin of Mound basin to a location across the Mound-Forebay basin boundary and terminates in the floodplain of the Santa Clara River (Figure 5.2-1). The black dashed lines in Figure 5.1-2 generally illustrate south-dipping stratigraphy roughly parallel to the land surface in the Mound basin. A distinct east-west synclinal axis that is mapped by some investigators is not readily apparent in this cross-section. There may be a synclinal form in Layer 2 south of the Ventura Fault and weakly represented in the warm tones of Layer 3 but this may also be the result of interpolation between sparse data points.

5.2.1 Oak Ridge Fault and Montalvo Anticline

The Oak Ridge Fault trends sub-parallel to the axis of the Montalvo anticline (Figure 5.2-1). Different investigators have mapped the Oak Ridge Fault following different traces with differing degrees of offset (United, 2012). A southern trace of the Oak Ridge Fault is identified as the Montalvo anticline by some investigators (Greene, 1978).

Cross-section SE Mnd-FB2 (Figure 5.1-2) traverses the Oak Ridge Fault to the north and the Montalvo anticline to the south. Modeled resistivity changes across the Mound-Forebay basin boundary are seen in the figure, suggestive of changes in depositional environments near the present day Santa Clara River floodplain. While distinct offsets in geoelectric layering due to faulting were not apparent from the data, the presence of vertically-oriented zones of lower resistivity is highly suggestive of faulting. The locations of these anomalies are coincident with mapped locations of the Oak Ridge Fault and the axis of the Montalvo anticline.

Cross-Section SE Mnd-FB2 is oriented roughly perpendicular to the mapped trace of the northern Oak Ridge Fault and the axis of the southern Montalvo anticline. Figure 5.1-2 and the mapped trace of the Oak Ridge Fault (Figure 5.2-1) indicate that the distance between the north and south geologic features (sub-vertical red dashed lines in Figure 5.1-2) is about 4,500 feet wide in east Mound basin. From the cross-section, the Oak Ridge Fault/ Montalvo anticline medial zone (labeled in Figure 5.1-2), Layer 1 displays notably low resistivities and Layer 2 displays anomalously high resistivities suggestive that the material that comprises this zone is highly-permeably aquifer material.

Two borehole electrical logs are superimposed on cross-section SE Mnd-FB2 (Figure 5.1-2) and show vertical offset near the Oak Ridge Fault, as indicated by the aquifer surface elevation profiles. There is approximately 150 to 300 feet of vertical offset seen in the logs that are approximately 1,800 feet apart. This offset corresponds well with the low resistivity anomaly annotated with a sub-vertical red dashed line in Figure 5.1-2. This is likely the Oak Ridge Fault trace shown on Figure 5.2-1. The Oak Ridge Fault is also discussed later in this report in sections 5.3.2 and 5.3.3 (Mound-Forebay basin boundary and Santa Paula-Forebay basin boundary respectively).

5.2.2 Ventura Fault

The Ventura Fault is an east-west oriented fault (Figure 2-1 and Figure 5.2-1) that runs from near the Santa Paula-Mound basin boundary west to the Pitas Point fault which continues in a northwest direction several miles offshore.

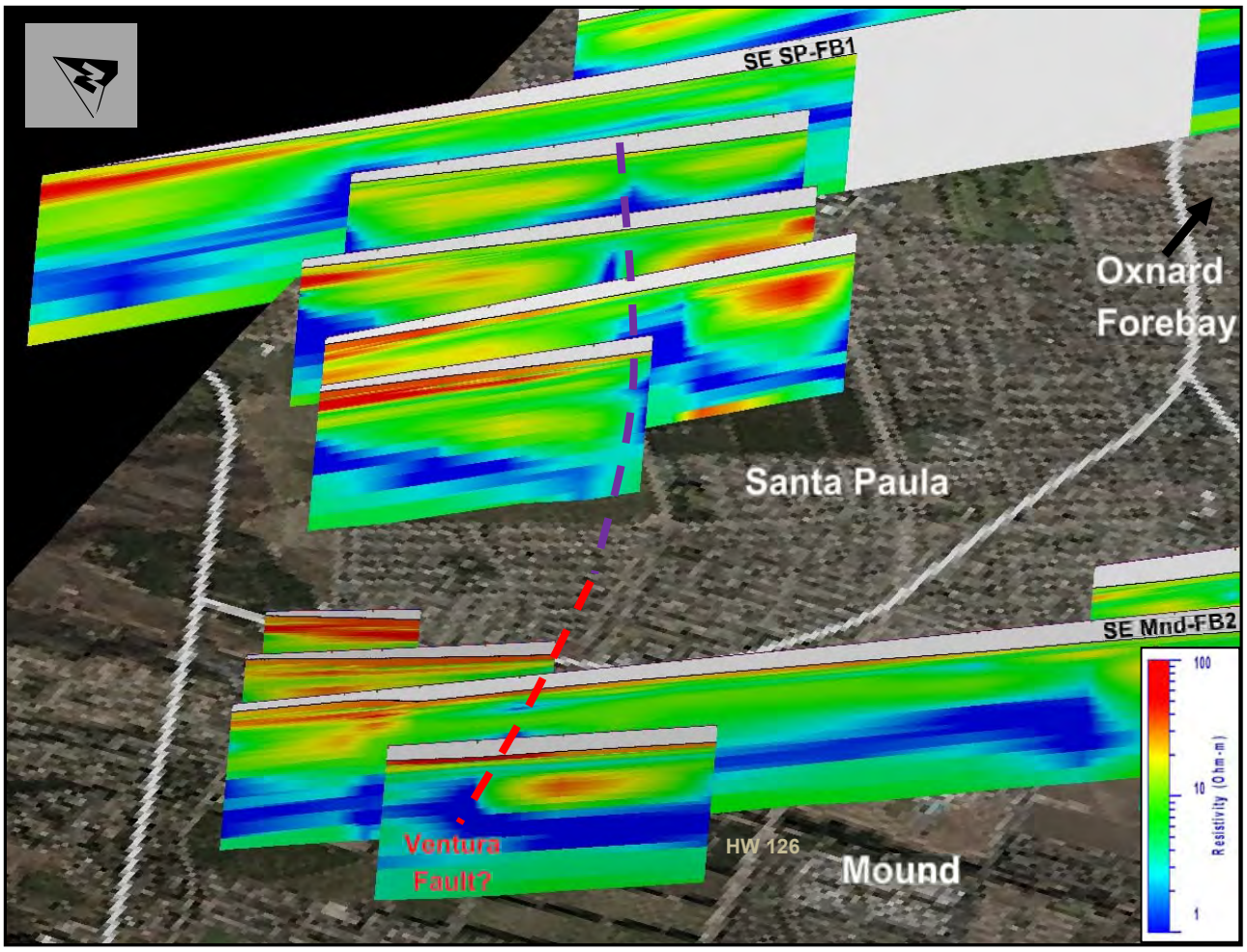

Figure 5.2.2-1. Fence diagram of select cross-sections (1 -100 Ohm-m color ramp) traversing the Ventura Fault looking obliquely east by northeast.

The mapped trace of the Ventura Fault terminates about 1,800 feet into Santa Paula basin (Yerkes, 1987). The low-resistivity anomalies seen in Figure 5.2.2-1 in Mound basin (red dashed line in figure) align well with the mapped Fault trace. These low-resistivity anomalies are highly suggestive of faulting.

Resistivity sections suggest that an unmapped extension of the Ventura Fault (purple dashed line in figure) may extend farther east into Santa Paula basin than has been traditionally recognized. From the resistivity sections, it trends roughly parallel to Telegraph Road (Figure 5.2-1). In the absence of other corroborating evidence (i.e. water level data, borehole geophysical logs or other surface geophysical studies), further investigation is needed to determine if this resistivity anomaly is an extension of the Ventura Fault or related to other undetermined subsurface conditions.

5.2.3 FOOTHILL FAULT

Cross-section SE SP-FB1 (Figure 5.2.3-1 and Appendix C) traverses the mapped trace of the Foothill Fault (see base map Figure 5.2-1). The section runs from Brown Barranca in Santa Paula basin southeast to the Santa Clara River floodplain.

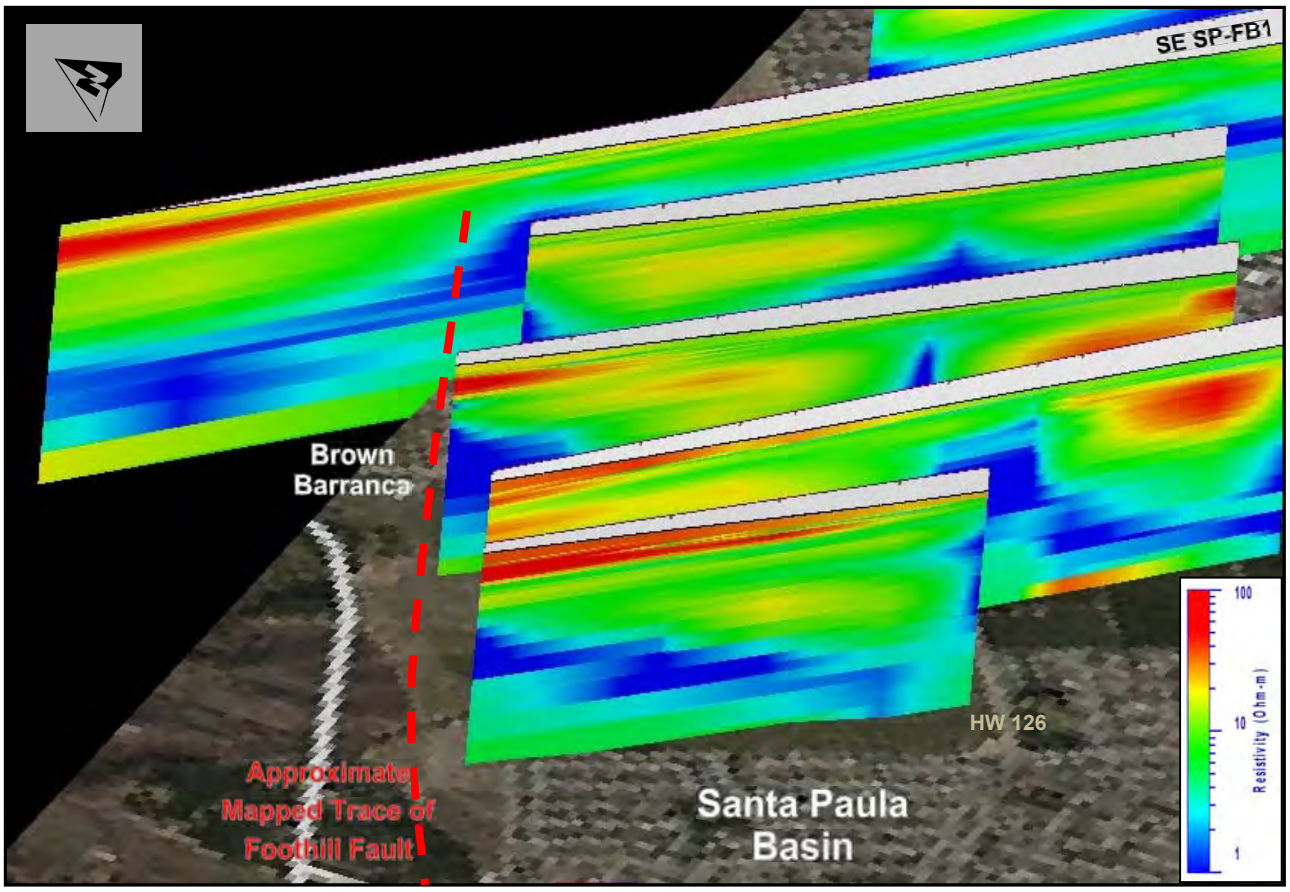

Figure 5.2.3-1. Fence diagram of select cross-sections (1 -100 Ohm-m color ramp) looking obliquely east by northeast with an approximate mapped trace of the Foothill Fault.

There is a vertical feature apparent near the topographic break in slope, near the third sounding from the left (sounding 130910s4) that may correspond to the Foothill Fault, but this single cross-section alone is not enough evidence to identify the fault. Cross-section SE SP-FB1 shows shallowing and thickening of the highly-conductive member of Layer 3a from northwest to southeast between sounding 140218s3 and 130910s4 (Appendix C). This is also seen in northernmost portions of cross-sections SE SP1, SE SP2, SE SP3 and SE SP4. These northernmost shallow low-resistivity zones suggest thinning of the alluvial basin fill near the northern edge of Santa Paula basin, and likely is not direct evidence of the Foothill Fault. The resistive Layer 1 seen on the northwest end of the cross-sections is likely the result of fluvial deposited alluvium (sands and gravels) within Brown Barranca.

5.3 BASIN BOUNDARIES AND OTHER PROMINENT GEOELECTRIC FEATURES

Faults and folds form the boundaries between the Santa Paula, Mound, and Forebay basins. The axis of the Montalvo anticline (Figure 5.2-1) generally is regarded as the boundary between the Forebay and Mound basins (Geotechnical Consultants, Inc., 1972). The northeast boundary of the Forebay is formed by South Mountain where the UAS is thin or absent, and the Fox Canyon aquifer and Santa Barbara Formation crop out at land surface. The boundary between Mound and Santa

Paula basins approximately coincides with the Country Club Fault (Figure 5.2-1). The boundary between the Santa Paula and Forebay basins coincides with the mapping of the Oak Ridge Fault.

5.3.1 Santa Paula-Mound Basin Boundary (Country Club Fault)

The mapped trace of the Country Club Fault that is generally accepted by other investigators and forms the Santa Paula-Mound basin boundary, but it largely underlies developed land where collection of usable TDEM data is not possible. The four cross-sections (NE Mnd SP2, NE Mnd SP3, NE Mnd SP4 and NE Mnd SP5) that cross the fault trace are blanked-out in this area due to the lack of data. Differences in the resistivity profiles are observed on either side of the blanked areas of these sections. These differences could be a result of offset of hydrostratigraphic units across the Country Club fault; however, insufficient TDEM data are available to confirm this hypothesis at present.

Developed land prevented the collection of TDEM data in all but the northwest portion of the mapped trace of the Country Club Fault (Figure 5.2-1). NE Mnd-SP2 (Figure 5.1-1 and Appendix C) shows a low-resistivity anomaly around 750 feet to the west of the mapped trace of the Country Club Fault (Figure 5.1-1 and Appendix C). This anomaly may correspond to a previously unmapped northwest extension of the fault.

5.3.2 Mound-Forebay Basin Boundary

Figure 5.3.2-1 shows fence diagrams of cross-sections SE Mnd-FB1, SE Mnd-FB2 (partial) and SE Mnd-FB3 that are oriented northwest-to-southeast across the boundary between the Mound and Forebay basins. The three cross-sections show a distinct resistivity pattern across the mapped boundary. The land surface elevation, represented on the cross-sections, decreases abruptly on the Forebay side of the basin boundary (to the southeast as the cross-sections obliquely transverse a terrace). There is a zone of low resistivity aligned with the basin boundary and the terrace, suggestive of folding and/or faulting that provide evidence in support of the current location of the Mound-Forebay basin boundary surface mapping (see Section 5.2.1 for Oak Ridge Fault discussion evidenced in Figure 5.3.2-1 below).

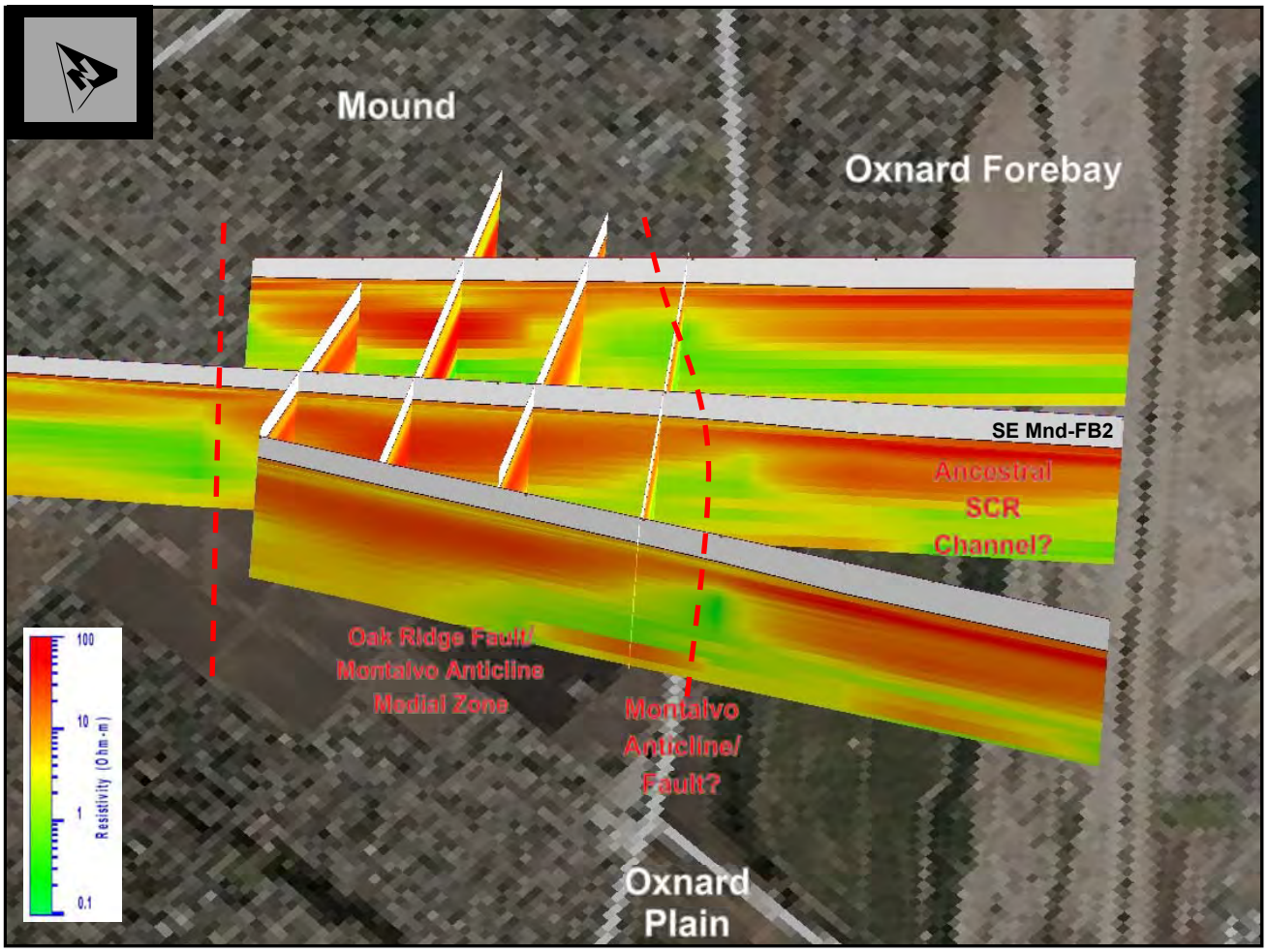

Figure 5.3.2-1. Fence diagram of cross-sections (0.1 -100 Ohm-m color ramp) across Mound-Oxnard Forebay basins boundary looking obliquely northeast.

Geoelectric Layer 1 is notably less resistive (conductive) on the northern side of the boundary in Mound basin. As mentioned earlier in the report, this may be the result of poor-quality (high mineral content) shallow groundwater.

5.3.3 Santa Paula-Forebay Basin Boundary

Figure 5.3.3-1 displays three northwest-to-southeast trending cross-sections (SE SP-FB3, SE SP-FB5 and SE SP-FB6) that traverse the Santa Paula-Forebay basin boundary. An additional northwest-to-southeast trending cross-section (SE SP-FB4) terminates just north of the basin boundary but shows a resistivity pattern similar to the other cross-sections labeled in the figure.

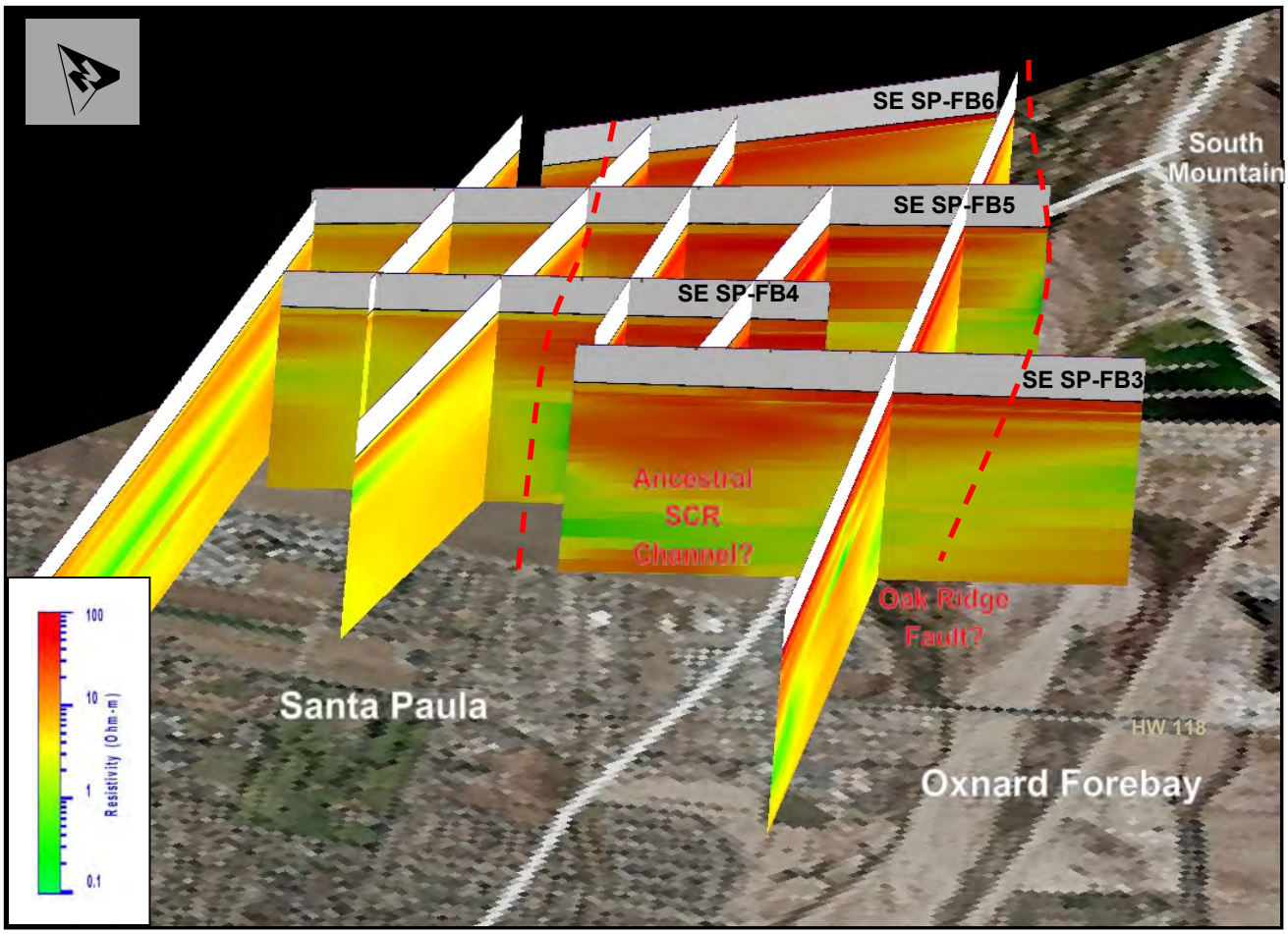

Figure 5.3.3-1. Fence diagram of cross-sections (0.1 -100 Ohm-m color ramp) across Santa Paula-Oxnard Forebay basins boundary looking obliquely northeast.

The geology is complex near the Santa Paula-Forebay basin boundary. As noted in Section 2, the Mugu and Hueneme aquifers are uplifted and eroded near the northeast boundary of the Forebay near the base of South Mountain. Figure 5.3.3-1 shows a thinning of the resistive Layers 1 and 2 on the southeast side of the cross-sections near South Mountain, consistent with previous studies detailing a thinning of the aquifers in this vicinity. A similar thinning of shallow alluvium was seen in the Forebay TDEM study in cross-section B-B' (UWCD, 2013).

The thinning of the high-resistivity Layers 1 and 2 on the far southeast side of the cross-sections labeled in Figure 5.3.3-1 could also be interpreted as a low-resistivity anomaly that may be evidence of a trace of the Oak Ridge Fault. If this is the case, the TDEM data provide evidence in support of the current mapped location of the Santa Paula-Forebay basin boundary. A few more soundings farther to the southeast could be collected to extend the cross-sections as long as there was enough offset contrast of the thick low-resistivity zone or a vertical anomaly to provide evidence of a trace of the Oak Ridge Fault.

5.3.4 Ancestral Santa Clara River Channel and Floodplain

The Santa Clara River has not always been confined to its current channel and adjacent floodplain that roughly follow the southern boundaries of Mound and Santa Paula basins (Figures 1.2-3, 1.2-4 and 3.3-1). As is common in fluvial-deltaic systems, the location of the main channel of the river has shifted across the Oxnard Plain over time.

Terrestrial sediments transported and deposited by the ancestral Santa Clara River were mined in the 20th century for construction aggregate. Mining of these sediments was banned in the active river channel in the mid-1980s as problems associated with significant river channel degradation related to these practices became increasingly evident. Several unused, off-channel gravel mining pits still exist in the Oxnard Forebay. United purchased one few of these pits, the Ferro property, to potentially use as an additional groundwater recharge facility for diverted Santa Clara River water. Two abandoned gravel mines are visible in Figure 5.3.4-1. The deepest of these, Brigham-Vickers pit, was mined to an elevation of a few feet below sea level. Groundwater is commonly exposed in these pits when the water table elevation in the Forebay is higher than the bottom of the pits. The shallow sands and gravels observed in these pits correlate with the shallow high resistivity values observed in the Oxnard Forebay TDEM cross-sections in the vicinity.

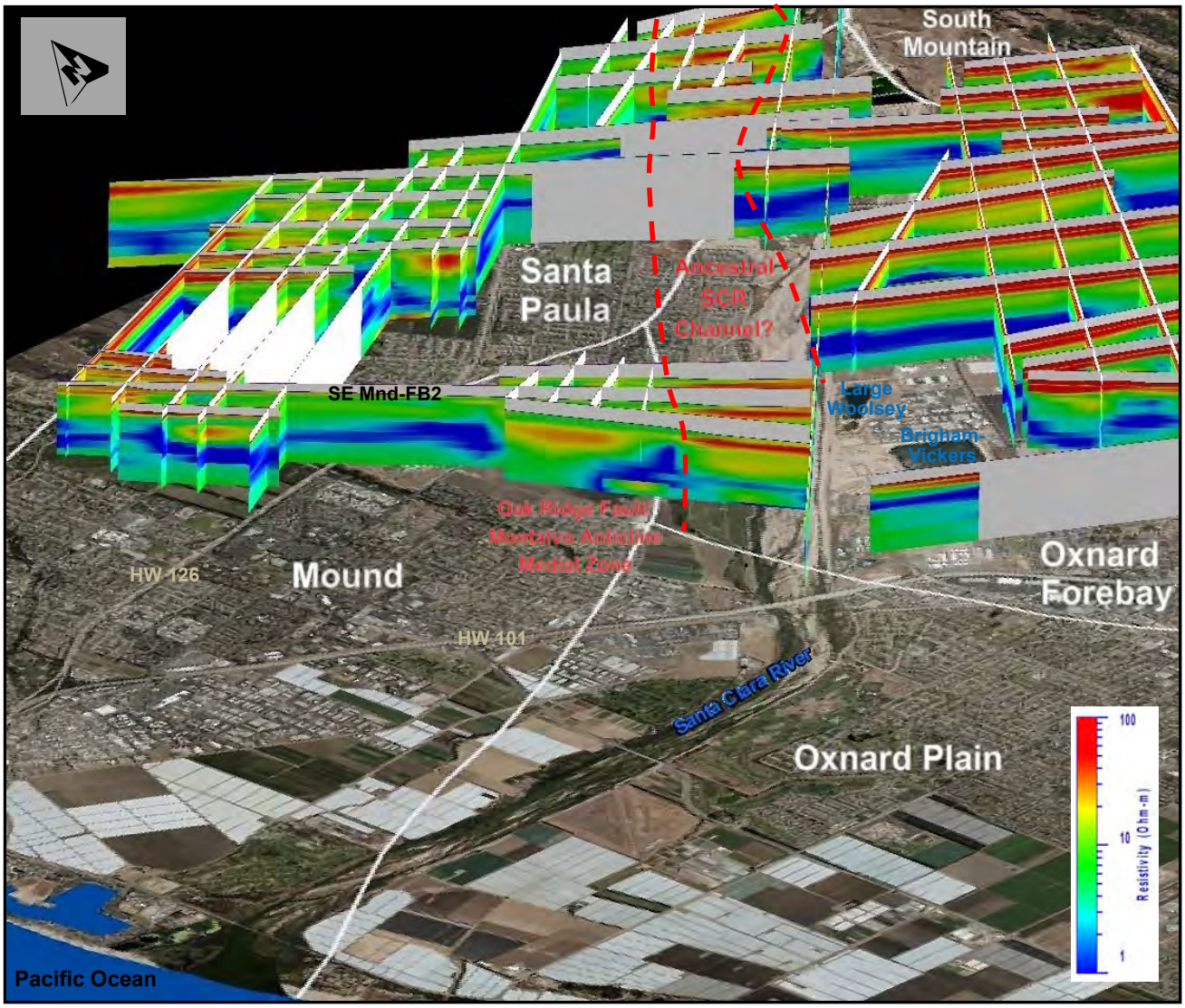

Figure 5.3.4-1. Fence diagram of select cross-sections (1 -100 Ohm-m color ramp) from the current study and the Forebay TDEM study looking obliquely northeast.

Buried paleo-channels are important features because they can provide preferential paths for groundwater flow. The TDEM method utilized in this report effectively delineated high energy paleo-channel deposits of the Santa Clara River. Figure 5.3.4-1 shows high-resistivity features, which are interpreted to represent coarse-grained deposits typical of high-energy depositional environments (active stream channels), in the area of the present-day Santa Clara River channel and adjacent floodplain. In the northeast portion of the study area, near South Mountain, the base of the high-resistivity features is at approximately -130 feet amsl (-40 meters) elevation and 300 feet (90 meters) depth. To the southwest, near the Forebay-Oxnard Plain basin boundary, the base of the high-resistivity features is approximately -200 feet amsl (-60 meters) elevation and 300 feet (90 meters) depth. The southern edge of the high-resistivity features align with the southern edge of the modern Santa Clara River floodplain, but the features extend hundreds to a few thousand feet farther north than the modern floodplain. This area likely contains paleo-channel deposits of the ancestral Santa Clara River.

In the northeast, near South Mountain at groundwater monitoring well 02N22W01P02S (NB1), the bottom of the Oxnard and Mugu aquifers are mapped at 175 and 266 feet below land surface respectively. In the southwest, near the Forebay-Oxnard Plain basin boundary at groundwater monitoring well 02N22W15L01S (TNC1), the bottom of the Oxnard and Mugu aquifers are mapped at 124 and 283 feet below land surface respectively (United, 2018). The depths to the bottom of the mapped Mugu aquifer generally align with the depth of the base of the TDEM high-resistivity features identified in these areas.

6 FINDINGS AND CONCLUSIONS

Following are conclusions resulting from the investigation:

- The large transmitter loop laid on the ground surface required to obtain the desired depth of investigation for this project produces notable lateral influence (averaging) of the modeled geoelectric layers. The TDEM method is suitable for determining the degree of continuity of units, but may not accurately define the depths of aquifer units. Comparison of geoelectric layers to modeled aquifer elevations and borehole electrical logs suggest that this method may be more useful in identifying structural features and less useful in delineating aquifer units and depths in the study area.

- Changes in resistivity were observed in the cross-sections across the Mound-Santa Paula and adjacent Forebay basin boundaries. Anomalous zones of high and low resistivity (indicating sands/gravels and silts/clays, respectively) were seen within the project area.

- The resistivity data can be roughly divided into three geoelectric layers. This grouping does not hold true for all of the soundings but are useful for the purpose of general interpretation of the data. Geoelectric Layer 1 is highly resistive in the northern portion of Mound and the northwest portion of Santa Paula basins, but not in the southern portions of these basins. It may be that shallow poor-quality water in the shallow alluvial aquifers the southern parts of these basins is causing this effect.

- Interpretation of the TDEM data collected for this project shows that resistivity of the sediments within the project area commonly decreases with increasing depth. This is expected since the age-equivalent lower Hueneme and Fox Canyon aquifers (San Pedro Formation) consist of more fine-grained marine sands (Layer 3), in contrast to the predominately coarse-grained terrestrial deposits of the age-equivalent Upper Hueneme/Lower Mugu (Layer 2) and Upper Mugu/Oxnard aquifers (Layer 1).

- Changes in the geoelectric layers are apparent in the cross-sections that transverse both the mapped Santa Paula-Forebay and Mound-Forebay basin boundaries. These geoelectric changes are interpreted to be changes in depositional/erosional environments and/or suspected faulting. The following sub-bullets are findings relating to specific geologic features identified in this report:

    - Developed land prevented the collection of TDEM data in all but the northwest portion of the mapped trace of the Country Club Fault. The four cross-sections that cross the fault are blanked-out in the area where the fault is mapped due to the lack of data. Differences in resistivity profiles are observed on either side of the mapped trace of the fault. One cross-section shows a low-resistivity anomaly around 750 feet to the west of the mapped trace of the Country Club Fault that may correspond to the most northwest portion of the fault.

- The presence of the vertically-oriented zones of lower resistivity are highly suggestive of faulting, although distinct offsets in geoelectric layering were not apparent. The locations of these anomalies coincide with mapped locations of the Oak Ridge Fault to the north and the axis of the Montalvo anticline to the south. Between these two features is an area where Layer 1 is notably conductive, and Layer 2 displays anomalously-high resistivities.

- Resistivity cross-sections suggest that an unmapped extension of the Ventura Fault extends farther east into Santa Paula basin than has been recognized by previous investigators. In the absence of other corroborating evidence, further investigation is needed to determine if this resistivity anomaly is an extension of the Ventura Fault or some other undetermined subsurface conditions.

- High-resistivity features in the area of the present-day Santa Clara River channel and floodplain may be evidence of buried paleo-channels. The base of these high-resistivity features generally coincide with the depth of the base of the Mugu aquifer as mapped as part of United's recent hydrogeologic conceptual model update. The southern edge of the high-resistivity features aligns with the southern edge of the modern Santa Clara River floodplain, but the features extend hundreds to a few thousand feet farther north than the modern floodplain.

7 RECOMMENDATIONS

It would be helpful to collect a few additional soundings in strategic areas that would extend a couple of the cross-sections presented in this report in order to clarify whether certain observed resistivities are actual changes in geologic character or data edge effect artifacts. Additional study is also needed to gain better understanding of the differences seen in the small loop and big loop data collected for this report.

In addition, because the TDEM study was useful for identifying subsurface features in a time- and cost-efficient manner, it is recommended that this method be applied to other areas, as follows: a similar geophysical investigation could be conducted on the agricultural land on either side of the Santa Paula-Fillmore basin boundary. This would likely provide useful data for comparison with historical basin boundary mapping, especially considering the continued development of agricultural land for commercial and municipal uses that will increasingly complicate future geophysical investigations in this area.

United also recommends a repeat of UWCD Open-File Report 2010-03, Oxnard Plain Time Domain Electromagnetic Study for Saline Intrusion. Following the recent extended drought, it would be informative to investigate the current landward extent of saline and brackish water in the southern Oxnard Plain basin.

8 REFERENCES

Aquifer Science & Technology: A Division of Ruekert | Mielke, Inc., 2008, Report on the Geophysical Investigations to Map Saline Groundwater in the West Coast Basin of Los Angeles County, CA: for Water Replenishment District of Southern California, September 2008, 2p.

California State Water Resources Control Board, accessed 2/28/2017, http://geotracker.waterboards.ca.gov/.

DeVecchio, D.E., and Keller, E.A., 2007, Earthquake Hazard of the Camarillo Fold Belt: An Analysis of the Unstudied Fold Belt in Southern California "Hot Zone". Final Report USGS/NEHRP, Award Number 07HQGR0040.

Dibblee, Thomas W. Jr., edited by Helmut E. Ehrenspeck. 1992a, Geologic map of the Santa Paula quadrangle: Ventura County, California: Santa Barbara, Calif., Dibblee Geological Foundation, Dibblee Foundation Map series, DF-41, scale 1:24,000.

Dibblee, Thomas W. Jr., edited by Helmut E. Ehrenspeck. 1992b, Geologic map of the Saticoy quadrangle: Ventura County, California: Santa Barbara, Calif., Dibblee Geological Foundation, Dibblee Foundation Map series, DF-42, scale 1:24,000.

Geotechnical Consultants, Inc., 1972, Hydrogeologic Investigation of the Mound Groundwater Basin for the City of San Buenaventura, California, unpublished consultants report prepared for City of San Buenaventura.

Greene, H.G., Wolf, S.C., and Blom, K.G., 1978, The Marine Geology of the Eastern Santa Barbara Channel, with particular emphasis on the Groundwater Basins Offshore of the Oxnard Plain, Southern California: U.S. Geological Society Open File Report 78-305.

Hanson, R.T., Martin, P. and Koczot, K.M., 2003, Simulation of Ground-Water/Surface-Water Flow in the Santa Clara–Calleguas Ground-Water Basin, Ventura County, California, U.S. Geological Survey, Water-Resources Investigations Report 02-4136, 32, 43, 157p.

Hopps, T.E., H.E. Stark, and R.J. Hindle, 1990, Website Titled: Ventura Basin Study Group Maps & Cross Sections, http://projects.eri.ucsb.edu/hopps/

Mukae, M., and Turner, J., 1975, Ventura County Water Resources Management Study, Geologic Formations, Structures and History in the Santa Clara-Calleguas Area, in Compilation of Technical Records for the Ventura County Cooperative Investigation: California Department of Water Resources, 28p.

Northwest Geophysical Associates, Inc., 2002, A Discussion of Geophysical Techniques: Time-Domain Electromagnetic Exploration.

Sylvester, A.G., and Brown, G.C., 1988, Santa Barbara and Ventura Basins; Tectonics, Structure, Sedimentation, Oilfields along an East-West Transect: Coast Geological Society Guidebook 64, Ventura, California, 167 p.

Turner, J.M., 1975, Aquifer delineation in the Oxnard-Calleguas area, Ventura County, in Compilation of Technical Information Records for the Ventura County Cooperative Investigation: California Department of Water Resources, 45p.

United Water Conservation District, 2010, Oxnard Plain Time Domain Electromagnetic Study for Saline Intrusion, United Water Conservation District Open-File Report 2010-003.

United Water Conservation District, 2012, Hydrogeologic Assessment of the Mound Basin, United Water Conservation District Open-File Report 2012-001, June 11, 2012 update.

United Water Conservation District, 2013, Aquifer Delineation within the Oxnard Forebay Groundwater Basin using Surface Geophysics, United Water Conservation District Open-File Report 2013-06.

United Water Conservation District, 2014, Groundwater Resource Management Fundamentals: Groundwater Basin Connectivity, United Water Conservation District Open-File Report 2014-03.

United Water Conservation District, 2018, Ventura Regional Groundwater Flow Model and Updated Hydrogeologic Conceptual Model: Oxnard Plain, Oxnard Forebay, Pleasant Valley, West Las Posas, and Mound Basins, United Water Conservation District Open-File Report 2018-02, July.

United States Geological Survey, 2011, Website Titled: Quaternary Fault and Fold Database of the United States, http://earthquake.usgs.gov/hazards/qfaults/

Yeats, R.S., Clark, M.N., Keller, E.A., and Rockwell, T.K. 1981, Active Fault Hazard in Southern California: Ground Rupture Versus Seismic Shaking: Geol. Soc. America Bull, Part 1, v. 92, 189-196p.

Yerkes, R.F., Sarna-Wojcicki, A.M., and La Joie, K.R., 1987, Recent Reverse Faulting in the Transverse Ranges, California: U.S. Geological Survey Professional Paper 1339.

APPENDIX A – FURTHER EXPLANATION OF METHODOLOGY AND DATA INTERPRETATION

The first panel in Figure A-1 shows the waveform of the transmitter current and primary magnetic field generated by the transmitter. The second panel shows the induced electromotive force (primary field impulse) which creates the secondary currents (referred to as eddy currents) immediately below the transmitter loop. These eddy currents approximate a mirror image of the transmitter loop. As the initial near surface eddy currents decay, they in turn induce eddy currents at greater depths. The third panel in Figure A-1 shows the waveform of the secondary magnetic field generated by the series of eddy currents induced in the ground. The magnitude and rate of decay of those secondary currents depend upon the conductivity of the medium (i.e. electrical resistivity of the soil) and the geometry of the subsurface. The TDEM receiver measures the decay of the magnetic fields (secondary magnetic fields) created by those secondary currents.

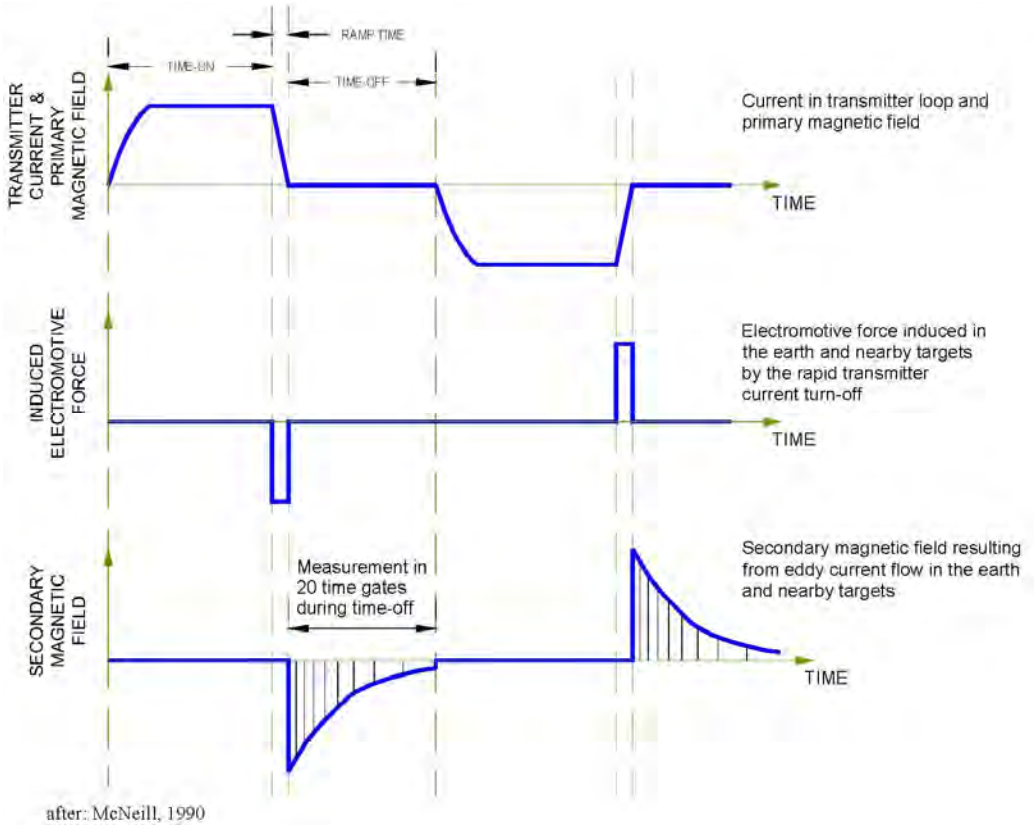

Figure A-1: TDEM Waveforms (from Northwest Geophysical Associates, 2002).

In TDEM techniques the inducing signal is a sharp pulse, or transient signal. The induced currents in the underlying sediment and rock (eddy currents) are initially concentrated immediately below the transmitter loop. This is depicted schematically in Figure A-2. Those currents will diffuse down and away from the transmitter with time. This is also depicted in Figure A-2. An analogy with smoke rings is often used to describe the behavior of the currents in the ground. Initially strong currents form in the ground adjacent to the transmitting loop. The “smoke ring” then expands, weakens, and travels down through the underlying sediment and rock. The rate of diffusion depends upon the underlying

sediment and rock resistivity. In resistive media the current will diffuse very rapidly. In conductive media (low resistivity) the currents will diffuse more slowly. A conductive layer at depth may "trap" currents in that layer, while currents elsewhere decay more rapidly.

Measurements of the secondary magnetic field are typically made in the time range from 10 micro-seconds to 10 milli-seconds following the "turn-off" of the primary field. Measurements are made in 20 to 30 discrete "time gates" (or time intervals) following the primary inducing pulse. For deeper exploration in conductive areas, measurement times can extend up to one second. Because measurements are made while the transmitting current is turned off, more sensitive measurements of the secondary field can be made.

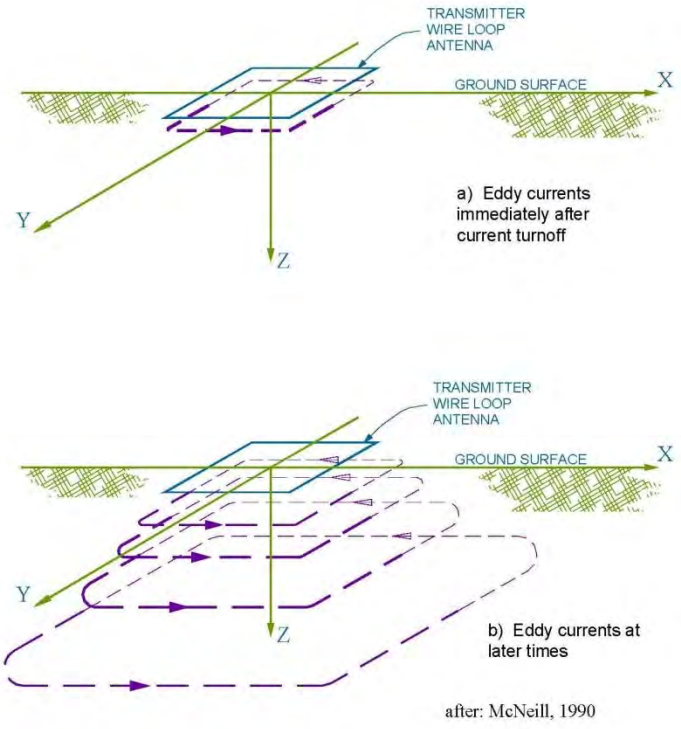

Figure A-2: TDEM Eddy Current Flow - a) early time and b) late time (from Northwest Geophysical Associates, 2002).

The measured decay values of the secondary magnetic field are used to generate values of apparent resistivity. Apparent resistivity is the resistivity of homogeneous and isotropic ground which would give the same voltage current relationship as measured. However, non-homogeneous and anisotropic media consist of different "true resistivities" which result in that measured value. Therefore, the data must be modeled to achieve a solution for resistivity structure and depth.

Interpretation procedures generally use forward and inverse modeling. A hypothetical layered earth model is generated and then the theoretical response for that model is calculated. The model is then refined until the calculated response matches the observed or measured field response. The model refinements can be made using an automated iterative process or "inversion modeling". There are several conditions that will affect the sounding data (perched aquifer, vadose zone, complex geology, etc.).

Figure A-3 shows the decay of the secondary magnetic field. It decays over three decades during the course of the recording from 0.006 milli-seconds (ms) to 7 ms. The electrical potential induced in the receiver coil is proportional to dBZ/dt and is reported as “normalized voltage”, normalized to the receiver coil moment and transmitter current of 2.6 amperes (A).

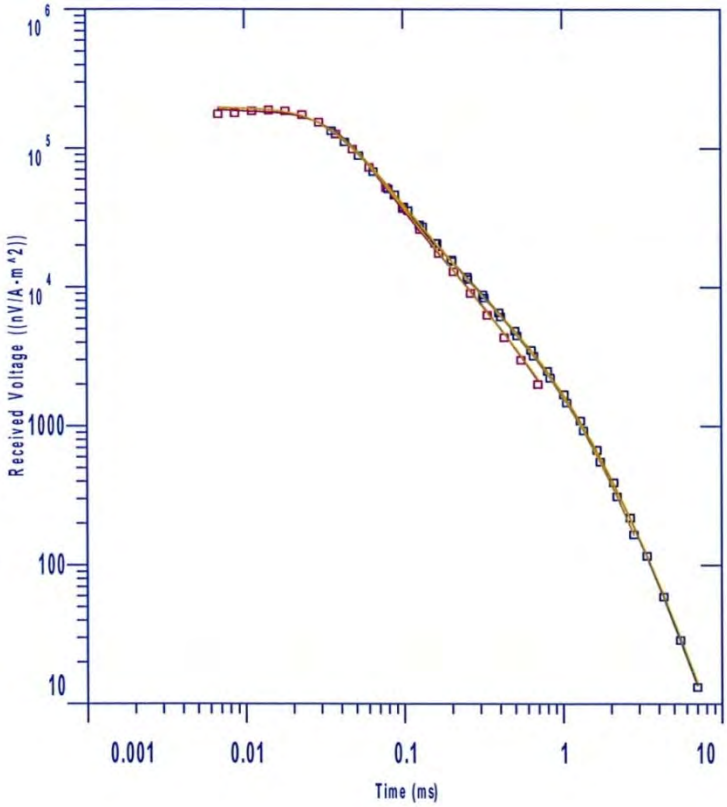

Figure A-3: TDEM Decay of Secondary Magnetic Field.

The right hand panel of Figure A-4 is a forward and inverse model refined using automated inverse modeling. The left hand panel shows a plot of the same data as Figure A-3 converted to “late stage” apparent resistivity. The apparent resistivity curve gives a somewhat more intuitive feel for the geoelectric section. However, as explained in the following paragraph, TDEM apparent resistivity is not a true apparent resistivity as observed in DC resistivity of frequency domain techniques.

In concept, the “apparent resistivity” is the resistivity of a uniform earth which will produce the observed instrument response. However, the observed TDEM field is a non-linear function of time and underlying sediment and rock resistivity. In fact, the instrument response is not a single valued function of the resistivity over the time range of the instrument.

For most TDEM soundings a “late stage” apparent resistivity is used, which is a “true” apparent resistivity only for a later stage of the decay curve. It is generally attempted to make measurements in this time range but often the first portion of the curve is not truly in late stage, hence the numerical values may not accurately indicate the underlying sediment and rock resistivity for the first few time gates. This discussed in Appendix B.

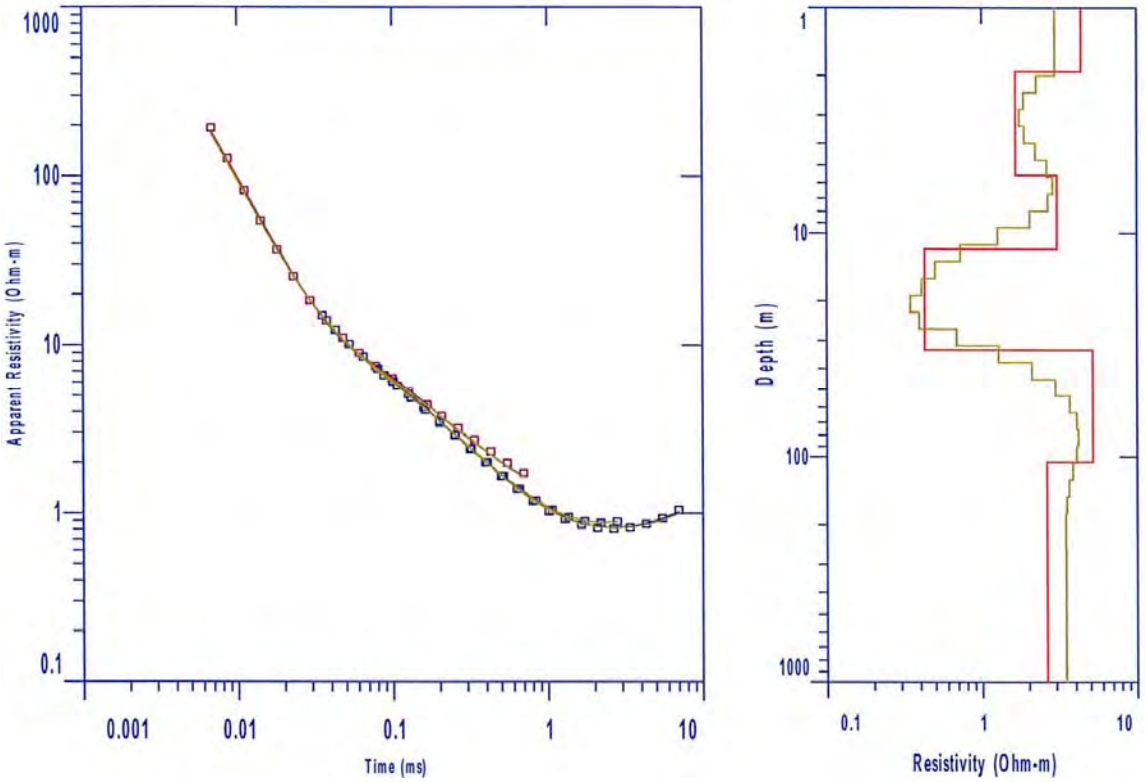

Figure A-4: TDEM Sounding in Late Stage and Model.

The green line in right hand panel of Figure A-5 shows the way in which the data was modeled for this project with the forward model (red line in right hand panel) approach superimposed on top of it. The model shown is the smooth model automatically generated using IX1D 3.51 modeling software. The modeled resistivity is considered to be the “true resistivity” which is used to calculate the given response in attempt to match the observed or field data (small squares on the left hand panel are apparent resistivity or measured data). The different resistivity values represent varying underlying sediment and rock materials with inherent true resistivities (sand versus clay versus silt versus rock, etc.). The true resistivity is dependent upon many factors some of which include: grain size, composition, water content, consolidation/lithification, weathering, etc..

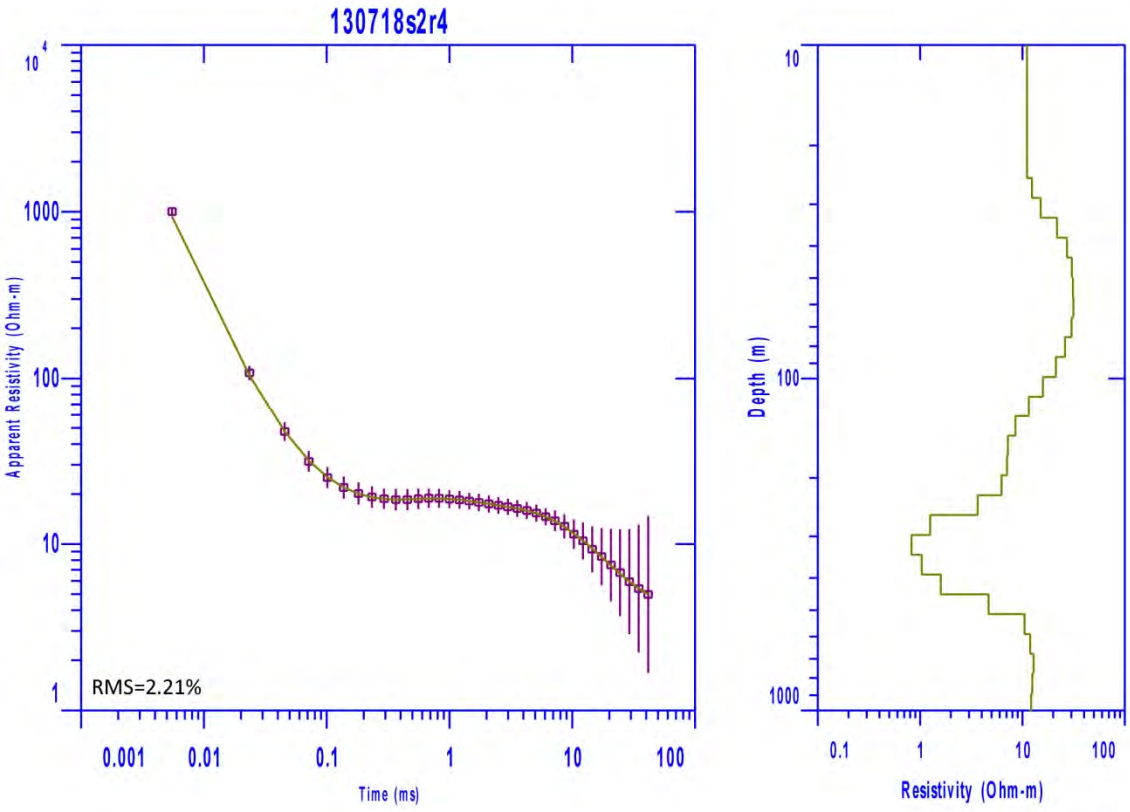

Figure A-5: TDEM Sounding and Model for Sounding 130718s2r4.

APPENDIX B – APPARENT RESISTIVITY IN TDEM SOUNDINGS

Figure B-1 shows, schematically, a linear plot of a typical TDEM transient response from the underlying sediment and rock. The vertical axis is instrument response (output voltage) in nV/m^2. It is useful to examine this response when plotted logarithmically against the logarithm of time for a homogeneous earth (i.e. the resistivity does not vary with either lateral distance or depth). Such a plot is shown in Figure B-2. It suggests that the response can be divided into an early stage (where the response is constant with time), an intermediate stage (response continually varying with time), and a late stage (response is now a straight line on the log-log plot). The response is generally a mathematically complex function of conductivity and time; however, during the late stage, the mathematics simplifies considerably, and it can be shown that during this time the response varies quite simply with time and conductivity as

$$e(t) = \frac{k_1 M \sigma^{3/2}}{t^{5/2}}, \qquad (1)$$

$e(t)$ = output voltage from a single-turn receiver coil of area 1 m^2
k_1 = a constant
M = product of Tx current x area (a-m^2)
σ = terrain conductivity (siemens/m = S/m = 1/Ωm)
t = time (s)

For conventional resistivity methods (DC resistivity) the measured voltage varies linearly with terrain resistivity. For TDEM, the measured voltage [e(t)] varies as $\sigma^{3/2}$, therefore, it is intrinsically more sensitive to small variations in the conductivity than conventional resistivity methods. Note that during the late stage, the measured voltage is decaying at the rate $t^{-5/2}$, which is very rapidly with time. Eventually the signal disappears into the system noise, and further measurement is impossible. This is the maximum depth of exploration for the particular system.

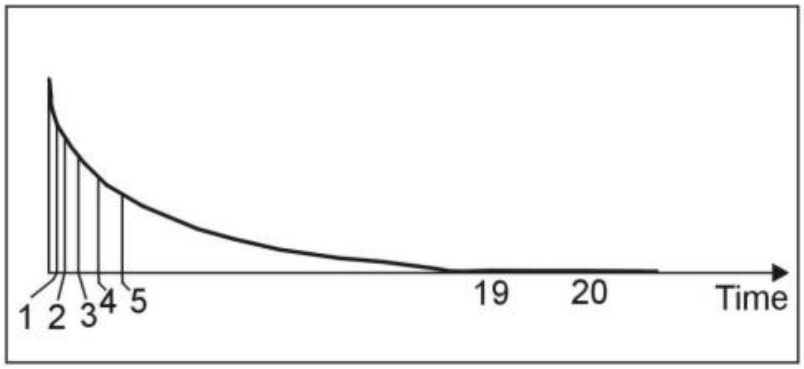

Figure B-1: Receiver time gate locations.

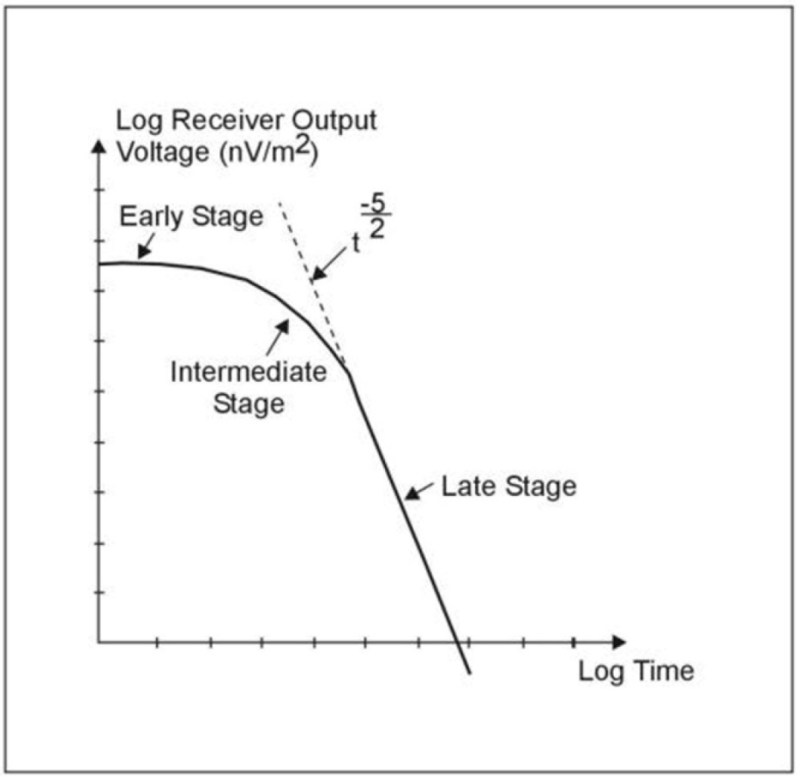

Figure B-2. Log plot-receiver output voltage versus time (one transient).

With conventional DC resistivity methods, for example the Wenner array, the measured voltage over a uniform earth can be shown to be

$$V(a) = \frac{\rho I}{2\pi a} \tag{2a}$$

a = inter-electrode spacing (m)
ρ = terrain resistivity (Ω-m)
I = current into the outer electrodes
V(*a*) = voltage measured across the inner electrodes for the specific value of *a*

In order to obtain the resistivity of the ground, equation 2a is rearranged to give equation 2b:

$$\rho = 2\pi a \frac{V(a)}{I}, \tag{2b}$$

If ground resistivity is homogeneous and isotropic (uniform half space), and the inter-electrode spacing (*a*) is increased, the measured voltage decreases directly with *a* so that the right-hand side of equation 2b stays constant, and the equation gives the true resistivity. Suppose now that the ground is horizontally layered (i.e., that the resistivity varies with depth). For example, it might consist of an upper layer of thickness *h* and resistivity ρ1, overlying a more resistive basement of resistivity (ρ2 > ρ1). This is called a two-layered earth. At very short inter-electrode spacing (*a*<<*h*), virtually no current penetrates into the more resistive basement, and resistivity calculation from equation 2b will give the value ρ1. As the inter-electrode spacing (a) is increased, the current (I) is forced to flow

to greater and greater depths. Suppose that, at large values of *a* (*a*>>*h*), the effect of the near-surface material of resistivity ρ1 will be negligible, and resistivity calculated from equation 2b will give the value ρ2. At intermediate values of *a*, the resistivity given by equation 2b will lie somewhere between ρ1 and ρ2.

Equation 2b is, in the general case, used to define an apparent resistivity which is a function of a ($\rho_a(a)$). The variation of $\rho_a(a)$ with *a*

$$\rho_a(a) = 2\pi a \frac{V(a)}{I}, \tag{3}$$

is descriptive of the variation of resistivity with depth. The behavior of the apparent resistivity $\rho_a(a)$ for a Wenner array for the two-layered earth above is shown schematically in Figure B-3. With conventional resistivity sounding, to increase the depth of exploration, the inter-electrode spacing must be increased. In the case of TDEM soundings it was observed earlier that as time increases, the depth to the eddy current loops increases. This phenomenon is used to perform the sounding of resistivity with depth in TDEM. Thus, in analogy with equation 3, equation 1 can be inverted to read (since ρ = 1/σ)

$$\rho_a(t) = \frac{k_2 M^{2/3}}{e(t)^{2/3} t^{5/3}}. \tag{4}$$

Suppose once again that resistivity does not vary with depth (uniform half-space) and is of resistivity ρ1. For this case, a plot of $\rho_a(t)$ against time would be as shown in Figure B-4. Note that at late time the apparent resistivity $\rho_a(t)$ is equal to ρ1, but at early time $\rho_a(t)$ is much larger than ρ1. The reason for this is that the definition of apparent resistivity is based (as seen from Figure B-2) on the time behavior of the receiver coil output voltage. At earlier and intermediate time, Figure B-2 shows that the receiver voltage is too low (the dashed line indicates the voltage given by the late stage approximation) and thus, from equation 4, the apparent resistivity will be too high. For this reason, there will always be, as shown on Figure B-4, a "descending branch" at early time where the apparent resistivity is higher than the half-space resistivity (or, as will be seen later, is higher than the upper layer resistivity in a horizontally layered earth). This is not a problem, but it is an artifact of which we must be aware.

Suppose the earth is two-layered with upper layer resistivity ρ1 (thickness *h)* and basement resistivity ρ2 (>ρ1). At early time when the currents are entirely in the upper layer of resistivity ρ1 the decay curve will look like that of Figure B-2. However, later on the currents will lie in both layers, and at much later time, they will be located entirely in the basement (resistivity ρ2). Since ρ2>ρ1, equation 4 shows that the measured voltage will now be less than it should have been for the homogeneous half-space of resistivity ρ1 (as indicated in Figure B-5). The effect on the apparent resistivity curve is shown in Figure B-6a. Since at late times all the currents are in the basement, the apparent resistivity $\rho_a(t)$ becomes equal to ρ2, completely in analogy with Figure B-3 for conventional resistivity

measurements. In the event that ρ2<ρ1, the inverse behavior is also as expected. At late times the measured voltage response, shown in Figure B-5, is greater than that from a homogeneous half-space of resistivity ρ1, and the apparent resistivity curve correspondingly becomes that of Figure B-6b, becoming equal to the new value of ρ2 at late time. Note that for the case of a (relatively) conductive basement, there is a region of intermediate time (shown as *t**), where the voltage response temporarily falls before continuing on to adopt the value appropriate to ρ2. This behavior, which is a characteristic of TDEM, is again not a problem, as long as it is recognized. The resultant influence of the anomalous behavior on the apparent resistivity is also shown on Figure B-6b at *t**.

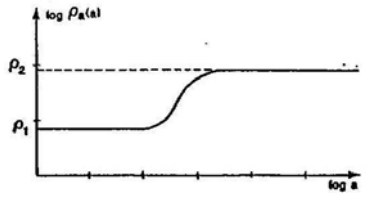

Figure B-3: Wenner array: apparent resistivity, two layer curve.

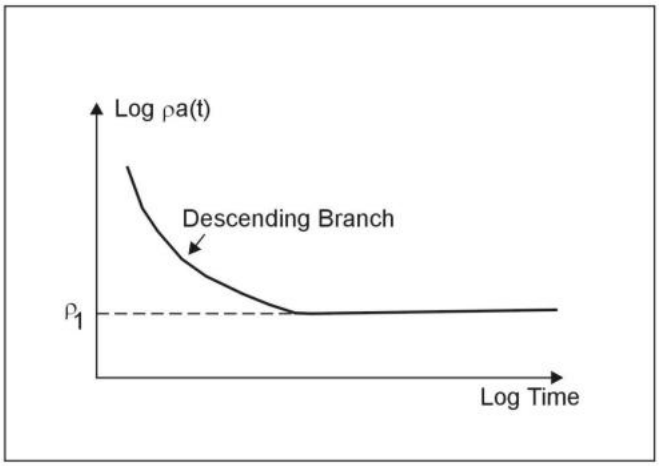

Figure B-4. Time Domain Electromagnetic (TDEM): apparent resistivity, homogeneous half space.

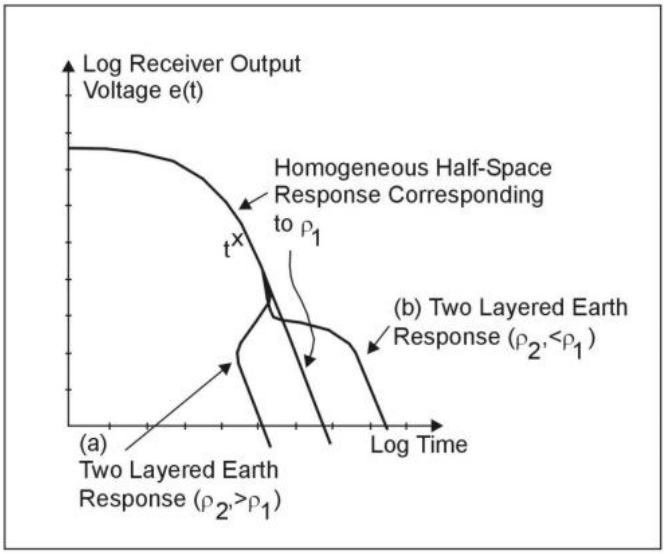

Figure B-5. Time Domain Electromagnetic (TDEM): receiver output voltage, two layer earth.

To summarize, except for the early-time descending branch and the intermediate-time anomalous region described above, the sounding behavior of TDEM is analogous to that of conventional DC resistivity if the passage of time is allowed to achieve the increasing depth of exploration rather than increasing inter-electrode spacing.

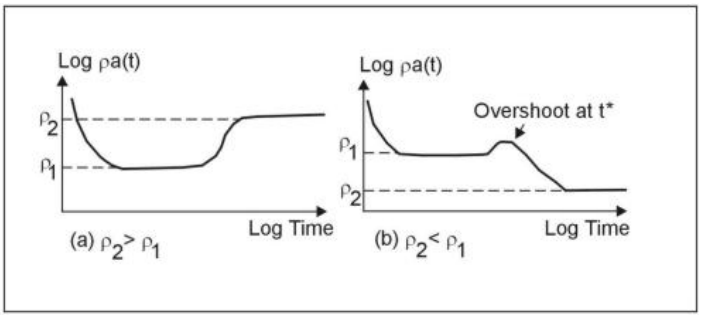

Figure B-6. Time Domain Electromagnetic (TDEM): apparent resistivity, two layered earth.

Curves of apparent resistivity such as Figure B-6 tend to disguise the fact, that at very late times, there is simply no signal, as is evident from Figure B-5. In fact, in the TDEM central loop sounding method, it is unusual to see, in practical data, the curve of apparent resistivity actually asymptote to the basement resistivity due to loss of measurable signal. Fortunately, both theoretically and in practice, the information about the behavior of the apparent resistivity curve at early time and in the transition region is generally sufficient to allow the interpretation to determine relatively accurately the resistivity of the basement without use of the full resistivity-sounding curve.

APPENDIX C – CROSS-SECTIONS

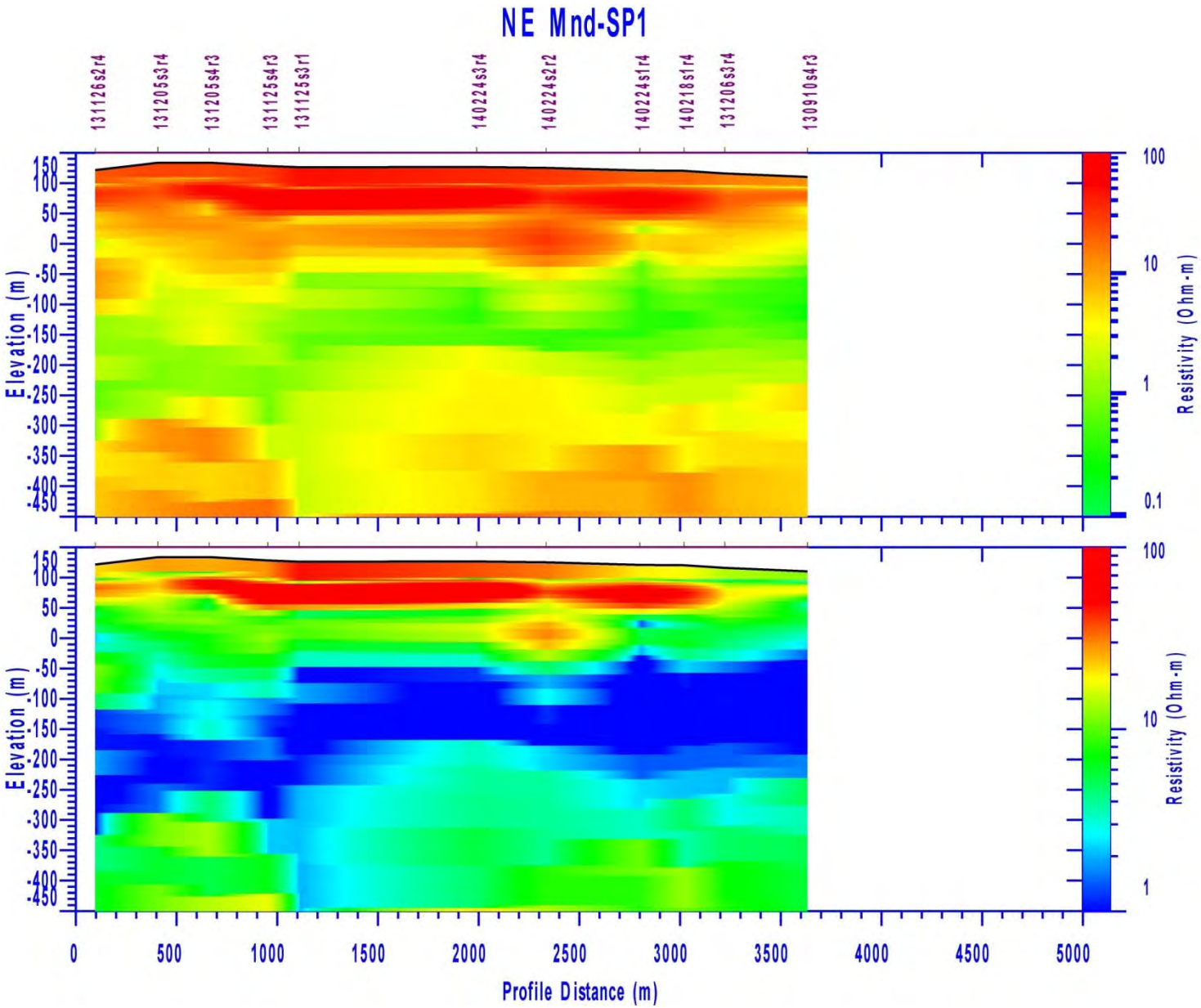

Figure C-1. Cross-section NE Mnd-SP1.

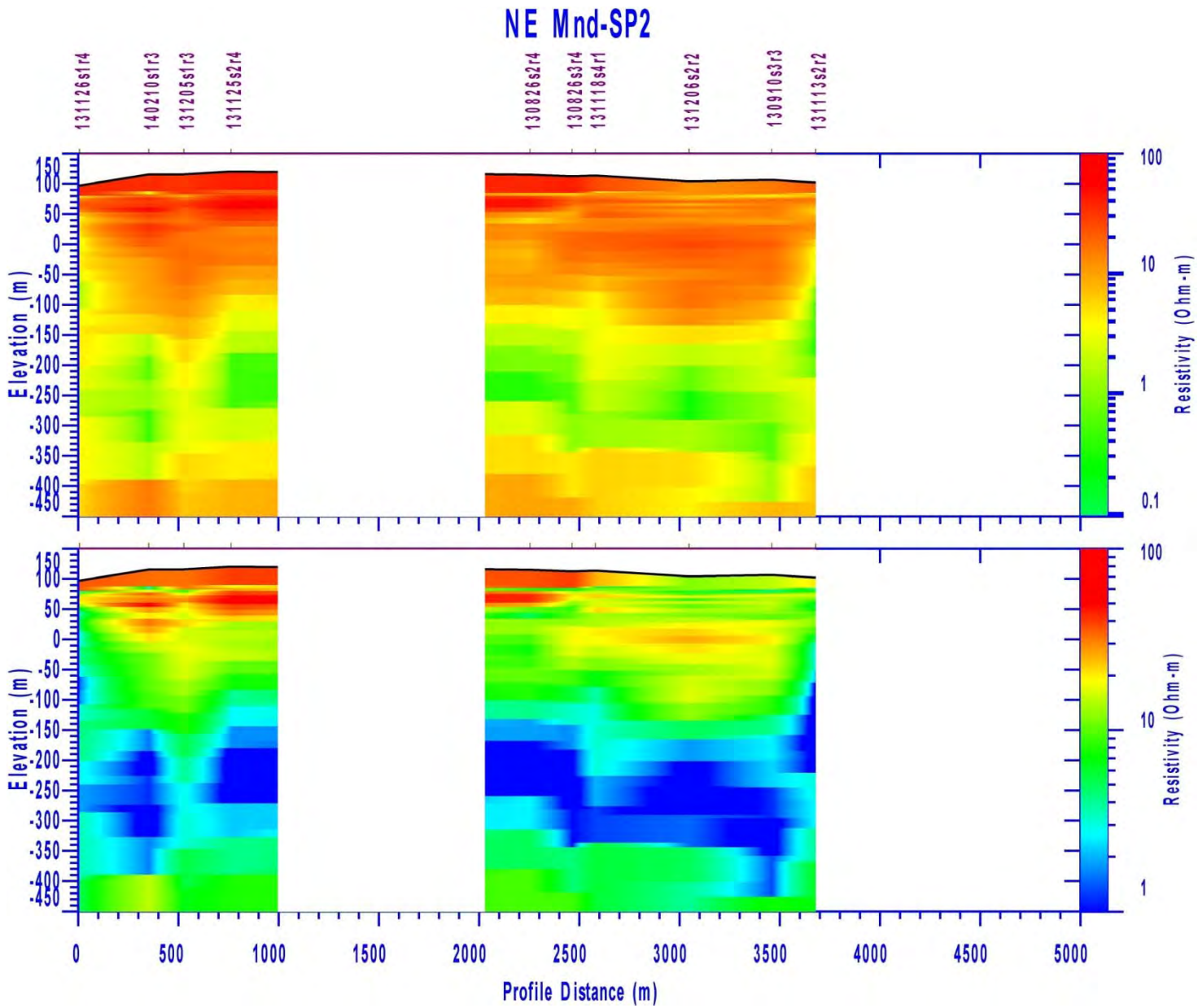

Figure C-2. Cross-section NE Mnd-SP2 (part of section blanked due to sparse data).

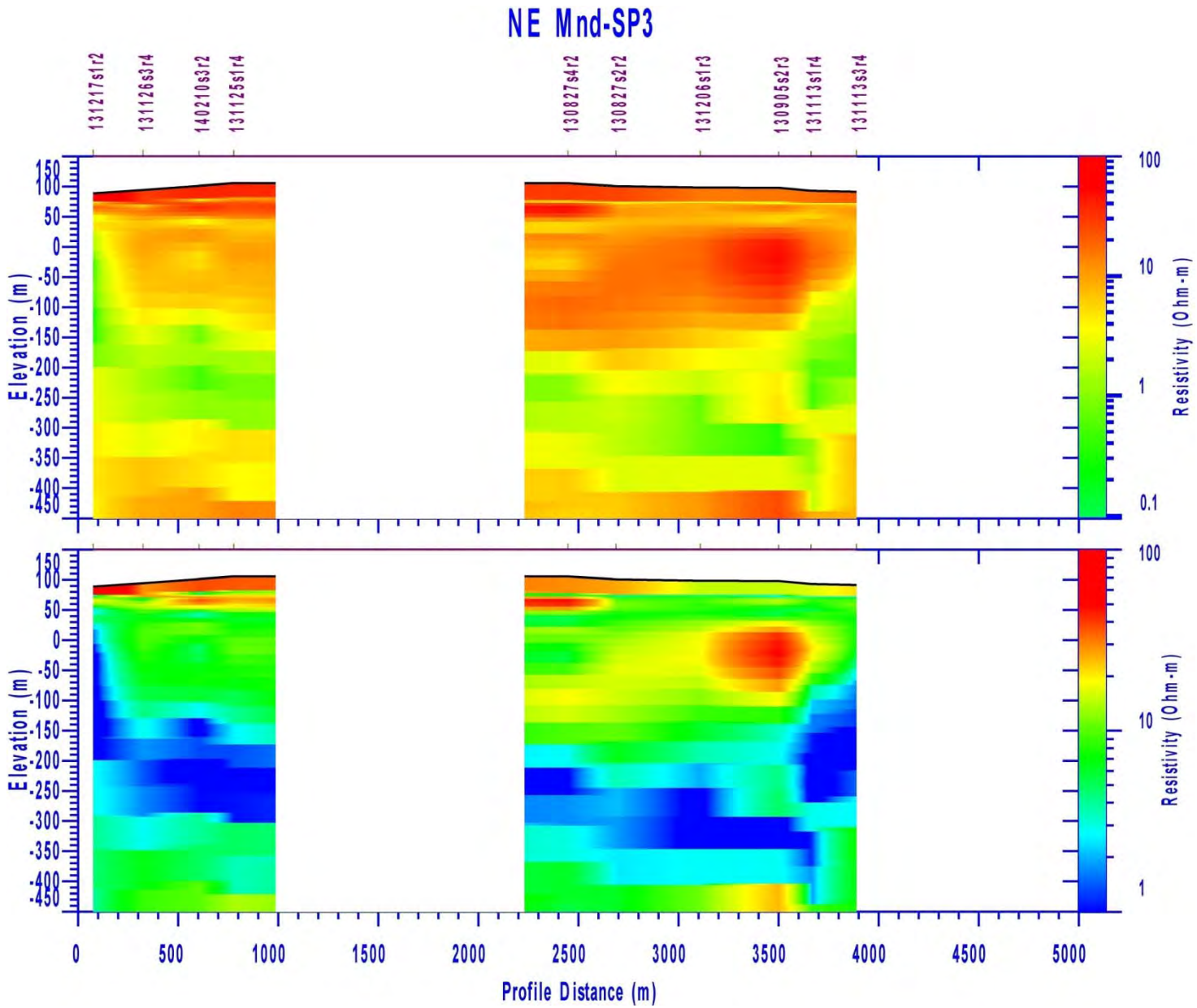

Figure C-3. Cross-section NE Mnd-SP3 (part of section blanked due to sparse data).

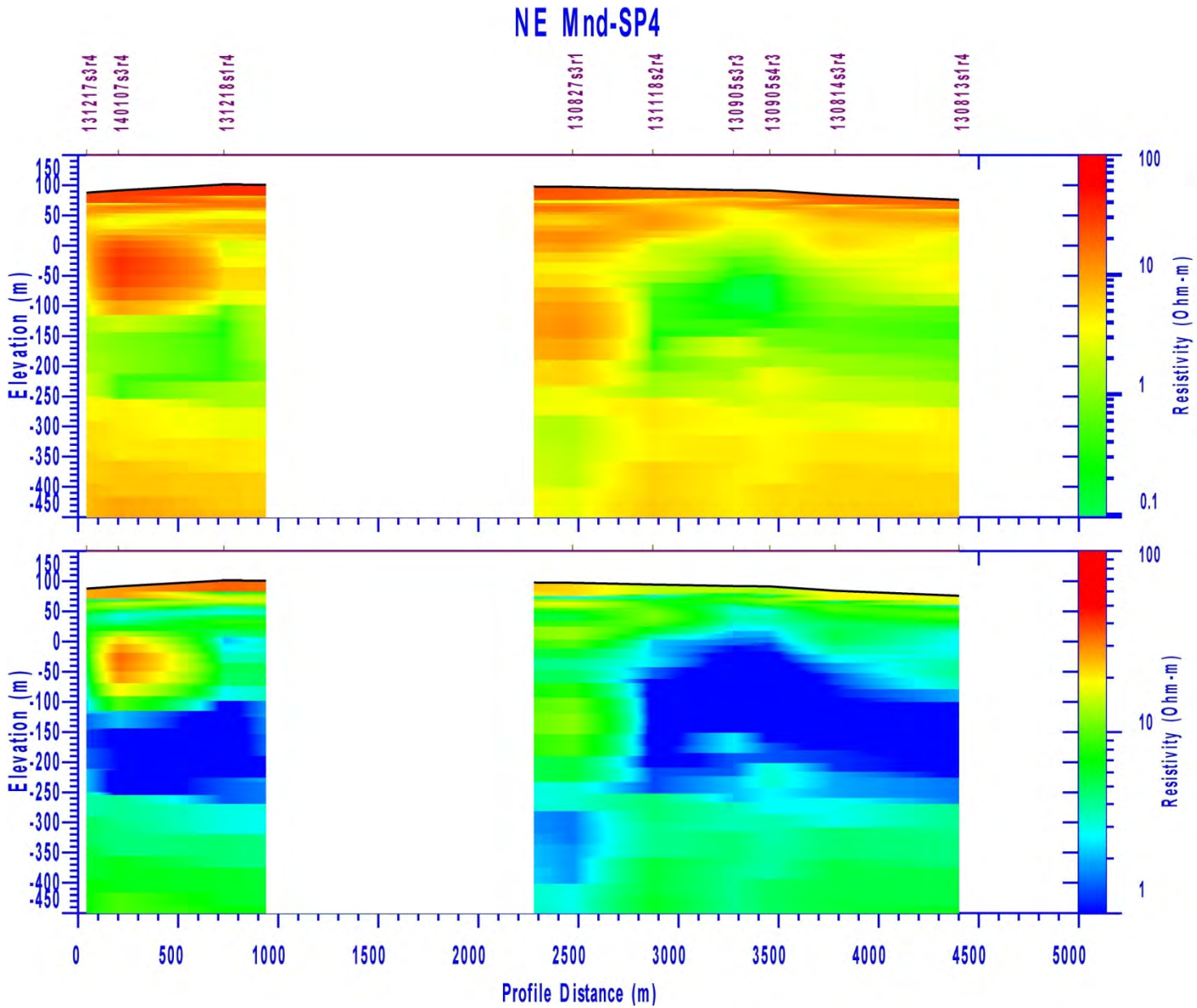

Figure C-4. Cross-section NE Mnd-SP4 (part of section blanked due to sparse data).

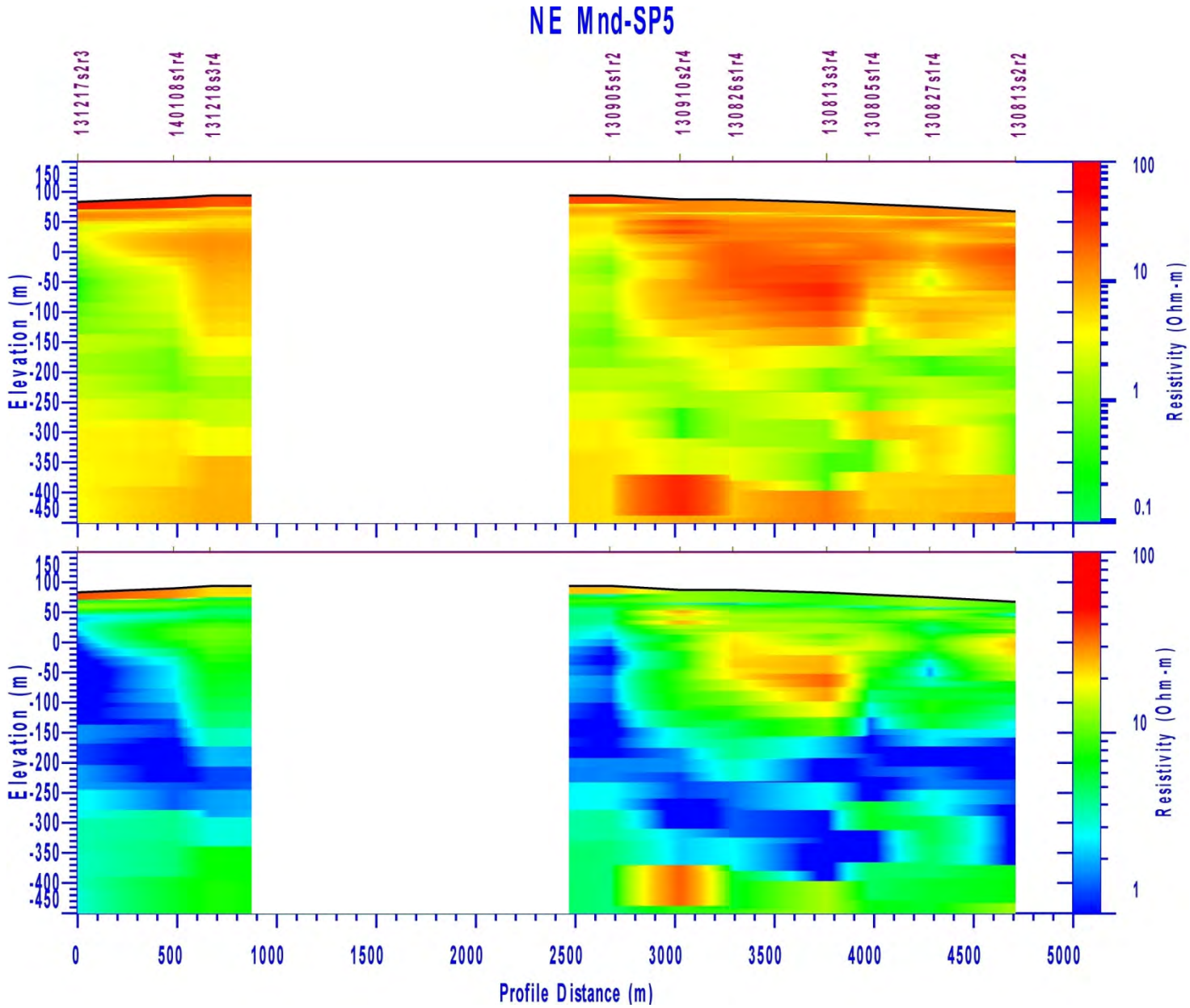

Figure C-5. Cross-section NE Mnd-SP5 (part of section blanked due to sparse data).

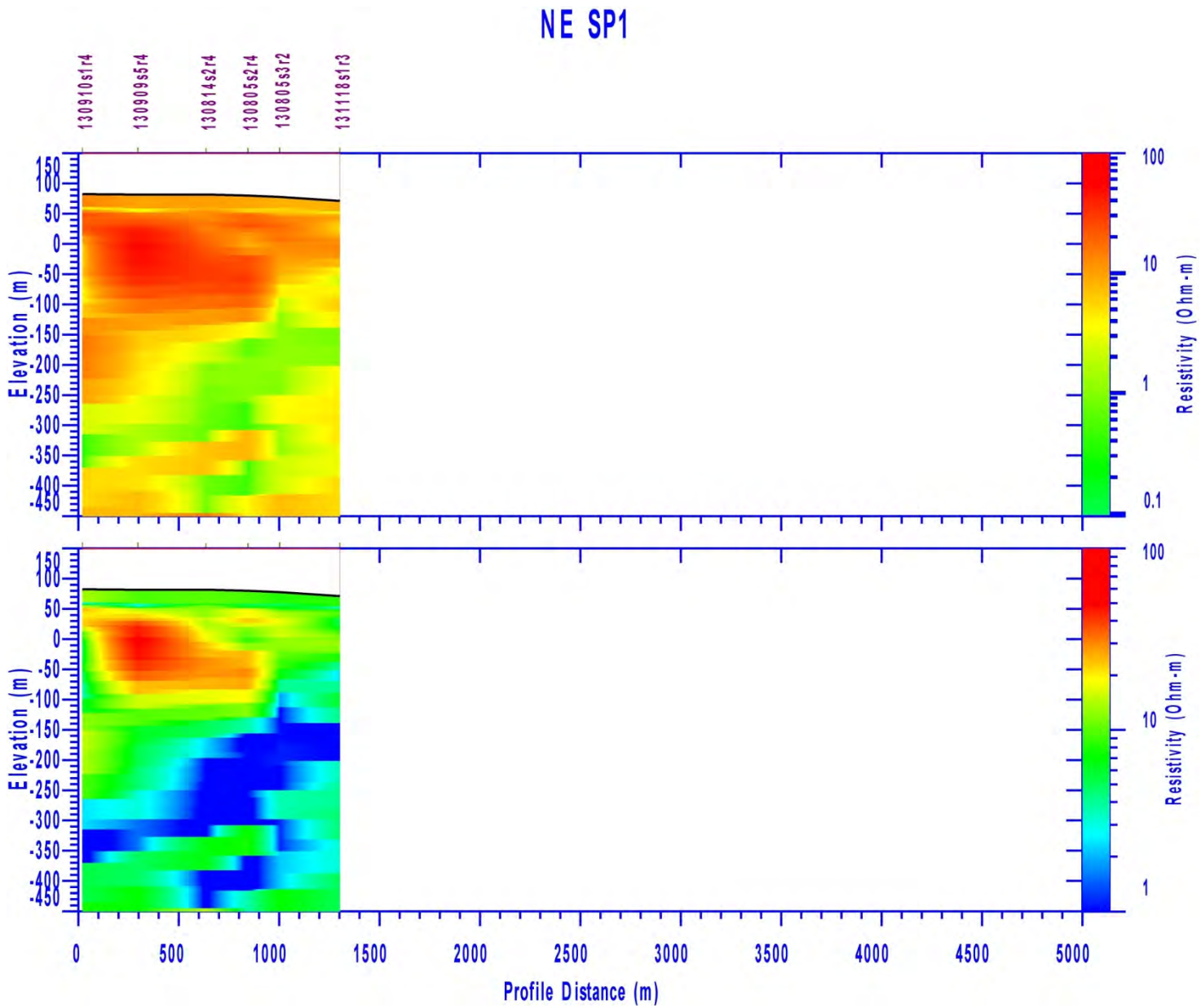

Figure C-6. Cross-section NE SP1.

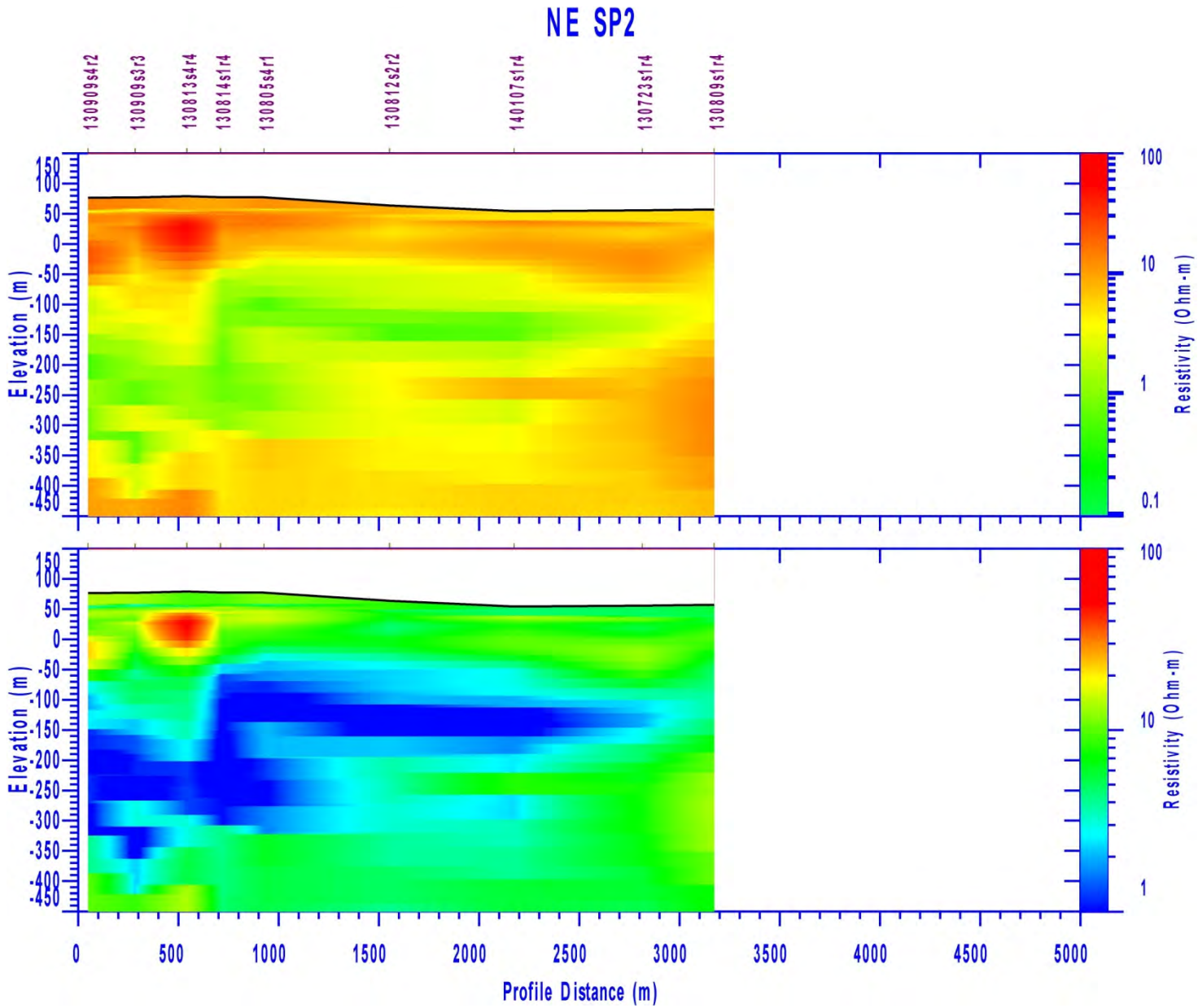

Figure C-7. Cross-section NE SP2.

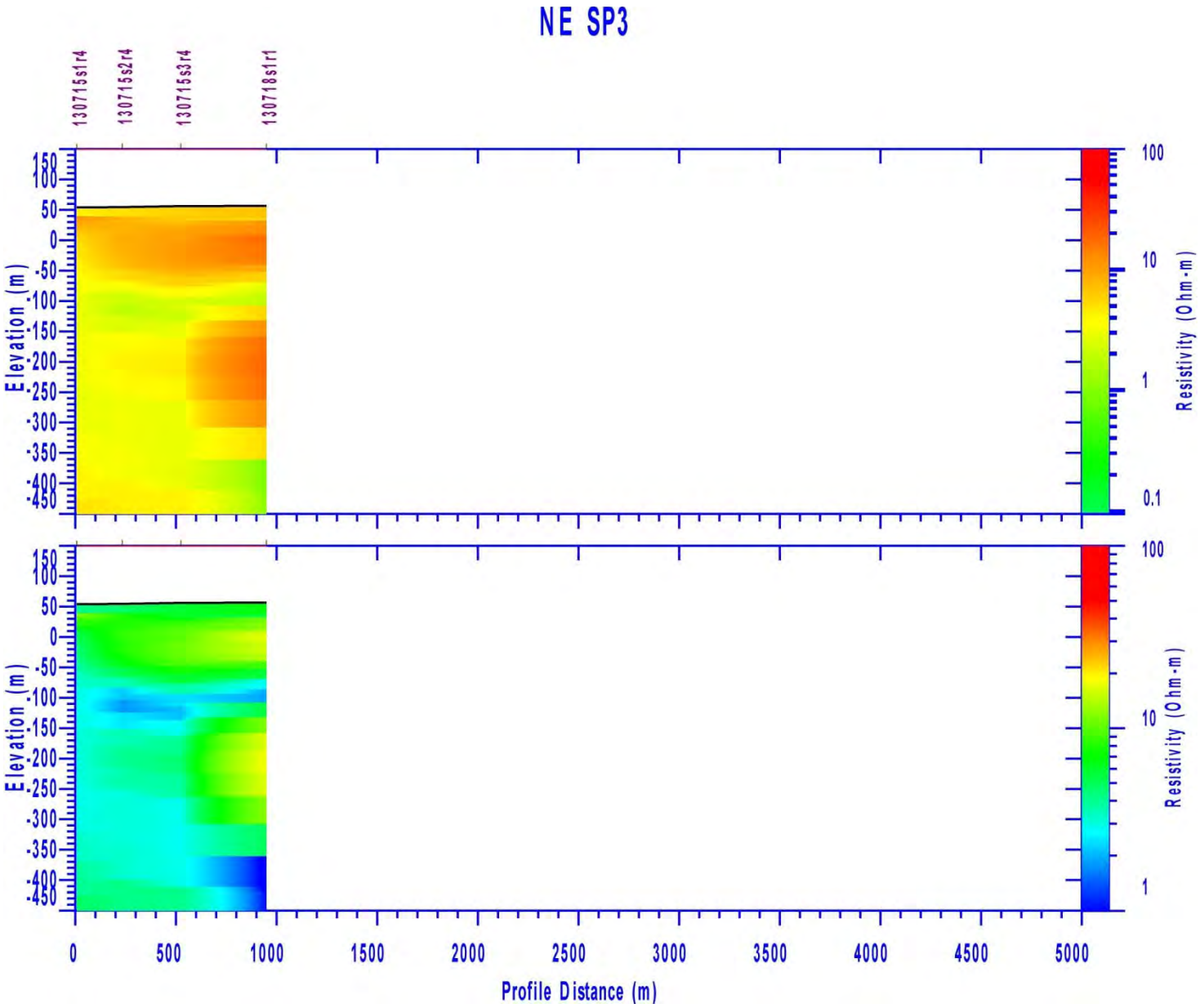

Figure C-8. Cross-section NE SP3.

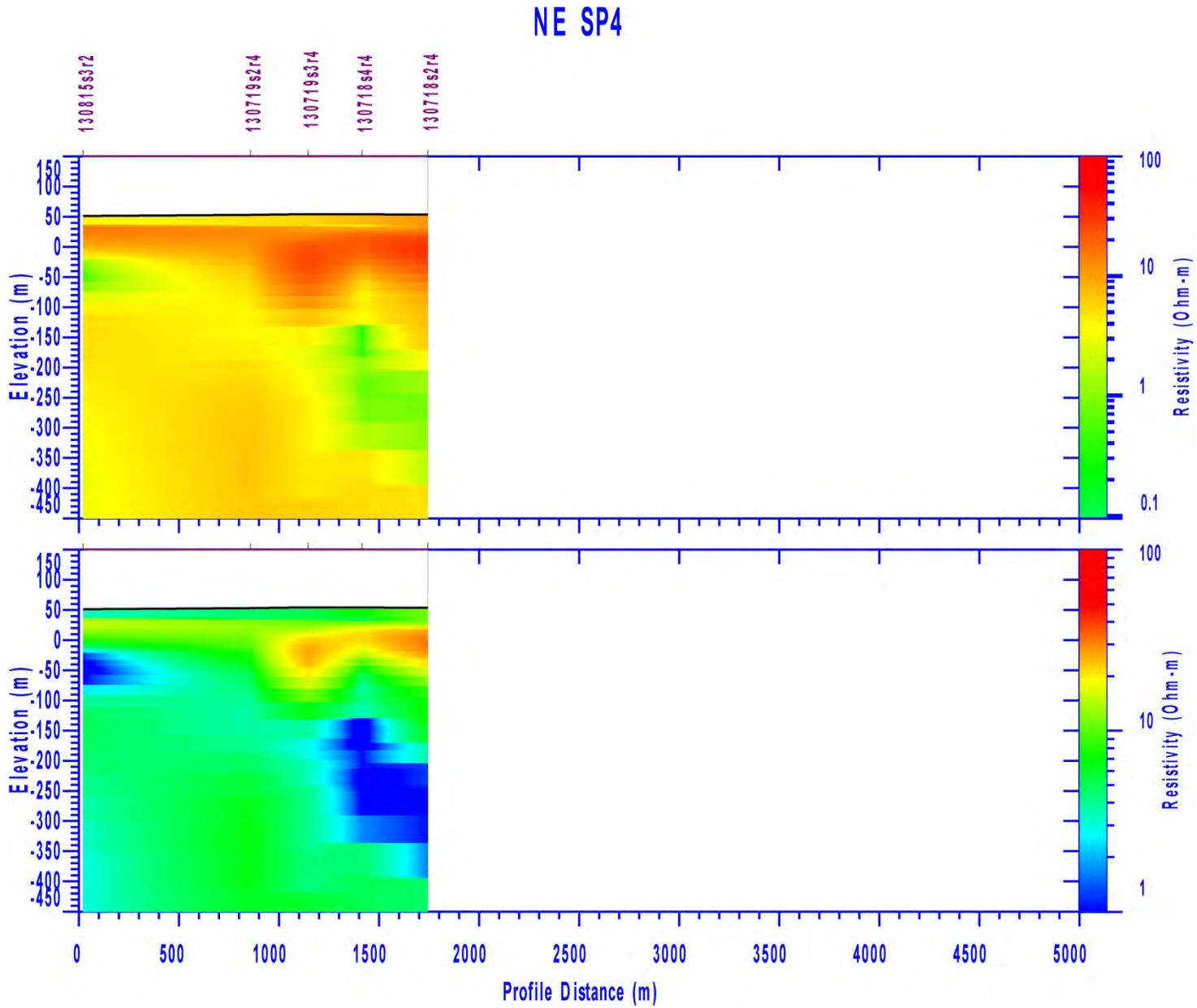

Figure C-9. Cross-section NE SP4.

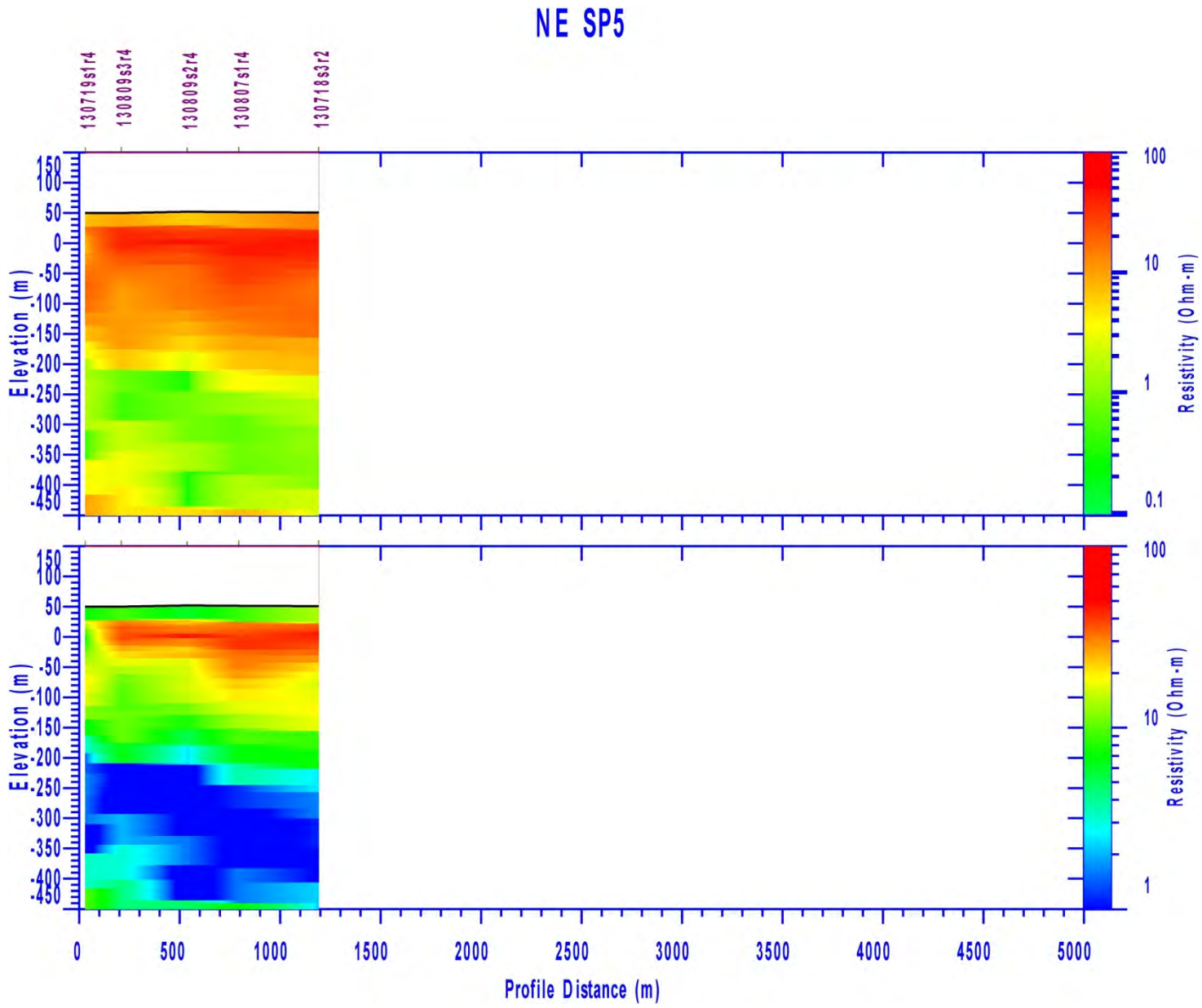

Figure C-10. Cross-section NE SP5.

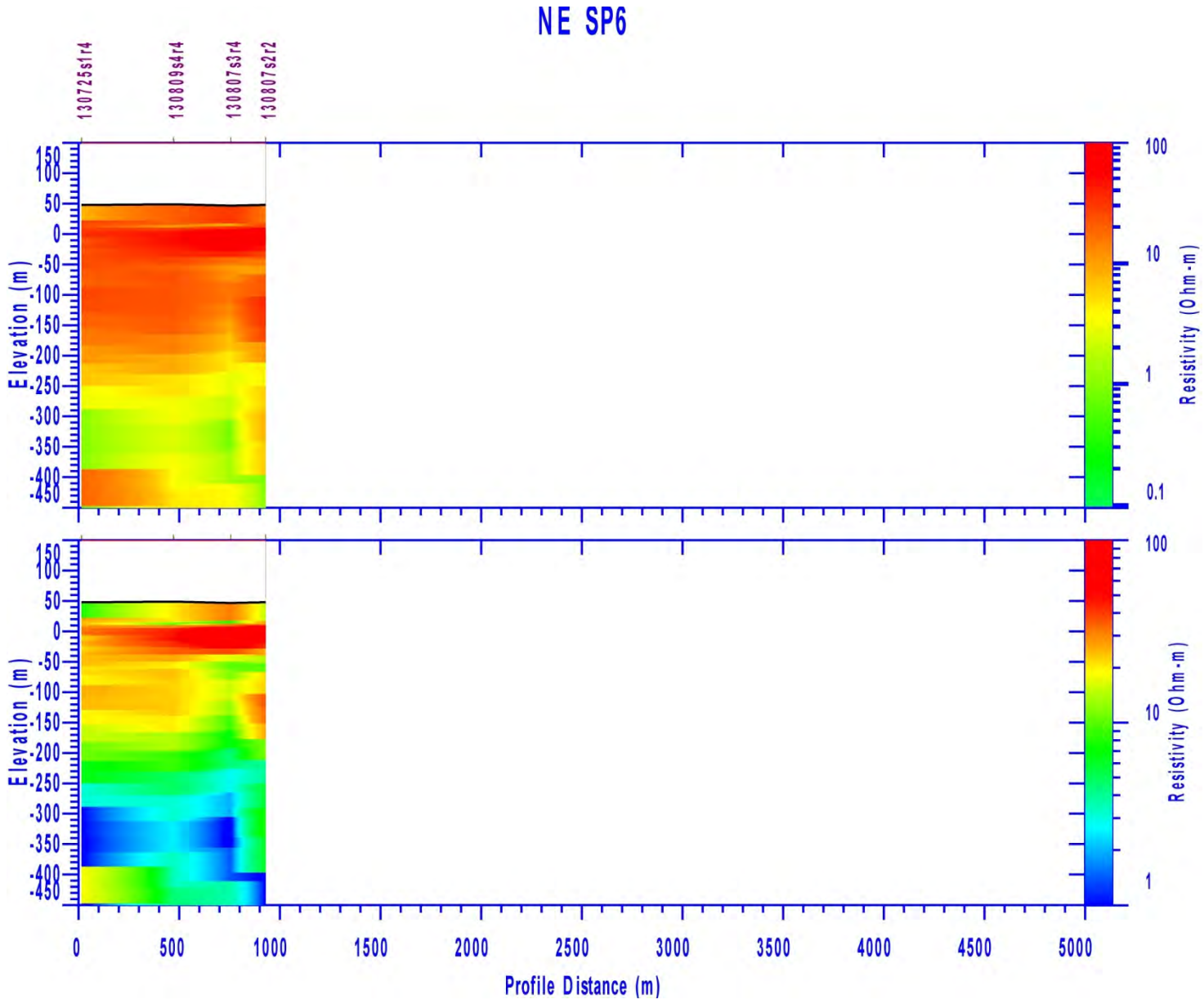

Figure C-11. Cross-section NE SP5.

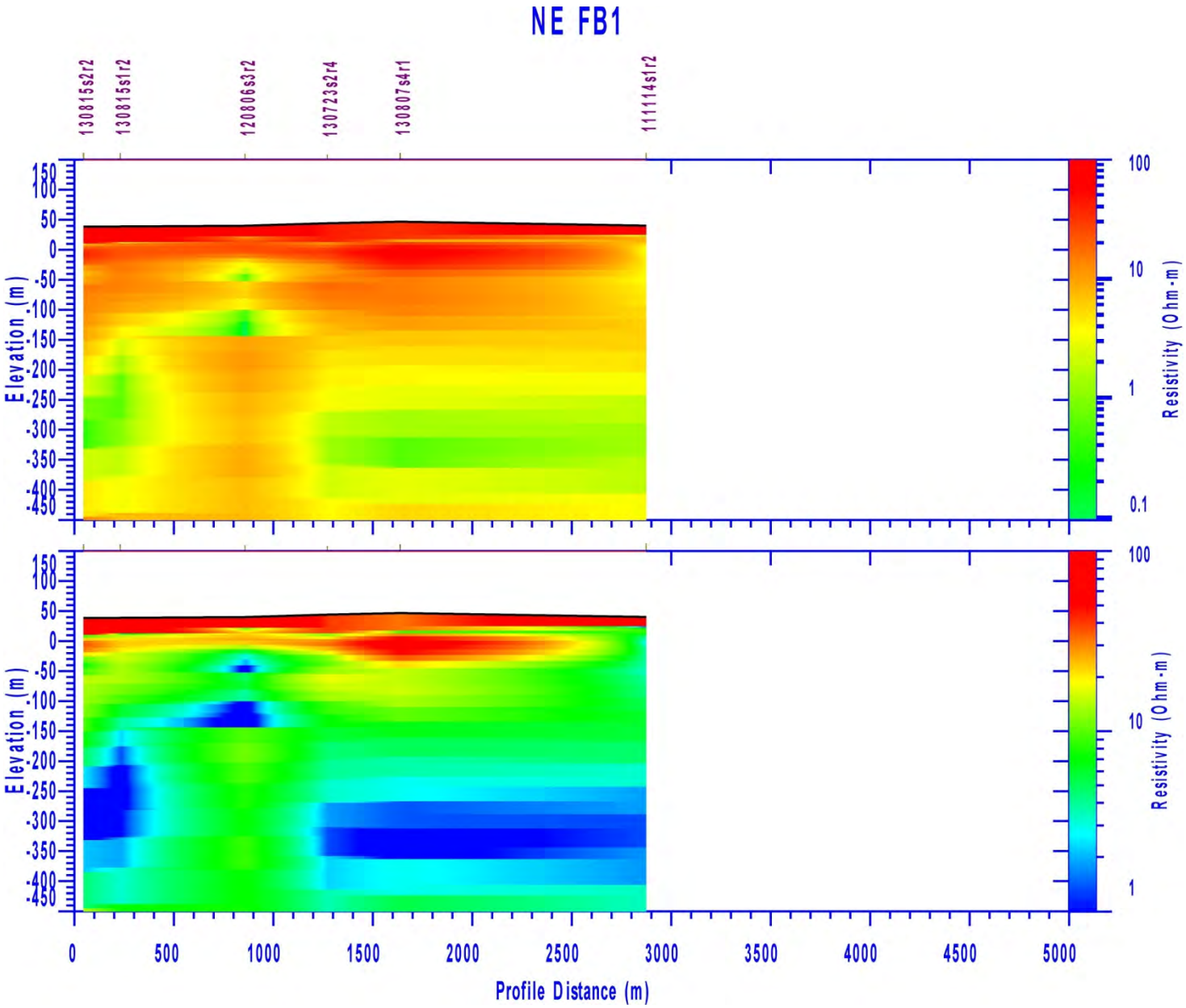

Figure C-12. Cross-section NE FB1.

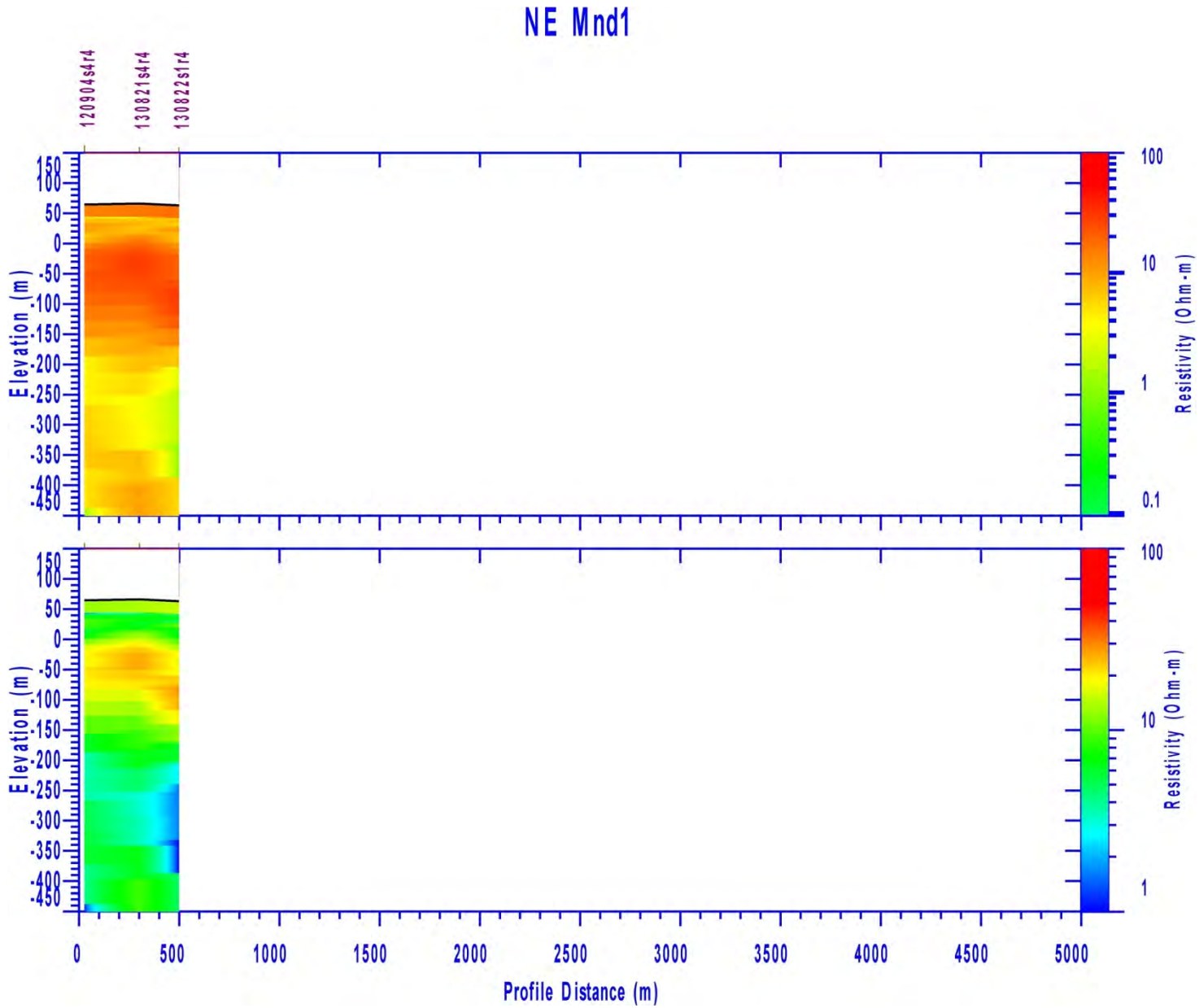

Figure C-13. Cross-section NE Mnd1.

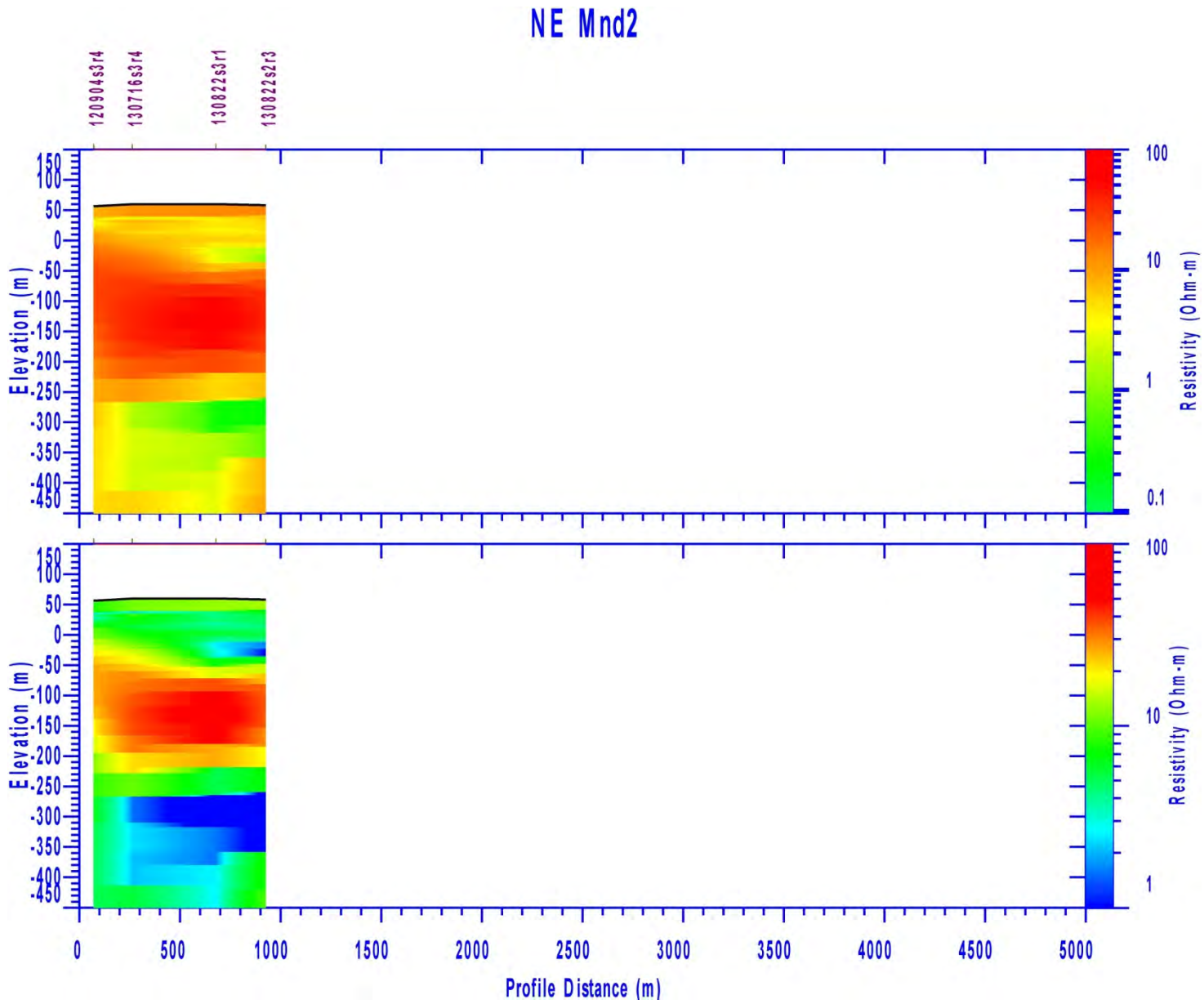

Figure C-14. Cross-section NE Mnd2.

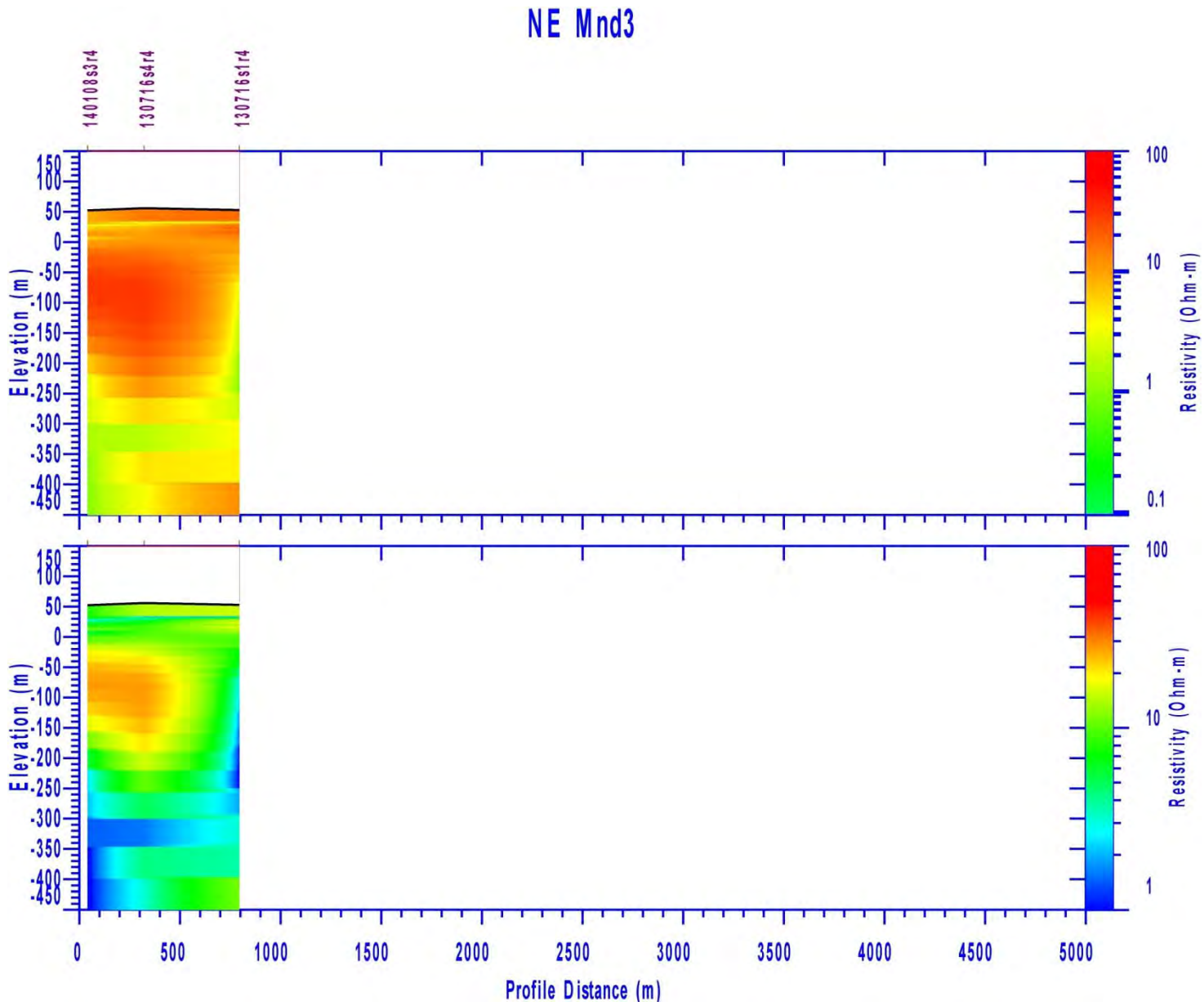

Figure C-15. Cross-section NE Mnd3.

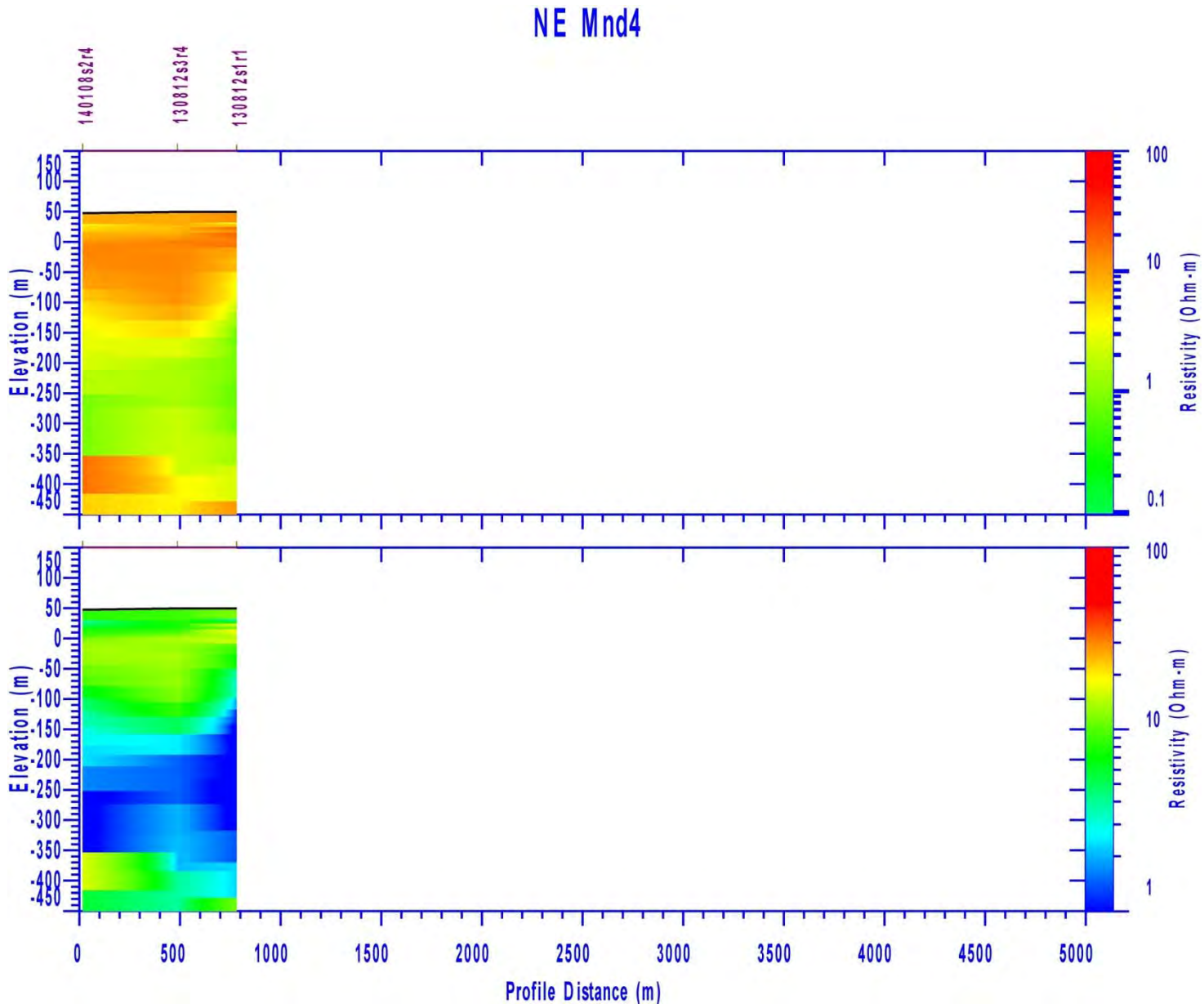

Figure C-16. Cross-section NE Mnd4.

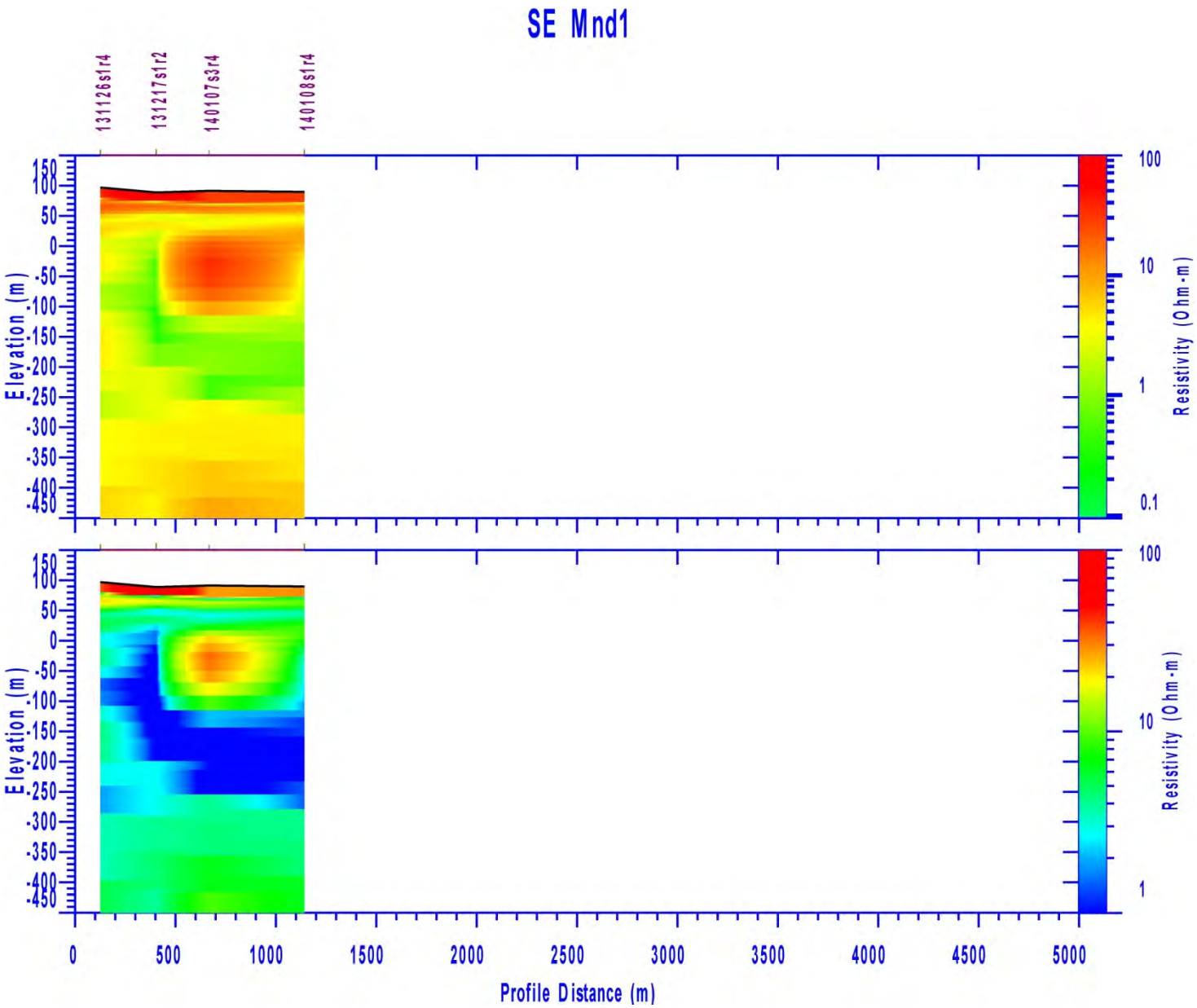

Figure C-17. Cross-section SE Mnd1.

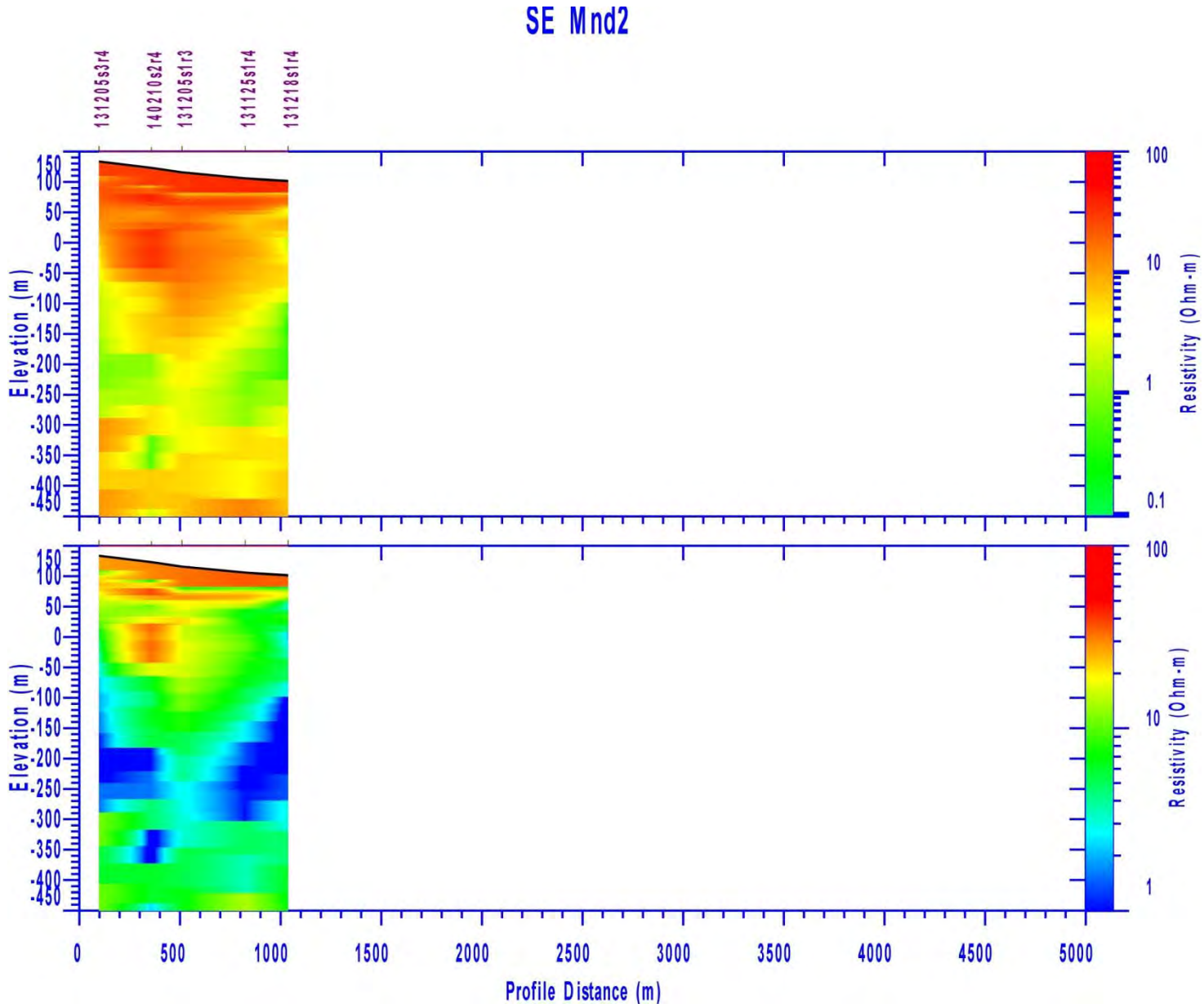

Figure C-18. Cross-section SE Mnd2.

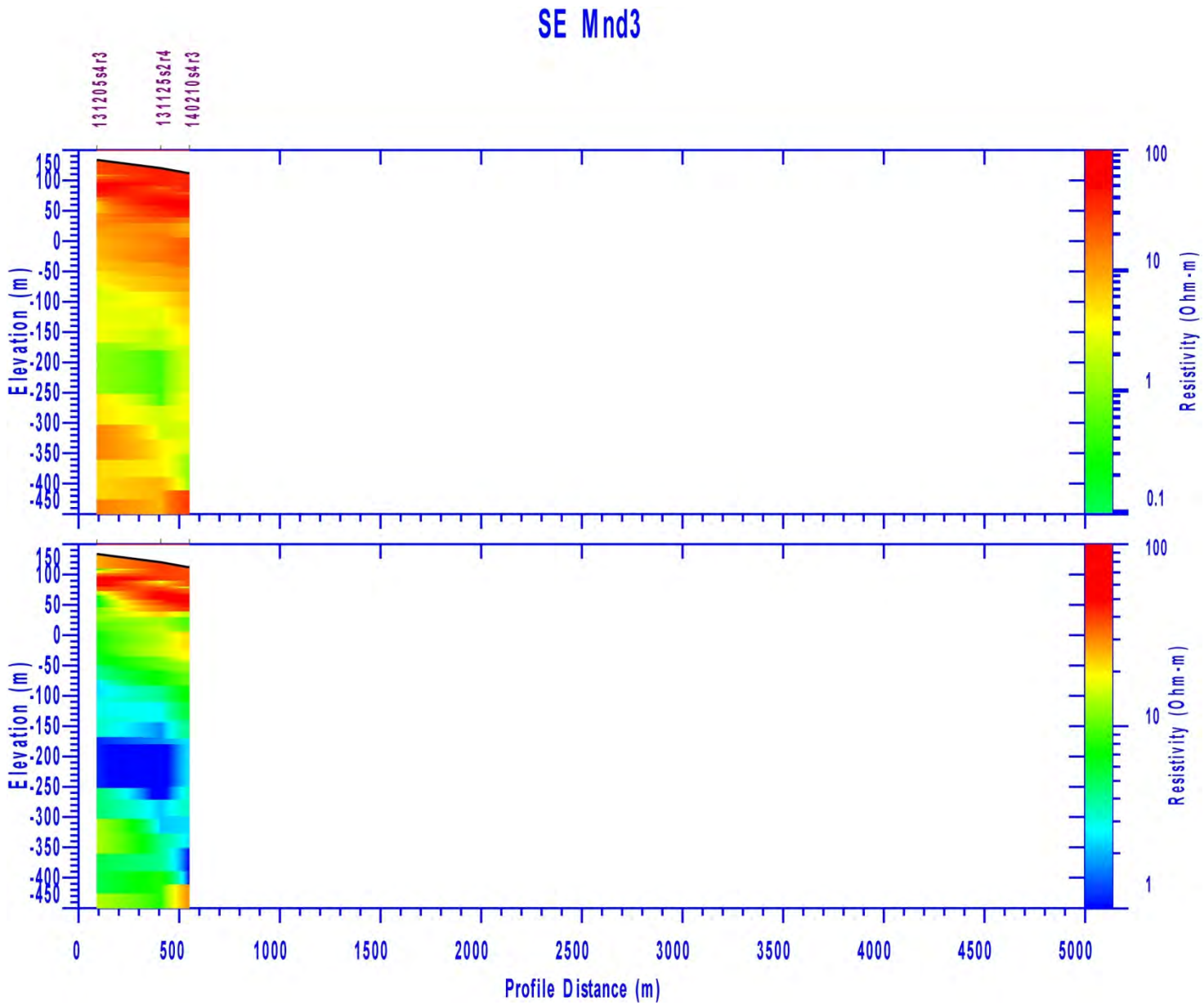

Figure C-19. Cross-section SE Mnd3.

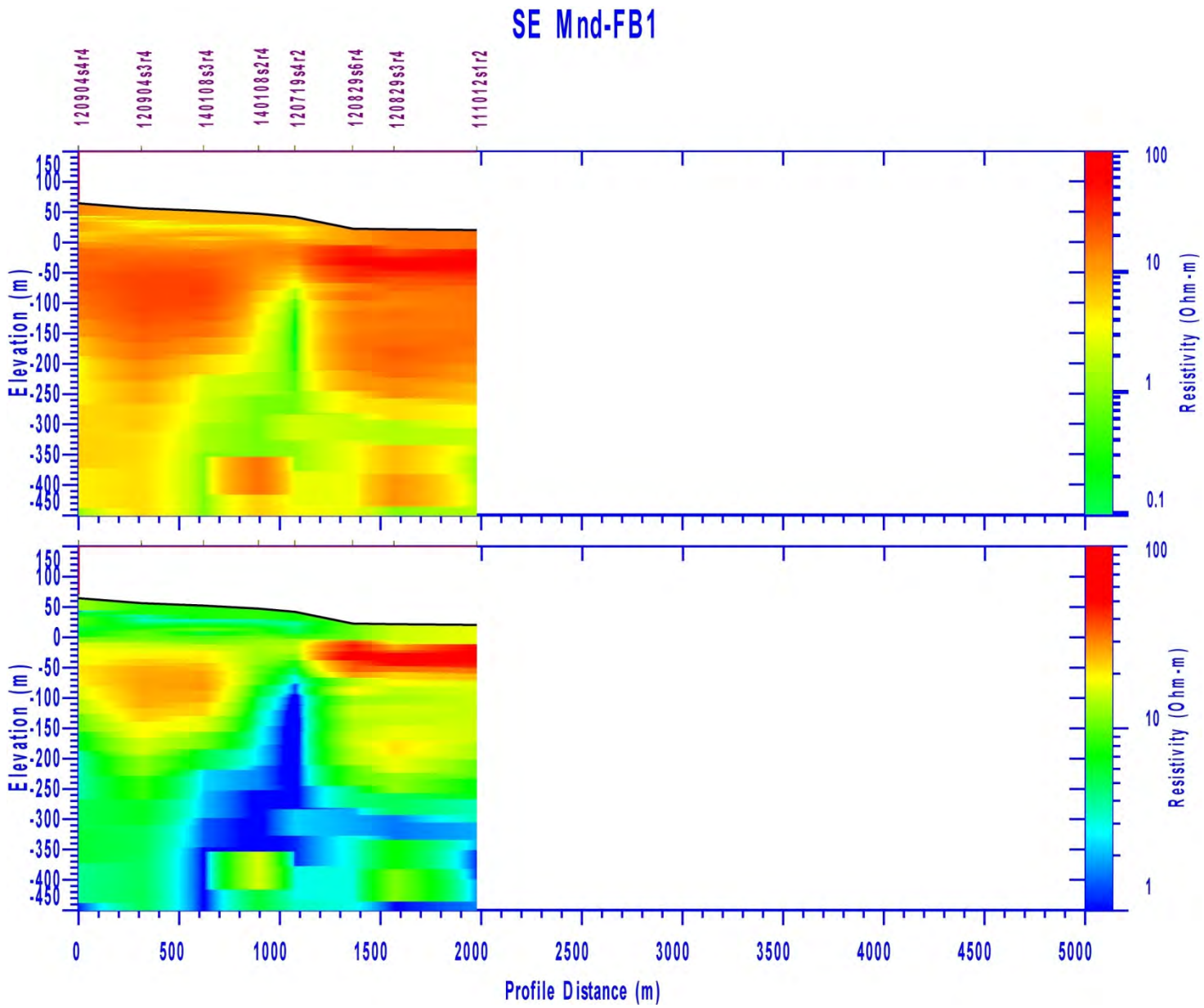

Figure C-20. Cross-section SE Mnd-FB1.

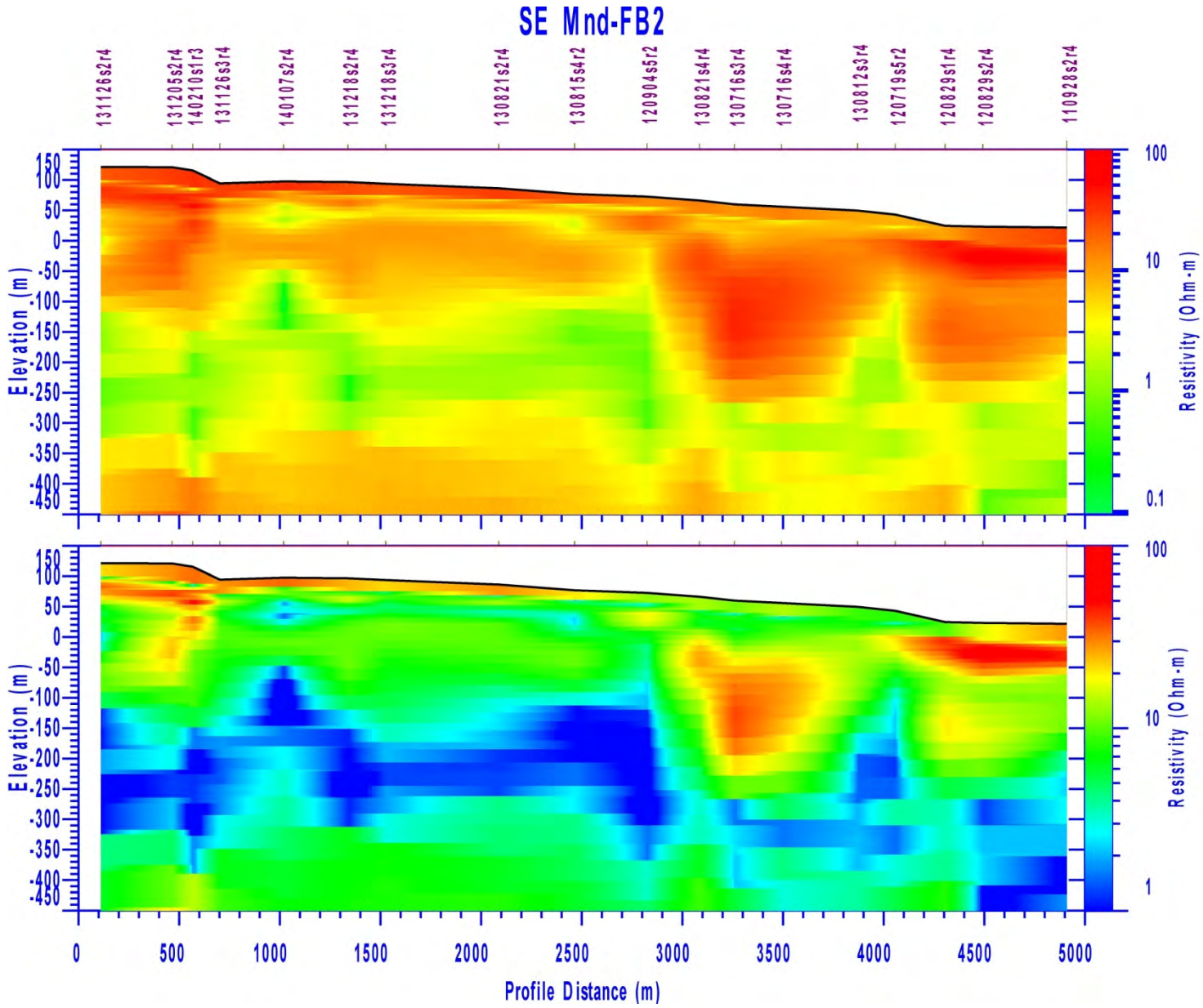

Figure C-21. Cross-section SE Mnd-FB2.

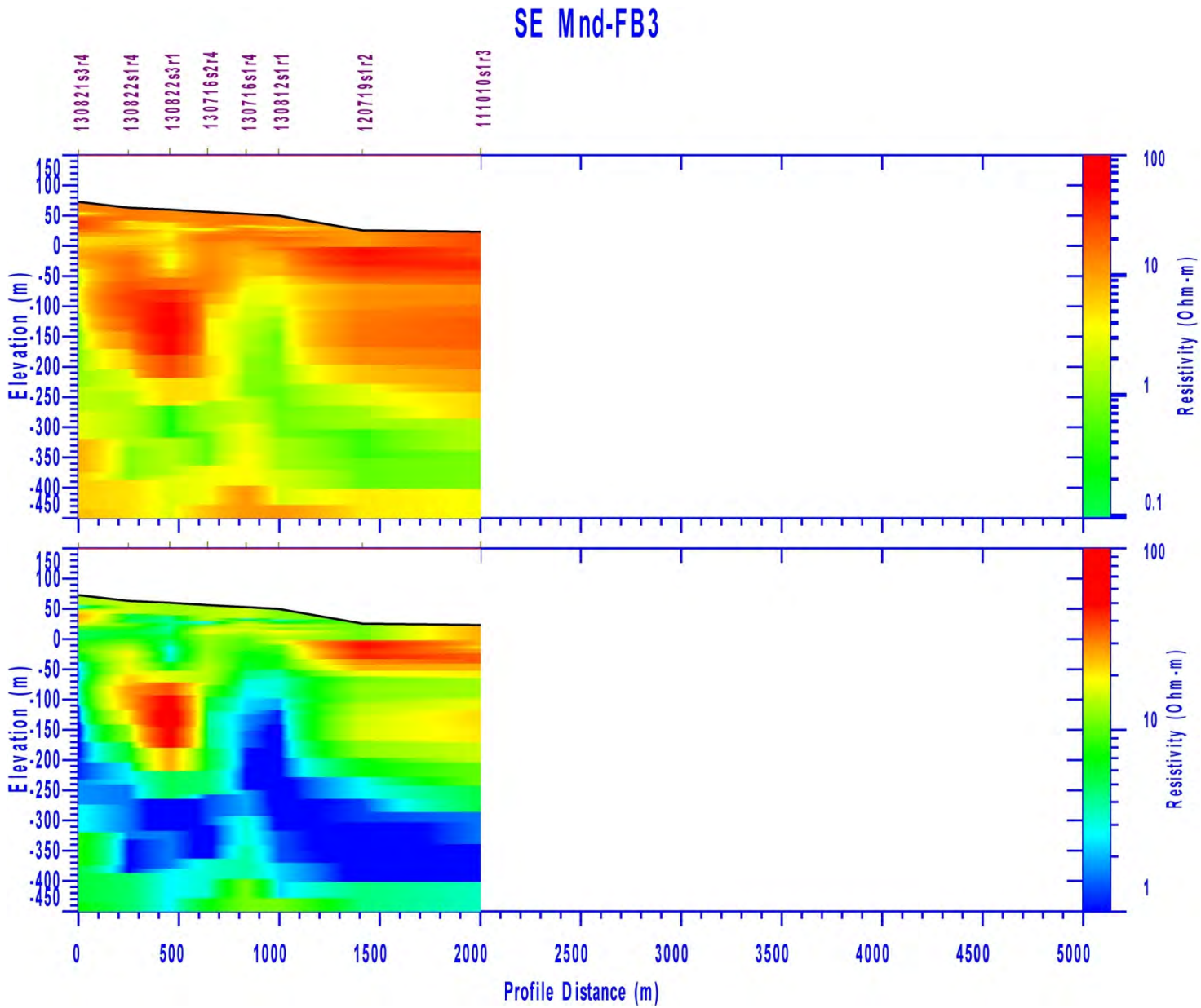

Figure C-22. Cross-section SE Mnd-FB3.

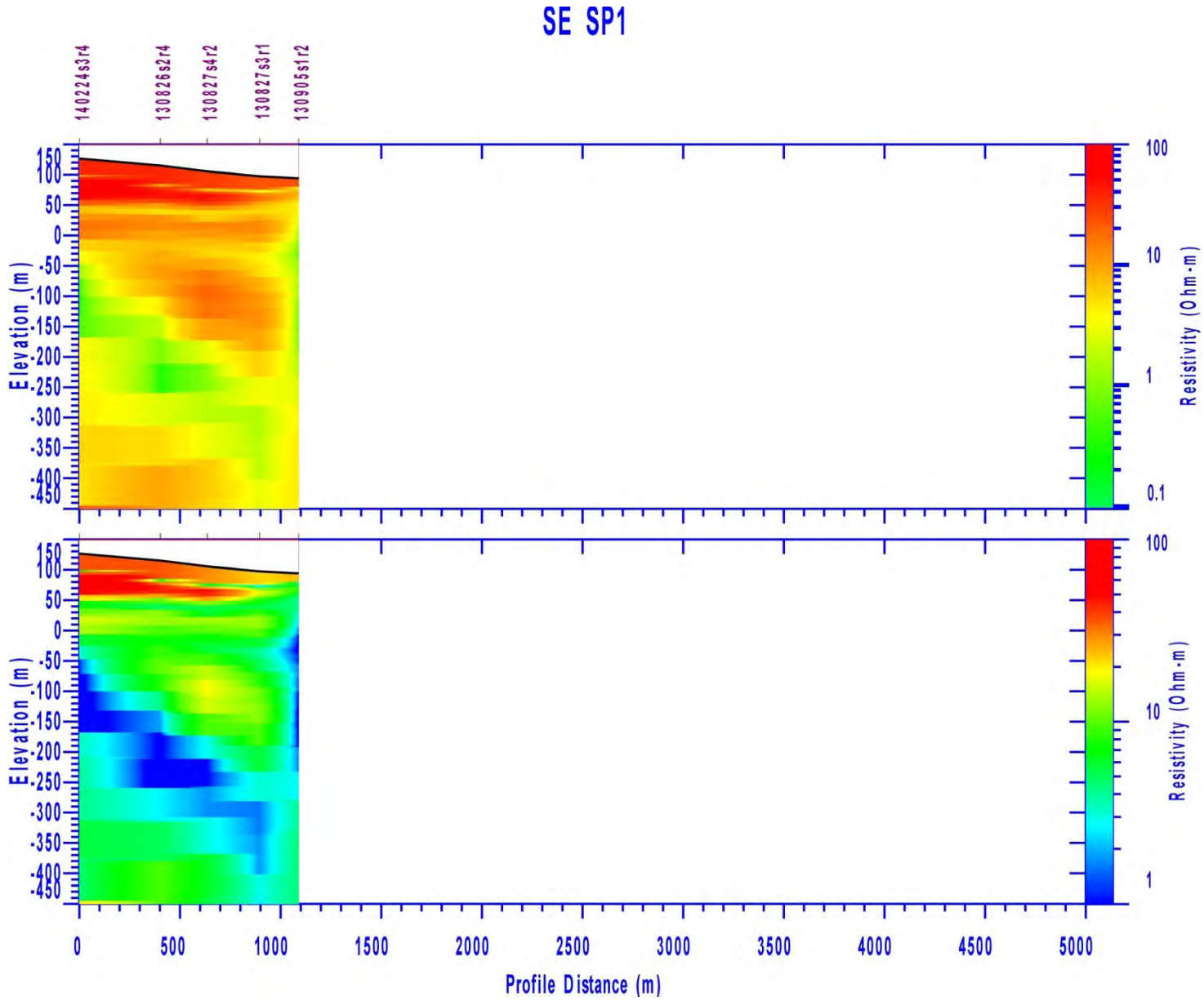

Figure C-23. Cross-section SE SP1.

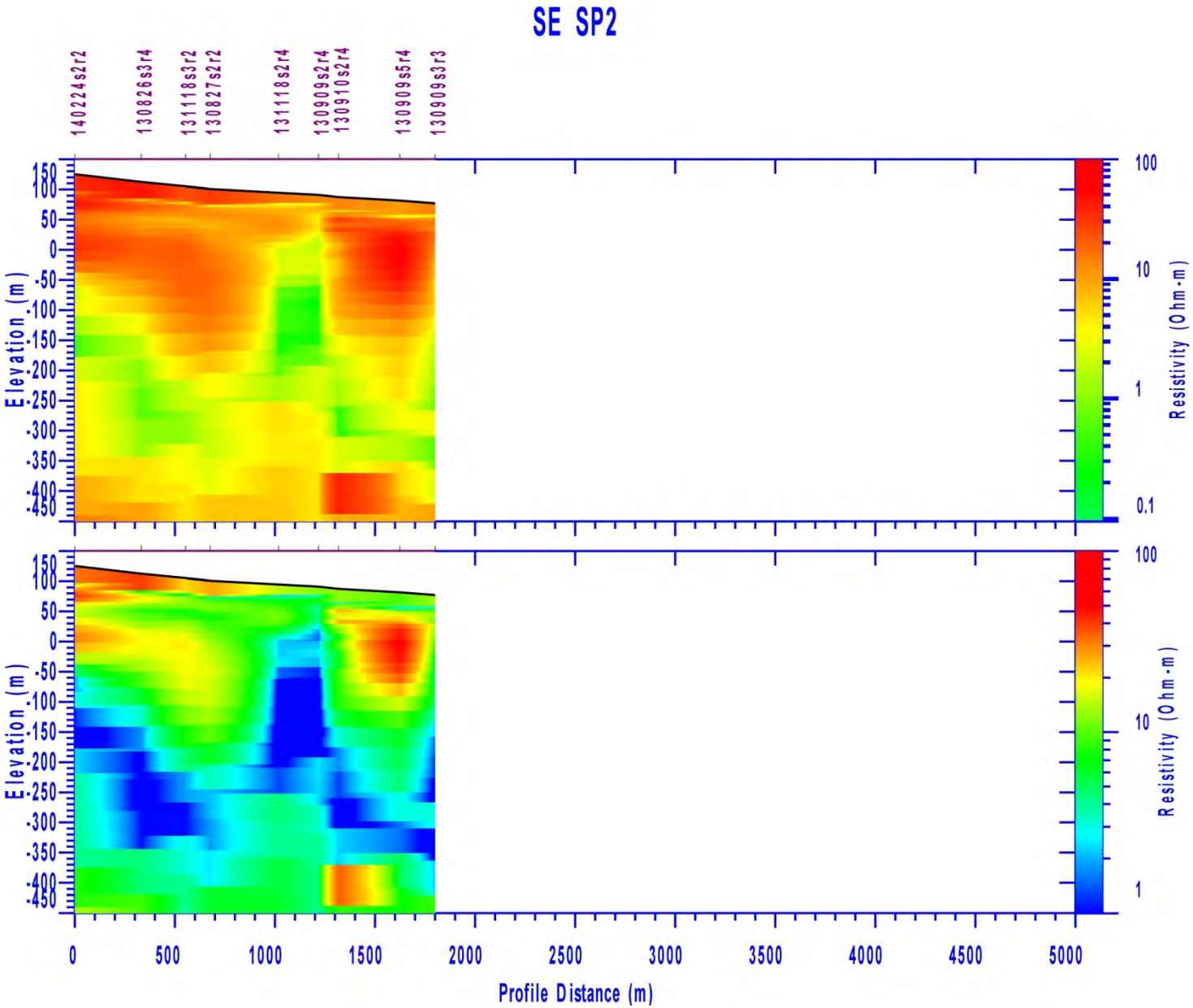

Figure C-24. Cross-section SE SP2.

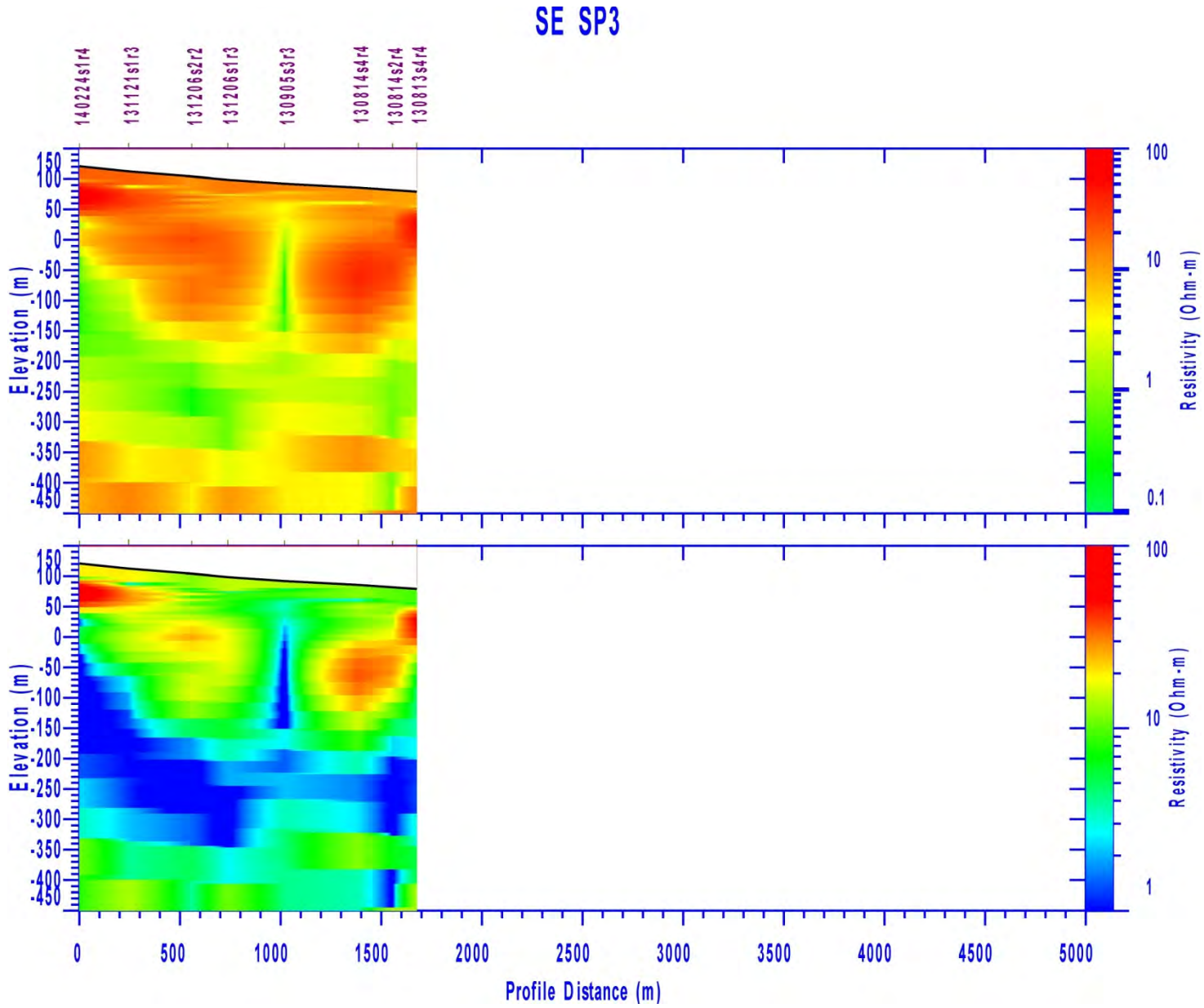

Figure C-25. Cross-section SE SP3.

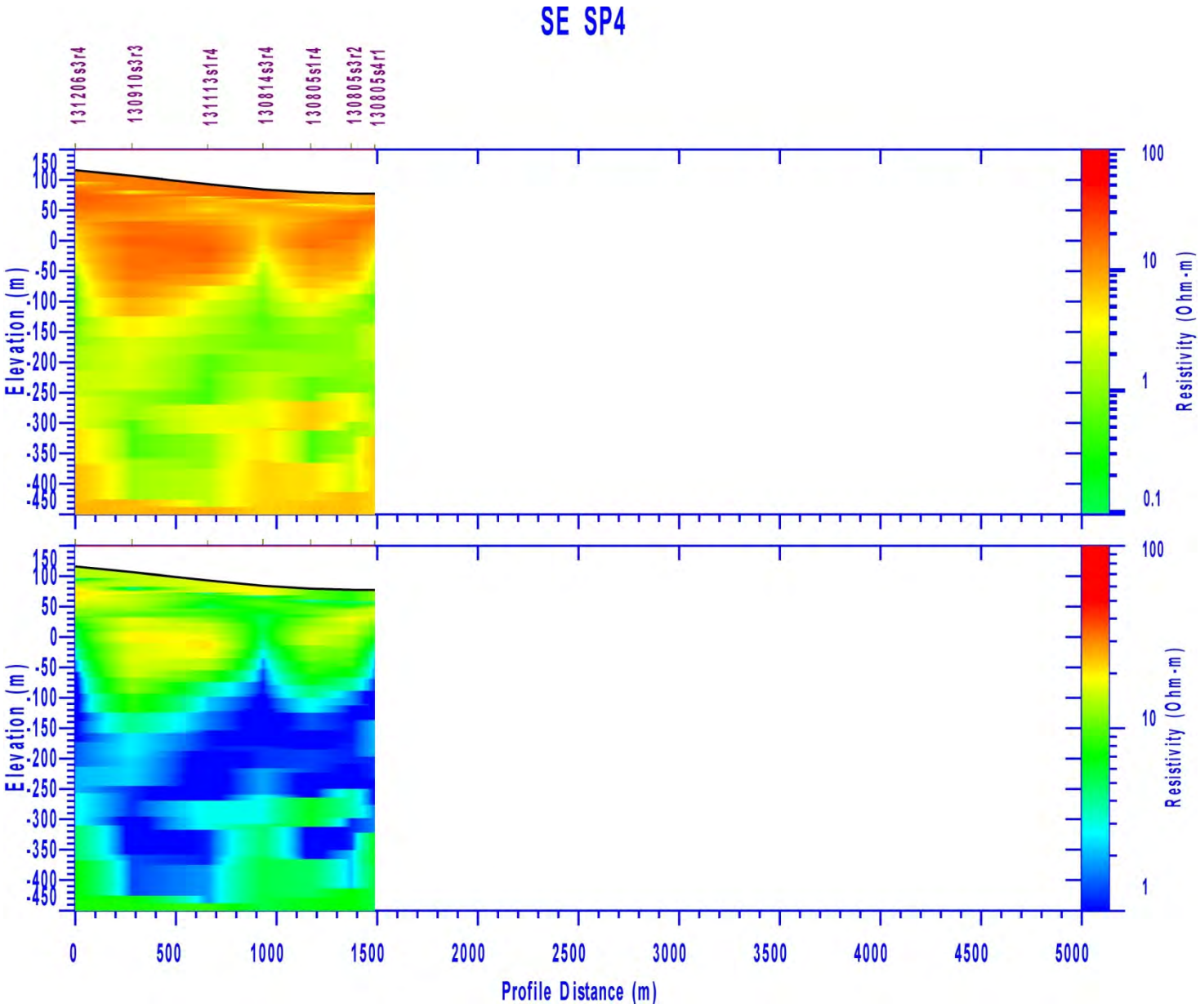

Figure C-26. Cross-section SE SP4.

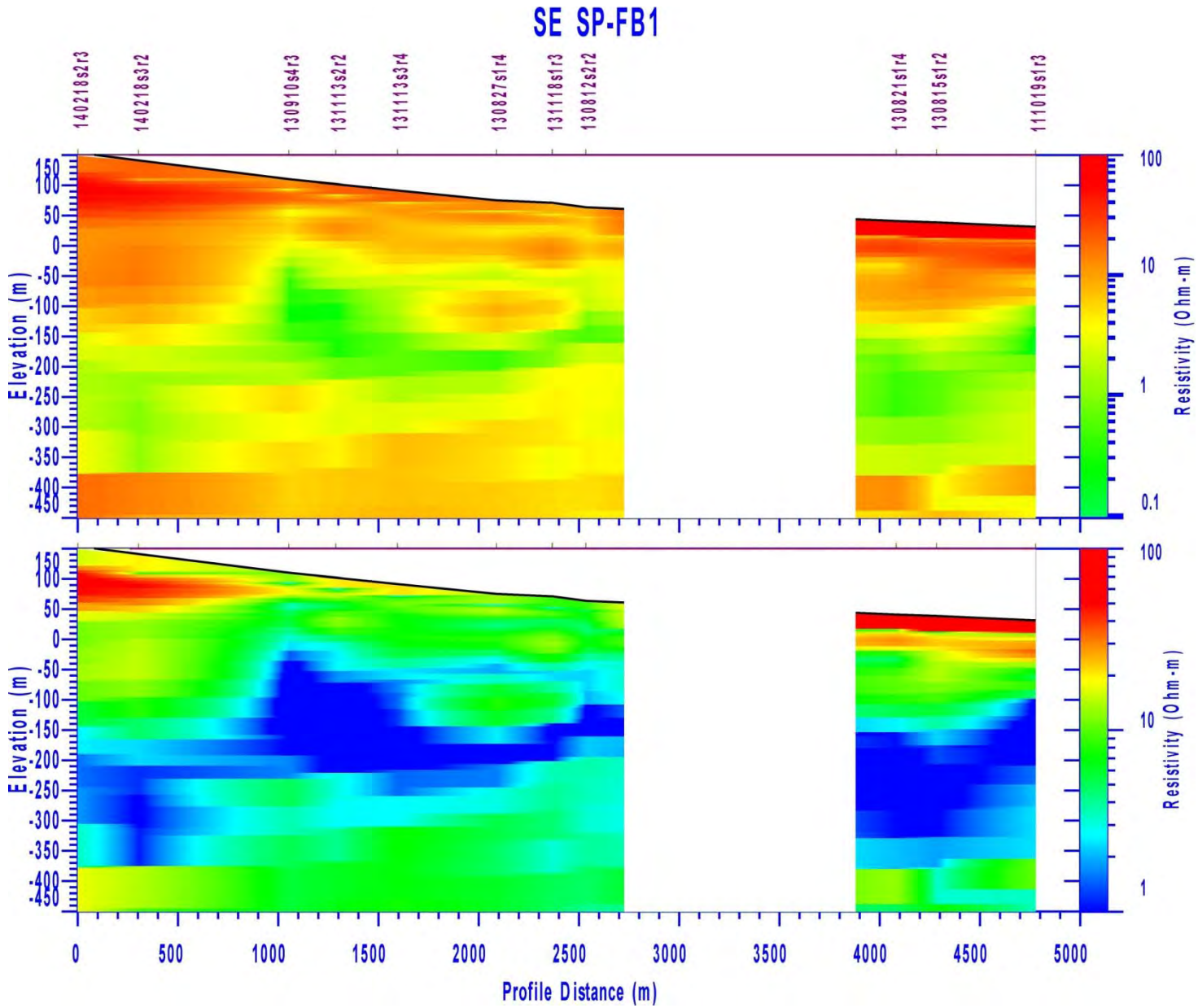

Figure C-27. Cross-section SE SP-FB1 (part of section blanked due to sparse data).

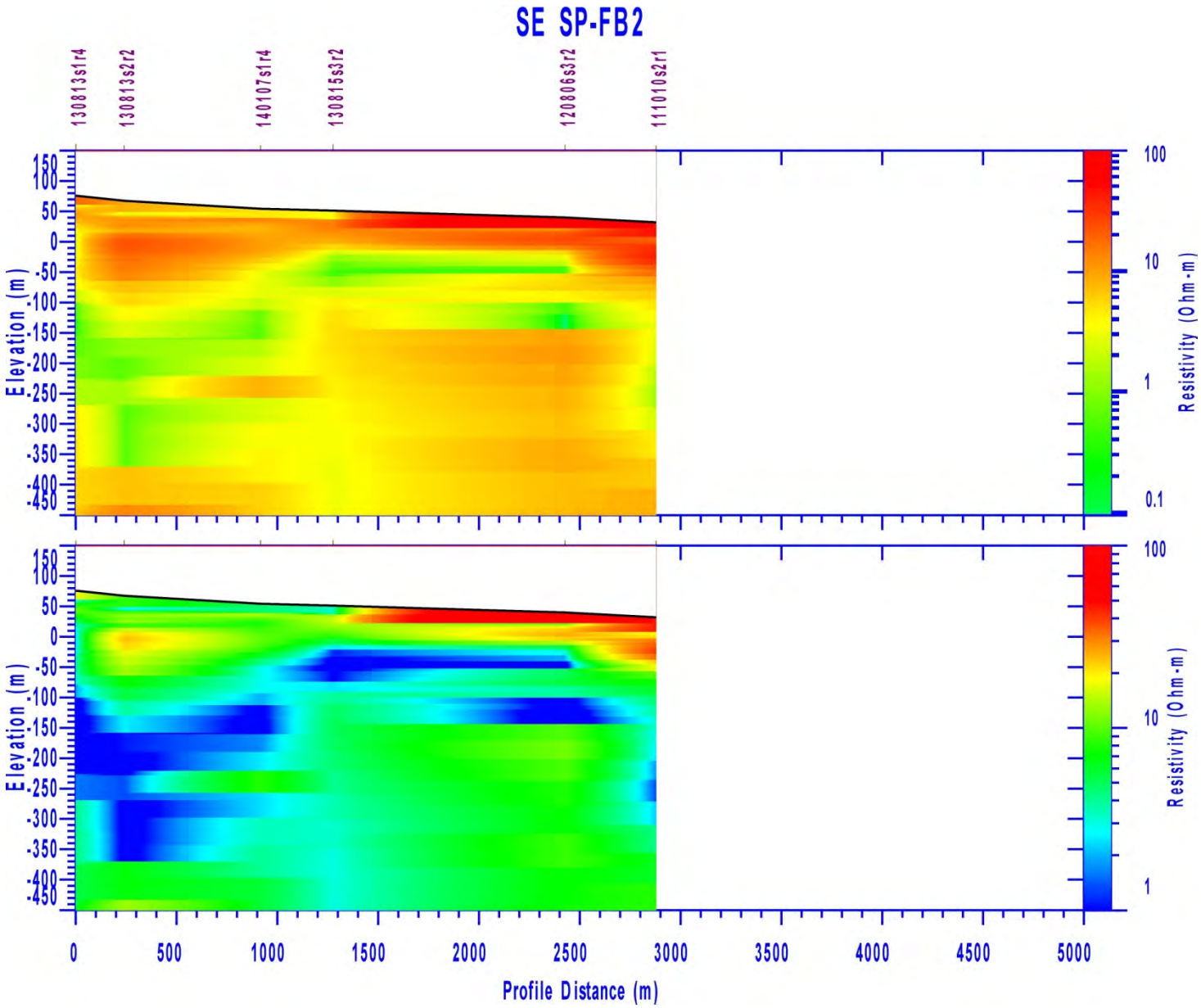

Figure C-28. Cross-section SE SP-FB2.

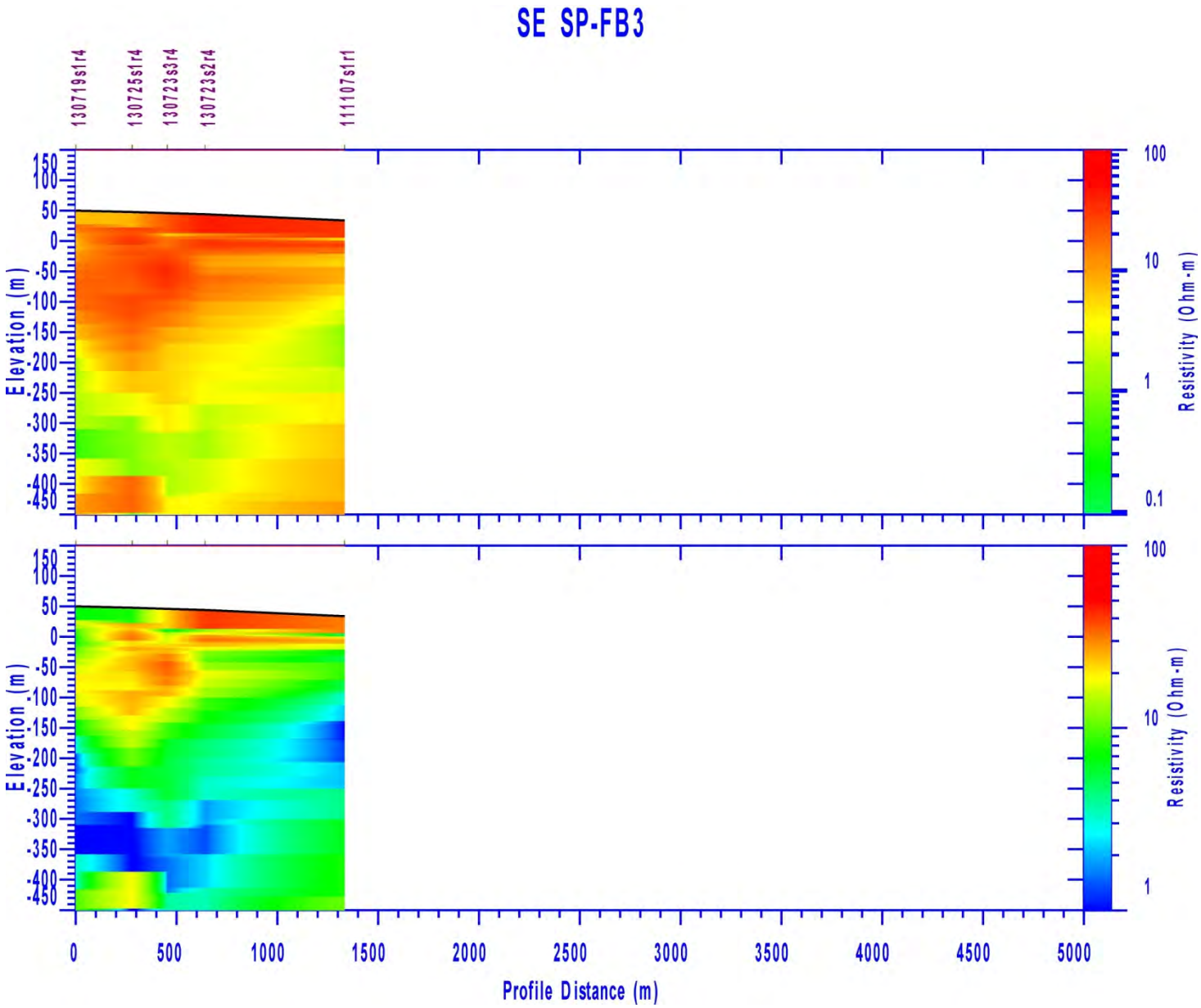

Figure C-29. Cross-section SE SP-FB3.

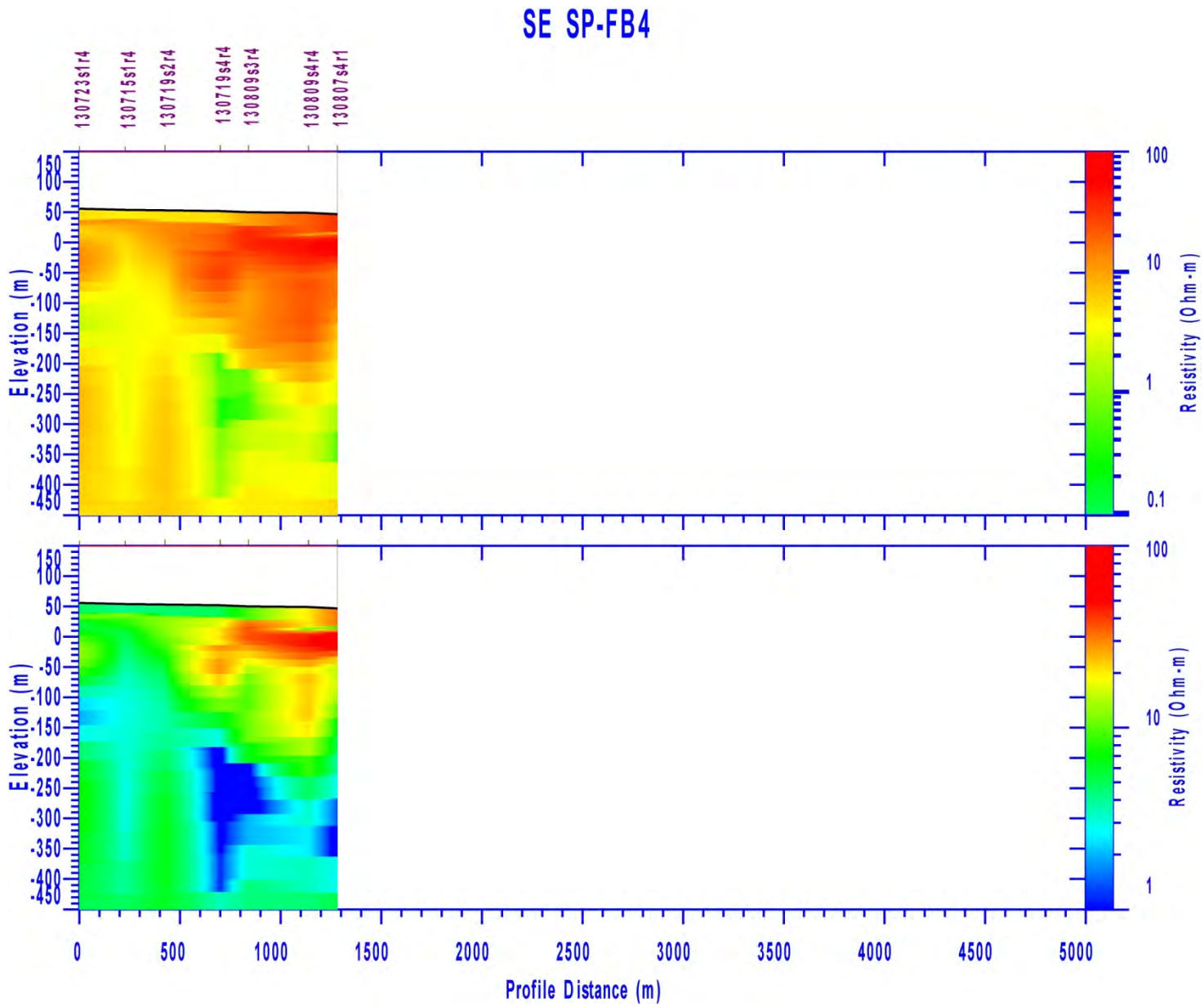

Figure C-30. Cross-section SE SP-FB4.

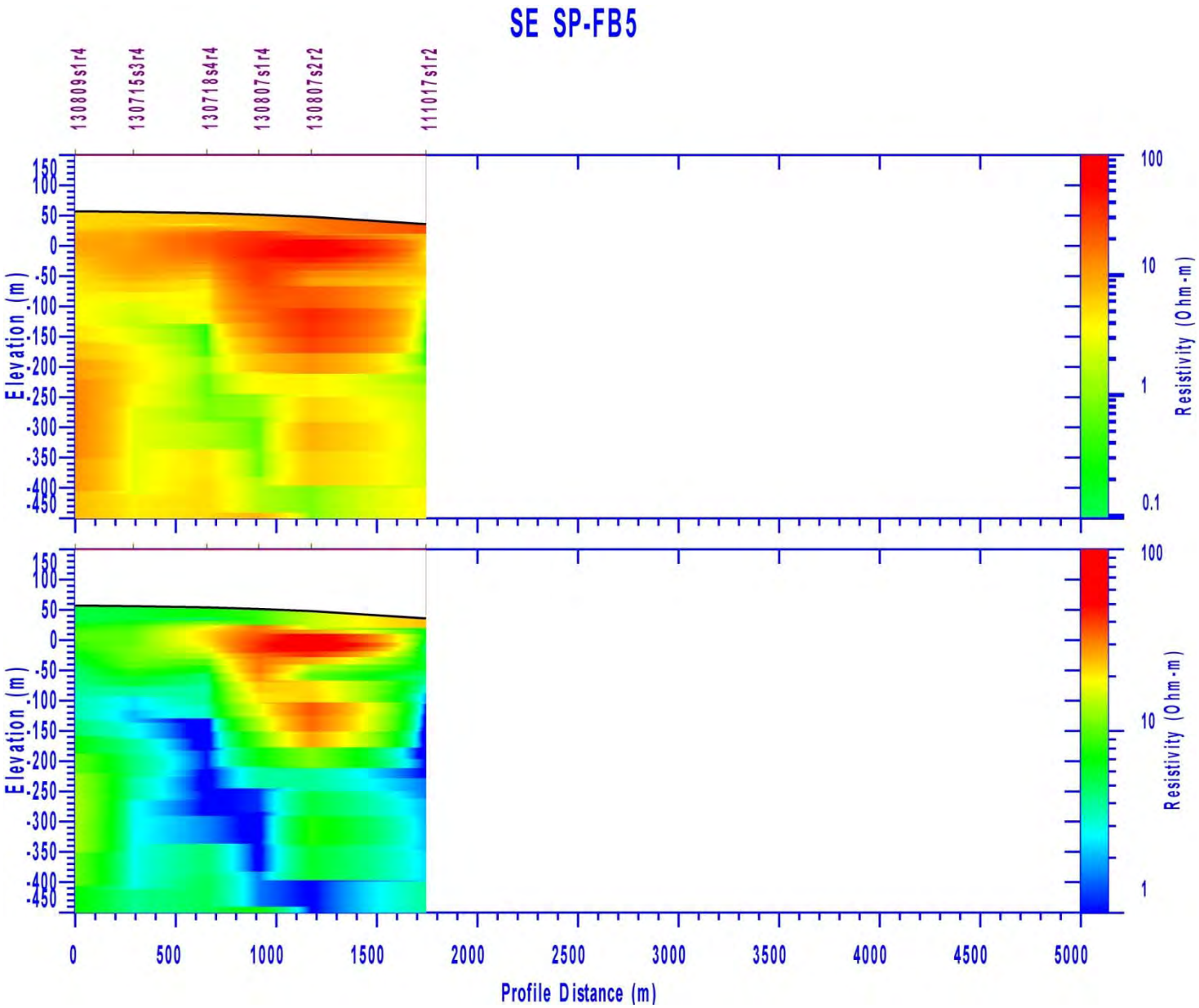

Figure C-31. Cross-section SE SP-FB5.

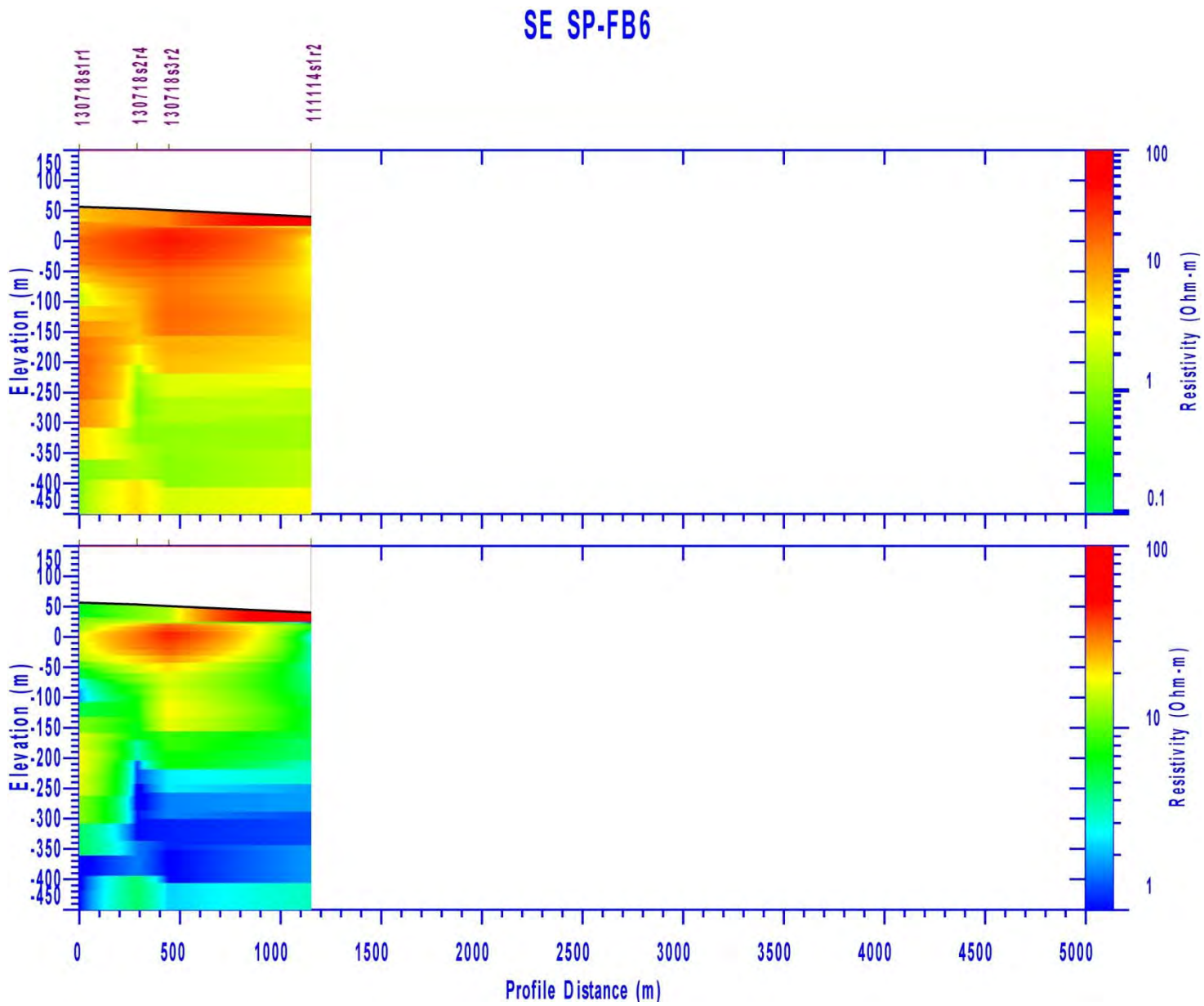

Figure C-32. Cross-section SE SP-FB6.